The Dissertation Committee for Kyle B. Guice Certifies that this is the approved version of the following dissertation:

Synthesis & Characterization of Temperature- and pH- Responsive Nanostructures Derived from Block Copolymers containing Statistical Copolymers of HEMA and DMAEMA

Committee:

Yueh-Lin Loo, Supervisor

Isaac Sanchez, Supervisor

Chris Bielawski

Venkat Ganesan

Don Paul

Nicholas Peppas

Synthesis & Characterization of Temperature- and pH- Responsive Nanostructures Derived from Block Copolymers containing Statistical Copolymers of HEMA and DMAEMA

by

Kyle B. Guice, B.S.

Dissertation

Presented to the Faculty of the Graduate School of

The University of Texas at Austin

in Partial Fulfillment

of the Requirements

for the Degree of

Doctor of Philosophy

The University of Texas at Austin

May, 2008

Dedication

To Ginger,

For your love and support on my hardest days.

And for Pappaw Cecil,

In loving remembrance.

Acknowledgements

I am very appreciative to those have helped me in the completion of my graduate studies. My advisor, Lynn, deserves tremendous credit for her support and encouragement of my research development. Her constant attention to detail and her desire to paint the entire picture are traits that I greatly admire. I would also like to thank several group members who have been very important to me during my graduate pursuits: Drs. Kimberly Dickey and Kwang Seok Lee, who provided excellent leadership for the group during my early years; Drs. Quinn Smith and Sally Peng Li, who provided invaluable guidance in polymer chemistry and characterization; Dr. Dmitry Krapchetov for assistance with FTIR experiments; and Joung Eun Yoo, Jacob Tarver, Reken Patel, Brian Goodfellow, Keith Gallow, and Dr. Enrique Gomez for numerous discussions. I would especially like to thank Tracy Bucholz, who provided far more support and discussion than I have room to mention. I would also like to gratefully acknowledge two undergraduate students, Raymond Teoh and Stephen Marrou, who have been instrumental in my research pursuits.

I would also like to acknowledge Dr. Chris Bielawski and members of the Bielawski research group, including Dan Coady, Kyle Williams, Brent Norris, and Dimitri Khramov, for use of and assistance with GC and GPC equipment, as well as for general discussion of chemistry-related issues. I would also like to thank Daniel Carr,

Steve Marek, and Adam Ekenseair for various discussions, and Dr. Steve Swinnea for assistance with SAXS.

I would like to acknowledge all the collaborators who have contributed to the work presented in this thesis. I am grateful to Dr. Brent Sumerlin and Dr. Sudershan Gondi for providing the RAFT chain transfer agents used in my work. I would also like to acknowledge Dr. Jan Genzer and Dr. Insun Park for LCST data.

I would like to thank Drs. Chris Bielawski, Venkat Ganesan, Don Paul, and Nicholas Peppas for providing research guidelines as members of my committee.

I would like to acknowledge the National Science Foundation for supporting my research with a Graduate Research Fellowship, and I would also like to thank the University and Bob West for a graduate fellowship. This work was supported by the National Science Foundation (DMR-0753148) and a Camille and Henry Dreyfus New Faculty award. Support from the Keck Foundation and Texas Materials Institute are also gratefully acknowledged.

Finally, I would like to thank my family for their enduring support during my graduate studies. Mom and Dad, I am very grateful for your efforts and your love. Ginger, I cannot imagine what it would have been like to go through this experience without you by my side. I am eternally thankful for your love and motivation.

Synthesis & Characterization of Temperature- and pH- Responsive Nanostructures Derived from Block Copolymers containing Statistical Copolymers of HEMA and DMAEMA

Publication No._____

Kyle B. Guice, Ph.D.

The University of Texas at Austin, 2008

Supervisors: Yueh-Lin Loo and Isaac C. Sanchez

Hydrogels containing of 2-dimethylaminoethyl methacrylate, DMAEMA, exhibit changes in their swelling properties in response to both pH and temperature. Accordingly, these materials are useful for a variety of applications, such as tissue scaffolds, responsive lenses, separations and drug delivery. The response of DMAEMA-containing hydrogels can be tuned by copolymerization with other monomers, such as 2-hydroxyethyl methacrylate, HEMA.

We have developed methodologies for the controlled synthesis of poly(HEMA-*co*-DMAEMA), PHD, statistical copolymers with uniform composition distributions, controlled molecular weights, and narrow molecular weight distributions using controlled free-radical polymerization techniques, such as atom transfer radical polymerization and radical addition-fragmentation chain transfer polymerization. We have also investigated the controlled synthesis and characterization of amphiphilic block copolymers containing

PHD statistical copolymers. These block copolymers microphase separate to form periodic nanostructures such as alternating lamellae, cylinders on a hexagonal lattice, or spheres on a body-centered cubic lattice, depending on the volume fraction of each block, the interblock segregation strength, and the choice of casting solvent. When swollen with water, these microphase-separated PHD-containing block copolymers form model hydrogels with uniform composition distributions.

Model block copolymer hydrogels containing PHD statistical copolymers are responsive to changes in pH or temperature. The response of these model block copolymer hydrogels can be tuned by adjusting of the DMAEMA content within the PHD block. Moreover, the response can be tuned by changing the hydrophobic block. Specifically, the use of a glassy hydrophobic block, such as polystyrene or poly(*tert*-butyl acrylate) at temperatures below its glass transition temperature, resulted in the preservation of the original block copolymer morphology during swelling. In contrast, the use of a hydrophobic block that is rubbery during swelling, such as poly(methyl acrylate), enabled reversible morphological transformations.

Table of Contents

List of Tables

List of Figures

Chapter 1. Introduction

Stimuli-responsive hydrogels represent a promising class of materials that are currently under investigation for a variety of applications, such as adaptive lenses,[1] tissue scaffolds,[2,3] biosensors,[2,3] bioseparations,[3] and drug delivery.[2,4] Hydrogels, or three-dimensional structures formed from polymeric materials that are highly swollen with water,[3] are generally useful for such bioapplications because they offer environments with similar mechanical properties to naturally-occurring biological systems.[5] Important hydrogel properties, such as elasticity and equilibrium water content, can also be tuned synthetically, thus affording investigators the ability to tailor the materials for each application.[5,6] Stimuli-responsive hydrogels allow for even greater tunability, as the properties of these hydrogels can also be altered by external triggers, such as changes in pH or temperature.[2,3,5]

One interesting monomer that is used in stimuli-responsive hydrogels is 2-dimethylaminoethyl methacrylate, DMAEMA, the chemical structure of which is shown in Figure 1.1. Poly(DMAEMA) exhibits responsiveness to two independent stimuli, pH and temperature.[7,8] Specifically, poly(DMAEMA) undergoes protonation when the pH of the surrounding solution is lowered below its pKa of 7.5.[9] In addition, poly(DMAEMA) undergoes a hydrophilic-to-hydrophobic transition upon heating, leading to a lower critical solution temperature (LCST) near 50°C in aqueous environments.[8,10] Due to their responsiveness to pH and temperature, DMAEMA-containing hydrogels have been investigated for a wide range of applications, including lenses,[1] nanofiltration systems,[11,12] tissue scaffolds,[13] and drug delivery.[7,14,15,16]

Often, it is desirable to copolymerize DMAEMA with other monomers, thereby tuning the responsiveness and/or incorporating additional chemical functionalities to the

hydrogel.[7,13,17] One comonomer that is commonly investigated in DMAEMA-containing hydrogels is 2-hydroxyethyl methacrylate, HEMA, the chemical structure of which is shown in Figure 1.2.[1,13,14,16,18] Poly(HEMA) is biocompatible and is water swellable, making it a useful biomaterial in its own regard.[19] In fact, poly(HEMA) was noted as a useful material for contact lenses as early as 1960.[20]

Copolymerization of HEMA and DMAEMA yields poly(HEMA-*co*-DMAEMA), PHD, hydrogels and enables the design of materials to meet specific performance requirements for each application. For example, a 10% increase in the DMAEMA content in PHD hydrogels was shown to increase the rate of diffusion of protamine through these hydrogels under acidic conditions by a factor of three.[16] For rapid release applications, higher concentrations of DMAEMA within PHD hydrogels are generally desirable.[7,15,16,18] In contrast, PHD hydrogels with low DMAEMA contents (< 1 mol%) resulted in the optimal proliferation of viable embryonic stem cells, when the hydrogels were investigated as tissue scaffolds.[13] In this case, the incorporation of a small amount of DMAEMA resulted in better adherence of embryonic stem cells to PHD hydrogel scaffolds.[13] In contrast, the incorporation of DMAEMA at higher concentrations was shown to result in reduced cell proliferation.[13]

While the utility of combining the attributes of HEMA and DMAEMA to tune the properties of the final hydrogel has been demonstrated, the ability to design PHD hydrogels with specific compositions is much less straight-forward. For example, Satish and coworkers found that the final DMAEMA content of PHD hydrogels that were synthesized in water was always less than that of the monomer feed, and that the difference between the DMAEMA content in the hydrogel and in the feed increased with increasing DMAEMA content in the feed.[14] In the most extreme case, the final concentration of DMAEMA in the hydrogel (60 mol%) was 14 mol% less than that in the

monomer feed (74 mol%).[14] Further, the addition of varying amounts of ethylene glycol dimethacrylate, a common crosslinking agent for PHD hydrogels, was also shown to affect the final DMAEMA content relative to HEMA in the hydrogel.[14] In these hydrogels, the final polymer composition is presumably also dependent on the total monomer conversion, as the final polymer composition at complete monomer conversion should be equivalent to that of the monomer feed. Because the composition of the monomers and crosslinker in the final hydrogel is a complex function of the feed compositions and the monomer conversion, the composition of the final hydrogel is difficult to predict.

In addition, the homogeneity of crosslink [21] and comonomer[22] distribution within these hydrogels is limited by the synthetic process. For two-monomer hydrogels synthesized in the presence of a chemical crosslinker, heterogeneities in the monomer sequence and crosslink[21] distributions are expected to arise not only from differences in the relative reactivities of the reactants (e.g., monomers and crosslinkers),[22] but also due to differences in monomer diffusion at polymerization conditions beyond the gel point, per the Trommsdorf effect.[4,23,24] Even in two component hydrogels consisting of a single monomer and a crosslinker, non-uniformities in compositional distributions have been demonstrated to result as a consequence of the synthetic process.[4,25-27] In some cases, large composition distributions within hydrogels can result in visible phase separation.[4] Such non-uniformities can significantly impact the swelling properties of gels. For example, increasing the non-uniformity in the crosslink distribution of cured epoxy resins resulted in a two-fold increase in their solvent uptake.[28] Ultimately, the presence of compositional non-uniformities within traditional hydrogels limits the ability to assess the structure-property relationships of the resulting materials.[21]

A potential technique to overcome non-uniformities in hydrogel crosslink distribution involves the self assembly of amphiphilic block copolymers.[4,29] Block copolymers are known to spontaneously microphase separate and self assemble to form periodic nanostructures, such as alternating lamellar sheets, hexagonally-packed cylinders, and spheres packed on a body-centered-cubic lattice, in the solid state.[30] The details of the morphology and characteristic dimensions of the block copolymer nanostructures depend on the volume fractions of the two blocks, the degree of polymerization, and the segregation strength between the two blocks.[31] Microphase-separated, amphiphilic block copolymers have been designed such that hydrophobic blocks occupy discrete nanostructures (e.g., cylinders, spheres) that are located periodically throughout hydrophilic matrices.[29] In these model block copolymer hydrogels, hydrophobic microdomains serve as physical crosslinks that are evenly distributed throughout a swellable matrix.[29]

Effective control over polymer molecular weight and molecular weight distribution, commonly achieved through controlled or "living" polymerization, is important in the design of well-defined amphiphilic block copolymer systems.[32] While anionic polymerization is generally considered the gold standard for "living" polymerizations,[32] this synthetic technique is not amenable to the direct polymerization of functional monomers, such as HEMA or DMAEMA.[33] Fortunately, several controlled free-radical polymerization schemes, including atom transfer radical polymerization (ATRP) and reversible addition-fragmentation transfer polymerization (RAFT), have been developed that are both controlled and highly tolerant to monomer functionalities.[34] Inherently, these polymerization schemes are not "living," as polymer termination in free-radical polymerizations cannot be entirely avoided.[34] If suitably designed, however, termination reactions can be suppressed with both ATRP and RAFT, thereby allowing

effective control over the polymerization.[34] Controlled polymerizations of HEMA[17,35,36,37] and DMAEMA[8,17,38-42] have been previously demonstrated by both ATRP and RAFT.

In the course of our investigation, we sought to design and assess microphase-separated, amphiphilic, PHD-containing block copolymers for use as model stimuli-responsive hydrogels. The synthesis of well-controlled PHD-containing block copolymers is complicated by the fact that HEMA and DMAEMA are copolymerized into a single block, because the comonomer distribution needs to be controlled in order to minimize non-uniformities in the resulting block copolymer hydrogels.

THESIS OVERVIEW

Chapter 2 provides an overview of the relevant theories and characterization techniques utilized in this work. The chapter also details the specific synthetic methodologies used throughout this work.

Chapter 3 highlights our efforts to control the synthesis of PHD copolymers. Specifically, Chapter 3 details the importance of the selection of the polymerization medium in controlling the compositional distribution within PHD copolymers.[44,45] Chapter 3 also describes the optimization of ATRP for the synthesis of PHD statistical copolymers with well-controlled molecular weights and narrow molecular weight distributions.[44, 45]

Chapter 4 extends the synthetic techniques elaborated in Chapter 3 to the design of amphiphilic block copolymers containing statistical PHD copolymers.[44,46] A multitude of PHD-containing di- and tri- block copolymers can be synthesized using controlled-free radical polymerization techniques. Chapter 4 further highlights that these block copolymers undergo microphase separation, resulting in well-defined nanostructured materials of predictable morphologies, depending on the volume fractions of the two

blocks, the degree of polymerization, the interblock segregation strength, and the choice of casting solvent.[44]

The response of PHD-containing amphiphilic block copolymer model hydrogels to pH and temperature are described in Chapters 5 and 6, respectively. In particular, Chapter 5 describes the pH-responsiveness of PHD-containing block copolymer hydrogels in which polystyrene, PS, forms the hydrophobic block. Because PS is glassy during these experiments, the microstructure originally defined by microphase separation is effectively preserved during swelling. This chapter identifies similarities in the swelling behavior of lamella-forming diblock and triblock copolymer hydrogels. It further highlights that the swelling of PS/PHD hydrogels can be tuned by synthetically adjusting the composition of the PHD block.

Chapter 6 describes the temperature response of PHD-containing block copolymer hydrogels in which poly(methyl acrylate), PMA, serves as the hydrophobic block. In contrast to the swelling observed for block copolymers with PS hydrophobic microdomains, Chapter 6 demonstrates that the swelling of PHD-containing hydrogels with PMA hydrophobic microdomains can result in morphological transformation within the hydrogels because PMA is rubbery during swelling. The chapter also highlights that the swelling of PMA/PHD hydrogels can be tuned with PHD composition.

Finally, Chapter 7 summarizes the major achievements of our research effort and presents suggestions for future work.

FIGURES

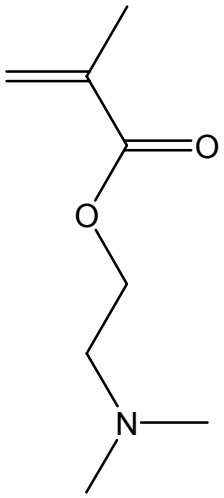

Figure 1.1. Chemical structure of 2-dimethylaminoethyl methacrylate, DMAEMA.

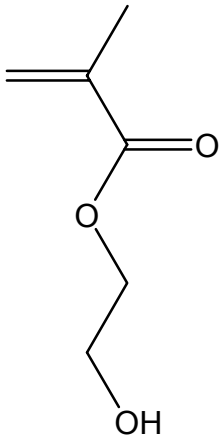

Figure 1.2. Chemical structure of 2-hydroxyethyl methacrylate, HEMA.

REFERENCES

1. Dong, L.; Agarwal, A. K.; Beebe, D. J.; Jiang, H. *Nature* **2006,** 442, 551-554.

2. Chaterji, S.; Kwon, I. K.; Park, K. *Progress in Polymer Science* **2007,** 32, 1083-1122.

3. Kopecek, J. *Biomaterials* **2007,** 28, 5185-5192.

4. Kopecek, J.; Yang, J. *Polymer International* **2007,** 56, 1078-1098.

5. Ulijn, R. V.; Bibi, N.; Jayawarna, V.; Thornton, P. D.; Todd, S. J.; Mart, R. J.; Smith, A. M.; Gough, J. E. *Materials Today* **2007,** 10, 40-48.

6. Bell, C. L. P., N.A. *Advances in Polymer Science* **1994,** 122, 129-173.

7. Brahim, S.; Narinesingh, D.; Guiseppi-Elie, A. *Biomacromolecules* **2003,** 4, 497-503.

8. Fournier, D.; Hoogenboom, R.; Thijs, H. M. L.; Paulus, R. M.; Schubert, U. S. *Macromolecules* **2007,** 40, 915-920.

9. Van de Wetering, P.; Moret, E. E.; Schuurmans-Nieuwenbroek, N. M. E.; Van Steenbergen, M. J.; Hennink, W. E. *Bioconjugate Chemistry* **1999,** 10, 589-597.

10. Cho, S. H.; Jhon, M. S.; Yuk, S. H.; Lee, H. B. *Journal of Polymer Science, Part B: Polymer Physics* **1997,** 35, 595-598.

11. Du, R.; Zhao, J. *Journal of Applied Polymer Science* **2004,** 91, 2721-2728.

12. Yilmaz, Z.; Akkas, P. K.; Sen, M.; Guven, O. *Journal of Applied Polymer Science* **2006,** 102, 6023-6027.

13. Kroupova, J.; Horak, D.; Pachernik, J.; Dvorak, P.; Slouf, M. *Journal of Biomedical Materials Research, Part B: Applied Biomaterials* **2006,** 76B, 315-325.

14. Satish, C. S.; Shivakumar, H. G. *Journal of Macromolecular Science, Part A: Pure and Applied Chemistry* **2007,** 44, 379-387.

15. Traitel, T.; Cohen, Y.; Kost, J. *Biomaterials* **2000,** 21, 1679-1687.

16. Brahim, S.; Narinesingh, D.; Guiseppi-Elie, A. *Biomacromolecules* **2003,** 4, 1224-1231.

17. Jin, X.; Shen, Y.; Zhu, S. *Macromolecular Materials and Engineering* **2003,** 288, 925-935.

18. Traitel, T.; Kost, J.; Lapidot, S. A. *Biotechnology and Bioengineering* **2003,** 84, 20-28.

19. Kwok, A. Y.; Qiao, G. G.; Solomon, D. H. *Polymer* **2004,** 45, 4017-4027.

20. Wichterle, O.; Lim, D. *Nature* **1960,** 185, 117-118.

21. Triftaridou, A. I.; Hadjiyannakou, S. C.; Vamvakaki, M.; Patrickios, C. S. *Macromolecules* **2002,** 35, 2506-2513.

22. Martin-Gomis, L.; Cuervo-Rodriguez, R.; Fernandez-Monreal, M. C.; Madruga, E. L.; Fernandez-Garcia, M. *Journal of Polymer Science, Part A: Polymer Chemistry* **2003,** 41, 2659-2666.

23. Gordon, M.; Roe, R.-J. *Journal of Polymer Science* **1956,** 21, 57-74.

24. Odian, G., *Principles of Polymerization*. 4th ed.; Wiley-Interscience: New York, 2004.

25. Haraguchi, K.; Takehisa, T. *Advanced Materials* **2002,** 14, 1120-1124.

26. Huglin, M. B.; Zakaria, M. B. *Polymer* **1984,** 25, 797-802.

27. Liu, R.; Oppermann, W. *Macromolecules* **2006,** 39, 4159-4167.

28. Kishi, H.; Naitou, T.; Matsuda, S.; Murakami, A.; Muraji, Y.; Nakagawa, Y. *Journal of Polymer Science, Part B: Polymer Physics* **2007,** 45, 1425-1434.

29. Nykaenen, A.; Nuopponen, M.; Laukkanen, A.; Hirvonen, S.-P.; Rytelae, M.; Turunen, O.; Tenhu, H.; Mezzenga, R.; Ikkala, O.; Ruokolainen, J. *Macromolecules* **2007,** 40, 5827-5834.

30. Leibler, L. *Macromolecules* **1980,** 13, 1602-17.

31. Matsen, M. W.; Bates, F. S. *Macromolecules* **1996,** 29, 1091-1098.

32. Hamley, I. W., Introduction to Block Copolymers. In *Developments in Block Copolymer Science and Technology*, Hamley, I. W., Ed. John Wiley & Sons: Chichester, 2004; pp 1-30.

33. Tsarevsky, N. V.; Pintauer, T.; Matyjaszewski, K. *Macromolecules* **2004,** 37, 9768-9778.

34. Matyjaszewski, K., General Concepts and History of Living Radical Polymerization. In *Handbook of Radical Polymerization*, Matyjaszewski, K.; Davis, T. P., Eds. Wiley-Interscience: New York, 2002; pp 361-406.

35. Beers, K. L.; Gaynor, S. G.; Matyjaszewski, K.; Sheiko, S. S.; Moeller, M. *Macromolecules* **1998,** 31, 9413-9415.

36. Weaver, J. V. M.; Bannister, I.; Robinson, K. L.; Bories-Azeau, X.; Armes, S. P.; Smallridge, M.; McKenna, P. *Macromolecules* **2004,** 37, 2395-2403.

37. Robinson, K. L.; Khan, M. A.; de Banez, M. V.; Wang, X. S.; Armes, S. P. *Macromolecules* **2001,** 34, 3155-3158.

38. Lee, S. B.; Russell, A. J.; Matyjaszewski, K. *Biomacromolecules* **2003,** 4, 1386-1393.

39. Mao, B.; Gan, L.-H.; Gan, Y.-Y.; Li, X.; Ravi, P.; Tam, K.-C. *Journal of Polymer Science, Part A: Polymer Chemistry* **2004,** 42, 5161-5169.

40. Bougard, F.; Jeusette, M.; Mespouille, L.; Dubois, P.; Lazzaroni, R. *Langmuir* **2007,** 23, 2339-2345.

41. Achilleos, M.; Krasia-Christoforou, T.; Patrickios, C. S. *Macromolecules* **2007,** 40, 5575-5581.

42. Sahnoun, M.; Charreyre, M.-T.; Veron, L.; Delair, T.; D'Agosto, F. *Journal of Polymer Science, Part A: Polymer Chemistry* **2005,** 43, 3551-3565.

43. Mathew-Krotz, J.; Mahadevan, V. *Macromolecular Chemistry and Physics* **1997,** 198, 1597-1604.

44. Guice, K. B.; Loo, Y.-L. *Macromolecules* **2006,** 39, 2474-2480.

45. Teoh, R. L.; Guice, K. B.; Loo, Y.-L. *Macromolecules* **2006,** 39, 8609-8615.

46. Guice, K. B.; Loo, Y.-L. *Macromolecules* **2007,** 40, 9053 -9058.

Chapter 2. Background and Experimental Techniques

INTRODUCTION

This chapter provides an overview of theories, experimental details, and characterization techniques associated with our work. First, we present the relevant background in polymer chemistry to understand the discussions in this thesis, including aspects of conventional free-radical polymerization, controlled free-radical polymerization, and the principles of copolymerization. We subsequently describe the phase behavior of block copolymers. Following that, we present a brief overview of pH-responsive hydrogels and that of aqueous polymer solutions that exhibit lower critical solution temperatures, both concepts we later utilize to design environmentally-responsive block copolymer hydrogels. Next, we present the experimental details relevant to the synthesis of polymers discussed in this work. Finally, we describe the analytical techniques used to characterize our materials, including differential scanning calorimetry, gas chromatography, gel permeation chromatography, Fourier transform-infrared spectroscopy, nuclear magnetic resonance, and small-angle x-ray scattering.

BACKGROUND

Free-Radical Polymerization

Free-radical polymerization[1] has proven to be a versatile technique for the polymerization of a wide variety of monomers, including many that are not amenable to polymerization by other chain polymerization techniques.[2] Free-radical polymerization involves three principle steps: initiation, propagation, and termination.[1] The steps of free-radical polymerization are shown schematically in Figure 2.1, which will be further summarized below.

First, free-radicals are generated through an initiation step, which most commonly involves the thermal or photo decomposition of an initiator, I, into a pair of radicals, R·. Common initiators for free-radical polymerization include azobisisobutyronitrile (AIBN), benzoyl peroxide (BPO), and *tert*-butyl peroxide (*t*BPO). After the radicals are generated, the first monomer, M, is added to the radical to generate M·, an initiated radical. The formation of this initiated radical is generally the rate limiting step for conventional free-radical polymerizations.[1] Additional monomers are then successively added to M· during propagation, resulting in a long-chain polymer radical, P_n·, where n represents the total number of M monomers that have been added to the radical during propagation. Finally, the polymer chain stops growing during termination. There are two specific termination pathways, combination or disproportionation, both of which require the presence of two polymer radicals. During combination, two polymer radicals undergo a head-to-head coupling reaction, resulting in a polymer chain whose length is the sum of the two coupled polymer radicals. Alternatively, the *beta*-Hydrogen of a polymer radical can be transferred to another polymer radical, resulting in two individual polymer chains, one with a saturated chain end and other with an unsaturated chain end. This termination mechanism is known as disproportionation and is by far more common than termination via combination.[1]

A side reaction that can potentially occur during the propagation step of conventional free-radical polymerization is chain transfer, whereby a free radical is transferred from a polymer chain end to another species (e.g., solvent or monomer), frequently resulting in the formation of a new radical species which can in turn propagate through subsequent monomer addition. In an effort to control the molecular weight during conventional free-radical polymerizations, chain transfer agents – species that promote this chain transfer reaction – are frequently added.[1] These compounds are

typically designed such that there is a high rate of transfer of radicals from existing polymer radicals to the chain transfer agents, resulting in the formation of new radical species that are capable of monomer addition. The introduction of chain transfer agent therefore increases the number of polymer chains produced given a specified initiator concentration, thereby reducing the average molecular weight of the resulting polymers.

Controlled Free-Radical Polymerization

One of the principle drawbacks of conventional free-radical polymerization is that it is difficult to synthesize polymers of prescribed molecular weights and narrow molecular weight distributions.[2] The poor control afforded by conventional free-radical polymerization is related to two specific aspects of the polymerization. First, the rate of initiation is significantly slower than the rate of propagation.[2] Second, the rate of termination is comparable to the rate of initiation at steady state, which typically occurs early in the polymerization.[1] As a consequence, polymers are being initiated and terminated throughout the polymerization, leading to polymers with molecular weight distributions that approach the most probable distribution at high conversions.[1]

If rapid initiation can occur and termination reactions can be suppressed, one can effectively control the polymer molecular weight and narrow the molecular weight distribution.[3] In conventional free-radical polymerization, this proposal seems paradoxical, given that a rapid rate of initiation leads to a rapid rate of termination.[1] Yet, a variety of controlled free-radical polymerization techniques have been successfully demonstrated.[2] Like conventional free-radical polymerization, controlled free-radical polymerization involves initiation, propagation, and termination steps. In addition to these basic steps, all controlled free-radical polymerization schemes include an equilibrium step in which polymer radicals exchange between active and dormant states.[2] In the active state, the polymers radicals are capable of undergoing propagation. In the

dormant or deactivated state, the polymer radicals are capped with protective end-groups and are therefore not able to add monomers or to undergo termination. The equilibrium radical exchange step insures that the total concentration of radicals is low at any point in the reaction, while still enabling a large number of polymer chains to undergo propagation while in the active state.[2] Two specific controlled free-radical polymerization schemes that utilize this principle, atom transfer radical polymerization (ATRP) and reversible addition-fragmentation chain transfer (RAFT), are described in greater detail below. We used each of these controlled free-radical schemes to synthesize PHD statistical copolymers, as well as block copolymers containing PHD.

Atom Transfer Radical Polymerization (ATRP)

Atom transfer radical polymerization (ATRP) is a controlled free-radical polymerization technique that utilizes a reversible equilibrium process based on a transition metal complex to activate and non-terminatively deactivate polymer radicals. The ATRP equilibrium[4] is generically shown in Figure 2.2, where P_n-X is the deactivated polymer radical and $P_n^{\bullet}$ is the activated polymer radical. The process is catalyzed by a ligand-transition metal complex, L_nM_t, which undergoes a one-electron oxidation to abstract the halide, X, off the polymer chain, thereby activating the polymer radical. While activated, the polymer radical is able to undergo both propagation and termination reactions.[1] Consequently, successful control of the polymerization requires that the equilibrium strongly favor the deactivated polymer radical, thus reducing the concentration of activated radical present at any point in the reaction, which suppresses termination reactions.[4] In Figure 2.2, this equilibrium is illustrated with a larger arrow favoring the deactivated polymer chain.

A variety of transition metals, M_t, have been investigated for use as ATRP catalysts. While ruthenium compounds have proven to be versatile catalysts for use in

ATRP,[5,6] copper halides (e.g., CuBr, CuCl) are by far the most common transition metal catalysts used in ATRP.[4] The activity of copper halides can be controlled with judicious selection of a nitrogen-containing ligand, many of which are commercially available.[7] In fact, it has been demonstrated that the activity of the catalyst can be changed by six orders of magnitude by changing the ligand,[8] thus allowing significant room for optimizing the ATRP equilibrium. One nitrogen-containing ligand that was commonly used in our polymerizations is N,N,N',N",N"-pentamethyldiethylenetriamine, PMDETA. PMDETA is a commercially-available ligand, and its use resulted in favorable control during PHD synthesis. The chemical structure of PMDETA is shown in Figure 2.3.

It is often beneficial to introduce the deactivating species ($M_t^{+(z+1)}X$; e.g., $CuBr_2$, $CuCl_2$) at the onset of polymerization in order to suppress termination reactions early during the reaction.[7] The addition of deactivating species shifts the ATRP equilibrium farther towards the deactivated polymer radical, thus further reducing its concentration. The addition of even larger amounts of the deactivating species may be necessary in protic solvents, due to the strong potential for dissociation of Cu^{II} and its ligand under protic conditions.[9] This technique has proven to be particularly useful in the polymerization of rapidly propagating monomers, such as methacrylates.[7,10,11]

ATRP is initiated by alkyl halides, with one initiating species required for each polymer chain.[4] Bromine-based alkyl halides can initiate at a faster rate than their chlorine-counterparts, due to differences in the C-Cl and C-Br bond strengths.[12,13] Figure 2.4 provides the chemical structures of commonly used alkyl bromides, include 1-bromoethylbenzene (Figure 2.4a), ethyl α-bromoisobutyrate (EB*i*B, Figure 2.4b), and ethyl α-bromopropionate (EBP, Figure 2.4c). In general, it has been observed that the initiation rate of alkyl bromides is faster than the propagation rate of structurally similar monomers.[4] Consequently, 1-bromoethylbenzene (Figure 2.4a) is commonly used to

initiate the polymerization of styrenic monomers, EBP for acrylates, and EB*i*B for methacrylates.[4]

To further improve the initiation efficiency, one can suppress the rate of propagation, relative to the initiation rate, through halogen exchange.[12,13] In this process, alkyl bromide initiators are used in conjunction with copper chloride catalysts. The use of such mixed halide systems results in fast initiation (by the alkyl bromide) but controlled propagation (due to copper chloride), which in turn improves control over molecular weights, and generally leads to narrower molecular weight distributions.[13] Provided that initiation is efficient and occurs at a rate that is faster than that of propagation, the degree of polymerization, N, can be related to the ratio of the initial monomer concentration to the initial initiator concentration, $[M]_o/[I]_o$, through Equation 2.1:[2]

$$N = x \cdot \frac{[M]_o}{[I]_o} \qquad \text{(Equation 2.1)}$$

Where x is the monomer conversion. The number-average molecular weight can be simply calculated from Equation 2.2:

$$M_n = M_o \cdot N \qquad \text{(Equation 2.2)}$$

Where M_o is the mer molecular weight.

Prediction of N in Equation 2.1, at any reaction time requires an understanding of the kinetics associated with the particular polymerization. The rate of monomer depletion associated with an ideal ATRP system is first-order with respect to monomer, resulting in overall kinetics that are first-order with respect to time, as shown in Equation 2.3:[14]

$$\ln \frac{[M]_o}{[M]} = \frac{k_p k_a [I]_o [Cu^I]_o}{k_d [Cu^{II}]_o} t \qquad \text{(Equation 2.3)}$$

Where [M] is the monomer concentration at time t, k_p is the rate constant of propagation, k_a is the rate constant of radical activation, k_d is the rate constant of radical deactivation, and $[Cu^I]_o$ and $[Cu^{II}]_o$ are the initial concentrations of Cu^I and Cu^{II}. The first-order kinetic model assumes that the radical concentration is constant, or that termination reactions are suppressed completely. As such, the equilibrium noted in Figure 2.2 does not shift during the polymerization. While the limit of zero termination is not valid during practical conditions of controlled free-radical polymerization, first-order kinetics have been observed for the polymerization of styrene.[14]

Deviations from first-order kinetics have been observed in many cases, leading to the development of other kinetic models. The persistent radical effect, first proposed by Fischer, accounts for termination reactions that cannot be completely eliminated from controlled free-radical polymerizations.[15,16] With specific consideration for ATRP, Fischer notes that termination of propagating radicals results in a build-up of halides, or what he refers to as "persistent radicals," in the system.[17] The increased availability of persistent radicals effectively shifts the ATRP equilibrium in the direction of the deactivated polymer radical with increasing reaction time.[15] As such, the polymerization slows down with time, and its kinetics obey a $t^{2/3}$ power law rather than being first order. The kinetic model taking the persistent radical effect into account is shown in Equation 2.4:[16,17]

$$\ln\frac{[M]_o}{[M]} = \frac{3k_p}{2}\left(\frac{k_a[I]_o[Cu^I]_o}{3k_d(2k_t)}\right)^{1/3} t^{2/3} \qquad \text{(Equation 2.4)}$$

Where k_t is the rate constant of termination.

Equations 2.3 and 2.4 are specifically derived for ATRP. We note, however, that equations for the zero-termination limit and that account for the persistent radical effect

can also be derived for other controlled free-radical polymerization schemes (e.g., RAFT).[15]

The kinetics of ATRP can be further complicated by the use of heterogeneous polymerization schemes, in which not all the components (e.g., Cu^{I} and Cu^{II}) are soluble in the reaction medium.[15] In order to account for these heterogeneous polymerization schemes, Snijder has proposed an alternate kinetic model.[18] The Snijder model accounts for termination reactions and also proposes a ceiling concentration of Cu^{II}, $[Cu^{II}]_c$, above which excess Cu^{II} falls out of solution and is no longer available to deactivate the polymer radicals.[18] The kinetics associated with the Snijder model are shown in Equation 2.5, where K_{eq} is the equilibrium rate constant (Figure 2.2):

$$\ln\frac{[M]_o}{[M]} = \frac{k_p\left[Cu^{II}\right]_c}{2k_tK_{eq}}\left\{\left(6k_t\left(\frac{K_{eq}}{\left[Cu^{II}\right]_c}\right)^2 t + [I]_o^{-3}\right)^{1/3} - [I]_o^{-1}\right\} \qquad \text{(Equation 2.5)}$$

ATRP is a versatile technique for the synthesis of well-defined block copolymers, either by sequential monomer addition in a single pot or by a macroinitiation strategy. For sequential monomer addition, the polymerization of one monomer is carried out to high conversions, upon which a second monomer is added.[19] Commonly referred to as one-pot synthesis, sequential monomer addition strategies are generally simple to implement and minimize the requisite amount of catalyst used in the process. However, well-defined block copolymers with chemically dissimilar blocks can be difficult to synthesize using this approach, as the optimal reagents (e.g., ligand, catalyst, solvent) may be significantly different for the polymerization of each of the monomers. Furthermore, unless the polymerization of the first monomer is carried to completion before the addition of the second monomer, the second block may contain residual amounts of the first monomer, thereby resulting in a gradient or a statistical block.[19] The

need to carry the polymerization of the first monomer to completion necessarily limits the use of one-pot polymerization for the synthesis of designer block copolymers because termination reactions become more significant at higher conversions.[7] The second strategy for the synthesis of block copolymers by ATRP uses a macroinitiator. Here, one block is synthesized, purified, and then used as the initiator to initiate (hence known as a macroinitiator) the polymerization of the second monomer.[19] This strategy is particularly useful as it allows the independent optimization of the polymerization conditions and parameters (e.g., solvent, ligand, catalyst) for each of the monomer, thereby enabling the well-controlled synthesis of block copolymers.

Reversible Addition-Fragmentation Chain Transfer (RAFT)

Reversible addition-fragmentation chain transfer (RAFT) is another controlled free-radical polymerization technique based on the concept of chain transfer, as is frequently used in conventional free-radical polymerizations. In contrast to the chain transfer agents (CTAs) employed in conventional free-radical polymerization, CTAs employed for RAFT are typically thiocarbonylthio compounds that enable the reversible transfer of radicals from one polymer chain to another.[3] The RAFT equilibrium step is shown in Figure 2.5,[3] where Z is a group that stabilizes the intermediate radical and R is the leaving group.

An assortment of CTAs with varying Z and R groups have been used in RAFT.[3] Typically, a good stabilizing group is one that contains aromaticity (e.g., Z = Ph), and a good leaving group is one that is stabilized as a radical (i.e., a tertiary carbon).[3] The transfer rate of the CTA can be extensively modified by judicious selection of the Z and R groups, thus allowing significant grounds for optimization for the controlled synthesis of a particular polymer by RAFT.[3] An appropriate CTA for the synthesis of DMAEMA-containing polymers is cumyl dithiobenzoate, CDB.[22] The molecular structure of CDB is

shown in Figure 2.6. The molecular structure of the bifunctional equivalent of CDB, 1,3-bis(2-(thiobenzoylthio)prop-2-yl)benzene, TBTPB, is also shown. Both CTAs were synthesized by Dr. Sudershan Gondi in the research group of Dr. Brent S. Sumerlin at Southern Methodist University.

Generally, the addition of RAFT CTAs does not change the overall rate of the polymerization.[3] In contrast, CDB has been demonstrated to inhibit the rate of polymerization at early reaction times.[3] Accompanying this slowing down of the polymerization rate, a slow consumption of the CTA has also been observed.[23,24] The origin of this inhibition period is not entirely known.[25] From a synthetic standpoint, the polymerization is controlled even with an inhibition period, and well-controlled polymers can still be produced and the kinetics of the polymerization quantified.[25]

RAFT makes use of conventional free-radical initiators (e.g., AIBN) to generate free-radicals for the subsequent polymerization.[3] However, if the CTA transfer rate is reasonably high, then many polymer chains can be simultaneously synthesized with the addition of small quantities of initiator. In this way, the overall radical concentration can also be greatly reduced relative to that in conventional free-radical polymerization, thus suppressing termination reactions.[3] Further, since the concentration of initiator is generally considerably lower than that of the CTA, the total number of polymer chains is heavily dependent on the amount of CTA used.[2] In this way, given the relevant monomer conversion, the degree of polymerization can be predicted from Equation 2.1, where the initial concentration of CTA, $[CTA]_o$, is substituted for the initial concentration of initiator.[3]

As in ATRP, one-pot synthesis schemes can be devised for the synthesis of block copolymers by RAFT. Because the vast majority of polymer chains at any point in the polymerization are capped with thiocarbonylthio groups, polymers from an initial RAFT

polymerization can easily be purified and used as a macro-chain transfer agent, macro-CTA, in the subsequent polymerization of a second monomer. In this manner, well-controlled block copolymers can also be synthesized by RAFT.[3]

Theory of Copolymerization

Two or more monomers (e.g., HEMA and DMAEMA) are often copolymerized to attain specific materials properties of the final copolymer.[26] It has been observed that the measured, or average, composition of a copolymer does not always reflect the composition of the monomer feed.[27] As such, an understanding of the relative rates with which monomers are added to growing polymer chains is necessary in order to reasonably predict the average composition of the polymer. Several models have been proposed to describe the relative rates of monomer addition to polymer radicals.[27-34] Particularly useful is the terminal model, in which the terminal monomer unit of a polymer radical determines the reactivity of that radical with respect to each monomer type.[28] From the terminal model assumption, reactivity ratios, r_i, can be used to describe the relative probability that a polymer radical with a terminal monomer of one type will add a like monomer instead of an unlike monomer, where i distinguishes the monomer type.[26] The instantaneous polymer composition, F_i, can thus be predicted from the reactivity ratios. For a two-monomer system composed of monomers M_1 and M_2 at an instantaneous monomer composition f_1, F_1 can described by the Skeist equation (Equation 2.6):[27]

$$F_1 = \frac{r_1 f_1^{\,2} + f_1(1 - f_1)}{r_1 f_1^{\,2} + r_2(1 - f_1)^2 + 2 \cdot f_1(1 - f_1)} \qquad \text{(Equation 2.6)}$$

To highlight the dependence of the instantaneous polymer composition on the reactivity ratios of the monomers, the instantaneous polymer composition, as estimated from the Skeist equation, for four different pairs of reactivity ratios are shown in Figure

2.7. The instantaneous polymer composition as a function of the instantaneous monomer composition in Figure 2.7a is generated assuming $r_1 = 1$ and $r_2 = 1$. In Figures 2.7b-d, the instantaneous polymer compositions are plotted for the cases $r_1 = 2$ and $r_2 = 0.5$, $r_1 = r_2 = 2$, and $r_1 = r_2 = 0.5$, respectively. As a reference, the dashed line in each plot corresponds to the condition where $F_1 = f_1$, which occurs when the instantaneous polymer composition is identical to the instantaneous monomer composition.

In Figure 2.7a, the instantaneous polymer composition is equal to the instantaneous monomer composition at all instantaneous monomer compositions. Because both r_1 and $r_2 = 1$, Equation 2.6 collapses into the simple relationship of $F_1 = f_1$. Accordingly, the ability to design statistical copolymers is straight-forward, as the instantaneous polymer composition, F_1, is equal to the total (average) polymer composition, $\overline{F_1}$, which is directly dictated by the monomer feed composition, $f_{1,o}$.

In Figure 2.7b, the instantaneous polymer composition is greater than that of the instantaneous monomer composition at all monomer compositions other than $M_1 = 0$ or 1. This scenario occurs for all cases in which $r_1 > 1$ and $r_2 < 1$, where the addition of M_1 to polymer radicals terminated with either M_1 or M_2 radicals is more likely than the addition of M_2.[1] As such, M_1 is always depleted at a faster rate than M_2, resulting in drift in the instantaneous monomer and polymer compositions with conversion.

In Figure 2.7c, F_1 is greater than f_1 in M_1-rich environments, but F_1 is less than f_1 in M_2-rich environments. Because $r_1 = 2$ and $r_2 = 2$, the polymer radicals preferentially add like monomers, and the monomer of higher initial concentration is consequently depleted at a faster rate. Since the probability of having the same monomers sequentially along the polymer chain is high, the resulting polymers tend to be "blocky" in nature. At most compositions, the instantaneous polymer composition, as predicted in Figure 2.7c, is not equivalent to the instantaneous monomer composition. There is, however, a single

condition, known as the azeotropic composition, where the instantaneous polymer concentration is equal to the instantaneous monomer composition. At the azeotropic composition, M_1 and M_2 are depleted at the same rate over the course of the polymerization. As a result, polymerization at this composition does not incur any changes in the instantaneous monomer or instantaneous polymer compositions, and the final polymer is a statistical copolymer in which the instantaneous polymer composition is equal to the average polymer composition. As shown in Figure 2.7c, the azeotropic composition for $r_1 = r_2 = 2$ is $F_1 = f_1 = 0.5$.

In Figure 2.7d, the opposite scenario to that shown in Figure 2.7c is presented. Specifically, the reactivity ratios are selected such that F_1 is less than f_1 in M_1-rich environments and is greater than f_1 in M_2-rich environments. Because $r_1 = 0.5$ and $r_2 = 0.5$, all polymer radicals preferentially add unlike monomers, and the monomer of the lower initial concentration is consequently depleted at a faster rate. The resulting polymers are therefore "alternating" in nature, meaning that there is a high probability that sequential monomers in a polymer chain are of different monomer types.[1] The instantaneous polymer composition is generally not equal to the instantaneous monomer composition, except at the azeotropic composition. In Figure 2.7d, the azeotropic composition for $r_1 = r_2 = 0.5$ is $F_1 = f_1 = 0.5$. The azeotropic composition will shift according to the reactivity ratios, and can be predicted from the Skeist equation by setting F_1 equal to f_1.

By the same token, the reactivity ratios can be easily determined from the Skeist equation given the instantaneous monomer and polymer compositions. The instantaneous polymer compositions, however, can be difficult to measure. In practice, the determination of reactivity ratios is accomplished using one of two primary methods. First, a series of polymerizations at various monomer feed compositions is carried out to

low conversions. If the monomer conversion is sufficiently low, the polymer composition measured at that juncture, though averaged over the course of polymerization thus far, can be approximated as the instantaneous polymer composition.[30,31] Alternatively, if the change in average polymer composition can be monitored as a function of monomer conversion, reactivity ratios can be regressed from a full range of monomer conversions by numerical integration of the Skeist equation over the measured conversion range, as we will describe in more detail in Chapter 3.[28]

Microphase Separation of Block Copolymers

Block copolymers are comprised of two or more homopolymers and/or statistical copolymers that are linked by covalent bonds. Block copolymers are able to undergo microphase separation due to an inherent chemical incompatibility between the chemically dissimilar blocks.[35] In the solid state, several well-ordered, periodic nanostructures have been observed for diblock copolymers, including alternating lamellae, hexagonally-packed cylinders, body-centered cubic lattice of spheres, and bicontinuous gyroid structures.[36] These solid-state nanostructures range from 5 nm to 500 nm, depending on the molecular weight of the diblock copolymer.[37] The phase behavior of diblock copolymers is, primarily, dependent on the volume fraction of one of the constituent blocks, v, and the incompatibility of the two blocks, χN, where χ is the Flory-Huggins interaction parameter, a measure of the chemical incompatibility between blocks that is inversely proportional to temperature, and N is the overall degree of polymerization.[36] From these two parameters, the phase behavior of diblock copolymers has been predicted using self-consistent field theory (SCFT), shown in Figure 2.8.[36]

As illustrated in Figure 2.8, symmetric ($v \approx 0.4$-0.6) block copolymers with $\chi N > 10.5$ microphase separate to form alternating lamellae. With increasing block asymmetry, block copolymers microphase separate to form the bicontinuous gyroid cubic

phase (v ≈ 0.35-0.4, 0.6-0.65), hexagonally-packed cylinders (v ≈ 0.2-0.35, 0.65-0.8), and spheres arranged on a body-centered cubic lattice (v ≈ 0.15-0.2, 0.8-0.85). At χN's below the order-disorder temperature, ODT, block copolymers are disordered, whereas the block copolymers self-assemble into ordered structures at χN's below the ODT. A block copolymer can also exhibit order-order transitions, OOTs, between different morphologies.[39,41,42] For example, a block copolymer with a constant v of 0.35 can microphase separate into alternating lamellae, a bicontinuous gyroid structure, or hexagonally-packed cylinders, with decreasing χN (and increasing temperature). Both ODTs and OOTs are reversible first-order phase transitions.[36]

Microphase separation can be induced from the melt or by solvent casting from a common solvent for the block copolymers.[35] In the latter case, the choice of solvent has been demonstrated to affect the final microstructure depending on the solubility parameter difference between the blocks and the solvent.[38,39] The role of solvent quality on the solid-state structure of PHD-containing block copolymers will be examined in Chapter 4. Importantly, the morphologies observed in a solid-state block copolymer might or might not represent the equilibrium morphology,[40] which is the morphology predicted by SCFT in Figure 2.8.

Swelling of Hydrogels

Hydrogels are crosslinked polymer networks that swell in water.[43] In general, equilibrium swelling in crosslinked polymer networks is related to a balance of the elastic and mixing chemical potentials of the network.[44] The incorporation of solvent into the network structure decreases the entropy of chain configuration but increases the entropy of mixing of solvent and polymer.[44] Flory and Rehner presented a derivation of the equilibrium swelling state for a crosslinked polymer network, as shown in Equation 2.7:[44]

$$\Delta F = 0 = RT\left[\chi \cdot v_2{}^2 + \ln(1 - v_2) + v_2 + \frac{V_1}{v \cdot M_c} \cdot \left(1 - \frac{2M_c}{M_n}\right) \cdot \left(v_2{}^{1/3} - \frac{v_2}{2}\right)\right]$$

(Equation 2.7)

Where ΔF is the change in the partial molal free energy (which is zero at equilibrium); V_1 is the molar volume of the swelling agent; v_2 is the polymer volume fraction in the network at equilibrium; v is the specific volume of the polymer; χ is the Flory interaction parameter between polymer and solvent; M_n is the number-average molecular weight before crosslinking; and M_c is the molecular weight between crosslinks. In Equation 2.7, the term containing M_c represents the elastic contribution, whereas the remainder of the equation describes the mixing contribution. Equation 2.7 was derived for a scenario in which the crosslinks connect four polymer chains.[44] The model also assumes that crosslinks are introduced in the dry state.[44] To account for hydrogels in which crosslinks are introduced in the swollen state (i.e., during solution polymerization), Peppas and Merrill derived a similar equation that describes equilibrium swelling, as is shown in Equation 2.8:[43]

$$\Delta F = 0 = RT\left[\chi \cdot v_2{}^2 + \ln(1 - v_2) + v_2 + \frac{V_1}{v \cdot M_c} \cdot \left(1 - \frac{2M_c}{M_n}\right) v_r \cdot \left[\left(\frac{v_2}{v_r}\right)^{1/3} - \frac{1}{2}\left(\frac{v_2}{v_r}\right)\right]\right]$$

(Equation 2.8)

Where v_r is the polymer volume fraction in the swollen state in which crosslinks are introduced but does not necessarily represent the equilibrium swelling state. When crosslinks are introduced in the swollen state, the elastic term in Equation 2.7 must be modified to account for v_r.

Both the Flory-Rehner and Peppas-Merrill equations describe the equilibrium swelling of hydrogels as a balance between mixing and elastic potentials. In many cases, ionic components are introduced into hydrogels in order to render the final materials pH-

responsive. The final equilibrium of ionic hydrogels can predicted by the Brannon-Peppas model, as shown in Equation 2.9:[45]

$$\left(\frac{K_b}{10^{pH-14}+K_b}\right)^2\left(\frac{V_1}{4I}\right)\left(\frac{v_2}{v}\right)^2 = \chi\cdot {v_2}^2 + \ln(1-v_2)+v_2+\frac{V_1}{v\cdot M_c}\cdot\left(1-\frac{2M_c}{M_n}\right)v_r\cdot\left[\left(\frac{v_2}{v_r}\right)^{1/3}-\frac{1}{2}\left(\frac{v_2}{v_r}\right)\right]$$

(Equation 2.9)

In Equation 2.9, I is the ionic strength and K_b is the dissociation constant. We also note that the parameter (v_2/v) describes the concentration, c, of ionic material present in the hydrogel (in mass per volume). The equilibrium swelling in the Brannon-Peppas model represents a balance between the ionic chemical potential, a new term that is pH-dependent, and the elastic and mixing chemical potentials that were previously described by Peppas and Merrill.[45] The Brannon-Peppas model was derived using the same assumptions used in the Peppas-Merrill model, i.e. four-point crosslinks that were introduced in solution.[45] Alternately, we can recast the Brannon-Peppas model by considering the case in which crosslinks are introduced in the dry state (Flory-Rehner[44]). The new equation describing the equilibrium swelling in ionic hydrogels thus becomes Equation 2.10:

$$\left(\frac{K_b}{10^{pH-14}+K_b}\right)^2\left(\frac{V_1}{4I}\right)c^2 = \ln(1-v_2)+v_2+\chi\cdot(v_2)^2+\left(\frac{V_1}{v\cdot M_c}\right)\cdot\left(1-\frac{2M_c}{M_n}\right)\cdot\left({v_2}^{1/3}-\frac{v_2}{2}\right)$$

(Equation 2.10)

In Chapter 5, we will consider the ionic swelling response of amphiphilic block copolymer hydrogels containing PHD. Because the physical crosslinks (or anchors) in our hydrogels are established in the solid state, we will use Equation 2.10 to analyze the equilibrium swelling of our model hydrogels.

Lower Critical Solution Temperature

Typically, polymers exhibit increased solubility on heating due to increases in the entropy of mixing with increasing temperature.[46] Polymers with favorable polymer-solvent interactions, however, can exhibit a lower critical solution temperature, LCST, above which the polymer phase separates from the solvent.[46] In hydrogen bonded systems, for example, it is possible that the enthalpy of mixing can decrease with increasing temperature, causing the polymer to fall out of solution upon heating.[46] Several polymers known to exhibit LCST behavior in water include poly(ethylene oxide),[46] poly(N-isopropylacrylamide),[47] and poly(DMAEMA).[48,49] In Chapter 3, we will demonstrate that the LCST of DMAEMA-containing polymers can be tuned by copolymerization with HEMA. In Chapter 6, we will also investigate LCST-type behavior in PHD-containing block copolymer hydrogels containing poly(HEMA-co-DMAEMA) in order to induce tunable transitions between the different block copolymer morphologies.[50]

SPECIFIC SYNTHETIC METHODS

The following section provides synthetic details for the various polymerizations considered in this work. Further discussion of these techniques will be provided as appropriate in Chapters 3 and 4.

Synthesis of bromine-terminated polystyrene macroinitiator by ATRP.

Polystyrene, PS, is hydrophobic and glassy at ambient temperatures (T_g = 105°C).[51] In Chapter 5, we will specifically explore polystyrene as the anchoring block in amphiphilic block copolymer hydrogels containing PHD. To make PS/PHD block copolymers, we employed the macroinitiation strategy. Here, we describe the synthesis of a PS macroinitiator by ATRP.

Styrene was passed through a column of activated basic alumina and stored over molecular sieves prior to use. Styrene (13.6 g, 127 mmol), CuBr (186 mg, 1.30 mmol), $CuBr_2$ (14.2 mg, 0.060 mmol), PMDETA (233 μL, 1.33 mmol), and 30 mL of anisole were added to a 100 mL flask equipped with a magnetic stirrer bar. The flask was sealed with a septum, placed in an oil bath that was preheated to 110 ^oC, and purged with N_2 for 30 min. The reaction was then initiated by the addition of 1-bromoethylbenzene (235 μL, 1.30 mmol) and was carried out for 3 h and 50 min. The reaction flask was removed from the oil bath and cooled to 0 ^oC, and the solution was exposed to air to terminate the polymerization. The solution was then diluted with THF and passed through neutral alumina to remove copper salts. Finally, the solution was concentrated and precipitated into methanol. The polymer (M_n = 6.5 kg/mol, M_w/M_n = 1.02) was collected by filtration and was dried *in vacuo* for 24 h. Polystyrene macroinitiators of varying molecular weight were synthesized by changing the ratio of initial monomer to initial initiator concentrations, and also by varying the polymerization time.

Synthesis of bromine-terminated poly(methyl acrylate) macroinitiator by ATRP.

Poly(methyl acrylate), PMA, is hydrophobic with a glass transition temperature below room temperature (T_g = 12.5°C).[52] As a result, amphiphilic block copolymer hydrogels containing PMA as the hydrophobic block are able to reorganize at or above ambient temperatures.[50] We used the following procedure to synthesize PMA macroinitiators, which were subsequently used for the synthesis of PMA/PHD block copolymers for these swelling studies.

Methyl acrylate was passed through a column of activated basic alumina and stored over molecular sieves prior to use. In a typical polymerization, methyl acrylate (50.0 g, 348 mmol), CuBr (255 mg, 1.74 mmol), $CuBr_2$ (19.4 mg, 0.087 mmol), and PMDETA (386 μL, 1.83 mmol) were added to a 100 mL flask equipped with a magnetic

stir bar. The flask was sealed with a septum, wired shut, placed in an oil bath that was preheated to 75°C, and purged with N_2 for 20 min. The reaction was then initiated by the addition of EB*i*B (235 μL, 1.30 mmol) and was carried out for 90 min. Positive N_2 pressure was maintained throughout the polymerization. Following polymerization, the reaction flask was removed from the oil bath and quenched in liquid nitrogen. The reaction contents were subsequently exposed to air, diluted with tetrahydrofuran, and mixed with silica gel to remove copper salts. Finally, the solution was concentrated and precipitated into hexanes. The polymer (M_n = 13 kg/mol, M_w/M_n = 1.02) was dried *in vacuo* for 24 h at 50°C. PMA macroinitiators of different molecular weights were synthesized by varying the polymerization time.

Synthesis of bromine-terminated poly(*tert*-butyl acrylate) macroinitiator by ATRP.

Poly(*tert*-butyl acylate), P*t*BA, is a hydrophobic polymer with a glass transition temperature of 43°C.[53] As such, amphiphilic block copolymer hydrogels containing P*t*BA are anchored by glassy PtBA microdomains at ambient temperatures, but the block copolymer hydrogels are able to reorganize when the hydrogels are heated above the glass transition temperature of P*t*BA. We used the following procedures to synthesize P*t*BA macroinitiators, which were subsequently used to initiate the copolymerization of HEMA and DMAEMA.

Tert-butyl acrylate was passed through a column of activated basic alumina and stored over molecular sieves prior to use. In a typical polymerization, *tert*-butyl acrylate (20.0 g, 154 mmol), CuBr (226 mg, 1.55 mmol), $CuBr_2$ (3.45 mg, 0.016 mmol), PMDETA (359 μL, 1.70 mmol), and 30 mL of acetone were added to a 100 mL flask equipped with a magnetic stir bar. The flask was sealed with a septum, wired shut, placed in an oil bath that was preheated to 50°C, and purged with N_2 for 20 min. The reaction was then initiated by the addition of EB*i*B (234 μL, 1.55 mmol) and was carried

out for 20 hr, yielding P*t*BA 15 (M_n = 13 kg/mol, M_w/M_n = 1.02). Alternately, the bifunctional ATRP initiator, dimethyl 2,6-dibromoheptanedioate (2Me2BrC7D), was used for the synthesis of P*t*BA with two active chain ends, which was subsequently used as a macroinitiator to synthesize PHD/P*t*BA/PHD triblock copolymers.

Synthesis of PHD statistical copolymers by ATRP.

DMAEMA was passed through a column of activated basic alumina and stored over molecular sieves prior to use. HEMA, was purified by vacuum distillation (40 mtorr, 65 ^oC) to remove ethylene glycol dimethacrylate prior to use.[54] HEMA (6.80 g, 51.2 mmol), DMAEMA (3.20 g, 20.0 mmol), CuCl (22.5 mg, 0.225 mmol), $CuBr_2$ (2.65 mg, 0.012 mmol), PMDETA (41.5 μL, 0.237 mmol), 6 mL of 1,2,4-trimethoxybenzene (gas chromatography standard), and 50 mL of DMF were added to a 100 mL flask equipped with a magnetic stir bar. The molar feed composition of DMAEMA, relative to the total monomer feed, was 0.28. As we will discuss in Chapter 3, this composition is the azeotropic composition for copolymerizations of HEMA and DMAEMA in DMF. Polymers synthesized at this composition are therefore statistical copolymers with uniform composition distributions.[55] The flask was sealed with a septum, placed in an oil bath that was preheated to 45 ^oC, and purged with N_2 for 30 min. The reaction was then initiated by the addition of EB*i*B (35.9 μL, 0.237 mmol). Positive N_2 pressure was maintained throughout the polymerization. To terminate the polymerization, the remainder of each aliquot was cooled to 0 ^oC and then exposed to air. The polymerization medium was subsequently diluted with tetrahydrofuran (THF) and passed through neutral alumina to remove copper salts. The solution was then dialyzed against THF (10 mL solution/100 mL THF) for 24 h to remove DMF. Upon further concentration, the solution was precipitated into hexanes. The filtered polymer (PHD_{28}, M_n = 46.0 kg/mol, M_w/M_n = 1.13) was dried *in vacuo* at room temperature for 24 h.

Synthesis of PHD copolymers at other compositions was carried out in dimethyl sulfoxide (DMSO) in a similar manner, except that $CuCl_2$ was used in place of $CuBr_2$, and the ratio of Cu^I to Cu^{II} to initiator was changed from 20:1:21 to 1:12:10. PHD statistical copolymers can be synthesized across the full range of compositions because the reactivity ratios of HEMA and DMAEMA are near unity in DMSO.[56] Polymers with different molecular weights were synthesized by varying the polymerization time.

Synthesis of PHD-containing block copolymers by ATRP.

PHD-containing block copolymers were synthesized in a similar manner to that of PHD statistical copolymers, except that bromine-terminated macroinitiators were used in place of EB*i*B to initiate the copolymerization of HEMA and DMAEMA. Briefly, the macroinitiators were first dissolved in a small amount of either DMF or DMSO to achieve a macroinitiator solution of approximately 10% by weight. The macroinitiator solution was purged with N_2 and was subsequently injected into the reaction mixture to initiate the copolymerization. Subsequent polymer cleanup proceeded similarly to that of PHD statistical copolymers.

Synthesis of PHD, and block copolymers containing PHD, by RAFT.

Due to the poor solubility of some macroinitiators (e.g., PS) in DMSO, we were unable to directly synthesize PHD-containing block copolymers at varying compositions from these macroinitiators. One can potentially swap the sequence of polymerization, i.e., first synthesize PHD and then use it to initiate the synthesis of the second block. This alternative, however, does not work because PHD copolymers suffer from a loss of halide endgroups, likely a result of polymer cleanup.[21] Accordingly, RAFT was explored as an alternate technique for the synthesis of PS/PHD diblock copolymers of varying PHD compositions and for the synthesis of PS/PHD/PS triblock copolymers with PHD midblocks. Because both RAFT and ATRP are controlled free-radical polymerization

schemes with identical propagation steps, the reactivity ratios of HEMA and DMAEMA in DMSO are assumed to be the same in both polymerization schemes. RAFT chain transfer agents, CDB (a monofunctional CTA) and TBTPB (a bifunctional CTA), which were provided by the Sumerlin research group at Southern Methodist University, were synthesized as follows:

Synthesis of cumyl dithiobenzoate (CDB). CDB was prepared following a method similar to that of Oae et al.[57] Specifically, dithiobenzoic acid[58] (11.1 g, 72.0 mmol) and α-methylstyrene (10.4 g, 88.0 mmol) were dissolved in carbon tetrachloride (40 mL), and the resulting solution was purged with nitrogen and stirred at 70 °C for 5 h. The crude product was obtained as a dark purple oil in 69% yield and was subsequently purified by column chromatography with neutral alumina as the packing material and hexanes as the eluent.

Synthesis of 1,3-bis(2-(thiobenzoylthio)prop-2-yl)benzene (TBTPB).[59] To prepare TBTPB, dithiobenzoic acid (20.0 g, 130 mmol), 1,3-diisopropenylbenzene (10.3 g, 64.8 mmol) and a catalytic amount of *p*-toluene sulfonic acid (1.0 g) were dissolved in carbon tetrachloride (80 mL). The resulting solution was heated at 70 °C for 18 h under a nitrogen atmosphere. The reaction mixture was cooled to room temperature, and a saturated solution of sodium bicarbonate (100 mL) was added. After extraction with dichloromethane (100 mL × 2), the organic layers were combined, washed with a saturated brine solution (200 mL), dried over $MgSO_4$ (10 g), and concentrated under reduced pressure to yield a red residual oil. Column chromatography with silica gel as the packing material and hexanes as the eluent yielded the product in 55% yield. ^{1}H-NMR (400 MHz, cdcl$_3$): 7.75-7.69 (dd, 4H, J = 7.5 Hz, SPh-C2***H*** & SPh-C6***H***), 7.36-7.32 (m, 3H, Ar-C5***H*** & SPh-C4***H***), 7.30-7.28 (m, 2H, Ar-C4***H*** ***&*** Ar-C6***H***), 7.24-7.16 (m, 5H, SPh-C3***H*** & SPh-C5***H,*** Ar-C2***H***), 1.89 (s, 12H, (Ar-***C***1-C[CH_3]$_2$). ^{13}C-NMR (100.6 MHz,

cdcl$_3$): 146.3 (Ph-***C***1-C=S), 143.7 (Ar-***C***1-C[CH_3]$_2$), 131.5 (Ar-***C***5H), 128.1 Ar-***C***4H & Ar-***C***6H), 128.0 (SPh-***C***4H), 126.5 (SPh-***C***3H and SPh-***C***5H), 125.4 (Ar-***C***2H), 124.8 (SPh-***C***2H & SPh-***C***6H), 56.4 (Ar-C1-***C***[CH_3]$_2$), 28.3 (Ar-C1-C[***C***H_3]$_2$). IR (KBr; expressed in units of wavenumber, cm^{-1}): 3050, 2970 (C-Cs), 1589, 1444 (C=C), 1264, 1040 (C=S) cm^{-1} 908, 765 (C-Cb). Elemental Analysis, calculated for $C_{26}H_{26}S_4$: C) 66.91%, H) 5.61%. Found: C) 67.09%, H) 5.67%.

Polymerization by RAFT. The RAFT polymerizations of PHD were carried out with either CDB or TBTPB at a total monomer : CTA (functional group) : AIBN molar ratio of 250:5:1. Each copolymerization utilized 20 g of total monomer (HEMA and DMAEMA) diluted in 40 mL of DMSO. For example, copolymerization of HEMA and DMAEMA (75 mol%) using TBTPB as the RAFT CTA consisted of DMAEMA (15.7 g, 99.7 mmol), HEMA (4.33 g, 33.2 mmol), TBTPB (0.12 g, 0.26 mmol), AIBN (0.01 g, 52 μmol), and 40 mL of DMSO in a 100 mL round-bottom flask equipped with a magnetic stir bar. The flask was sealed with a septum and purged with N_2 for 15 min. The flask was then placed in an oil bath that was preheated to 70 ^oC to initiate the RAFT copolymerization. The polymerization was carried out for 8 hr. Positive N_2 pressure was maintained throughout the copolymerization. The polymerization was quenched by freezing the flask in liquid nitrogen, then exposing the solution to air and diluting with THF. To remove DMSO, the solution was dialyzed against THF (10 mL polymerization medium/ 300 mL THF). The resulting solution was then precipitated into hexanes, and the filtered polymer (PHD_{75}, M_n = 20.0 kg/mol, M_w/M_n = 15) was dried in vacuo at room temperature for 24 hr. Subsequent polymerization of styrene was accomplished by using the purified PHD as the macro-chain transfer agent in DMF at 90 ^oC, with a styrene : PHD : AIBN molar ratio of 650:4:1. For example, the synthesis of a PS/PHD/PS triblock copolymer (PS/PHD_{75}/PS 5.9/20/5.9, M_n = 32 kg/mol, M_w/M_n = 1.19) consisted of

styrene (5.33 g, 51.2 mmol), PHD_{75} (bifunctional, M_n = 20.0 kg/mol, 0.75 g, 37.5 μmol), AIBN (0.002 g, 9.38 μmol), and 12.2 mL of DMF. The polymerization was carried out for 7 hr, followed by termination, dialysis, and precipitation as described above.

EXPERIMENTAL TECHNIQUES

In this section, we will discuss the characterization techniques used in this work.

Differential Scanning Calorimetry (DSC)

Differential scanning calorimetry measures the energy absorbed or evolved during thermal transitions, including melting, crystallization, or glass transitions. Specifically, the heat that is required to flow into and out of a sample pan to maintain a constant temperature between the sample and reference pans is monitored during a temperature ramp. A first-order transition (e.g., melting) thus appears as a peak when the heat flow is plotted against temperature. The glass transition temperature, a pseudo-second-order phase transition, appears as a step in similar graphs. DSC experiments were performed on a Perkin Elmer DSC 7 equipped with an intracooler, at a ramp rate of 10 ^{o}C/min. DSC was used to measure the glass transitions of polymers investigated in this work. All glass transition temperatures and melting temperatures were extracted at the midpoint of a step change in heat capacity during the second heat following controlled cooling at a rate of 5 ºC/min. Crystallization temperatures were extracted upon cooling at a rate of 5 ºC/min.

Gas Chromatography (GC)

Gas chromatography is an established technique for determining the concentration of chemical species through separation by differences in boiling points. We used this technique to track the changes in HEMA and DMAEMA monomer concentrations, relative to an inert standard, which was used to determine monomer conversion during copolymerization. In this manner, we quantitatively determined monomer conversion during copolymerization of HEMA and DMAEMA. GC was carried out on an Agilent

Technologies 6850 Series II Network GC system equipped with a polydimethylsiloxane capillary column (12 m x 200 μm x 0.25 μm) with H_2 as eluent at a flow rate of 1.5 mL/min and with a temperature ramp rate of 10 ^oC/min, and a flame ionization detector (FID) operating at 300 ^oC with a H_2 flow rate of 40 mL/min. GC was performed in the laboratory of Dr. Chris Bielawski, with assistance from Dan Coady.

Gel Permeation Chromatography (GPC)

Gel permeation chromatography is a size exclusion technique for measuring the molecular weight and molecular weight distribution of polymers. Dilute polymer solutions are passed through porous columns, and the polymer elutes on a time (or volume) scale inversely proportional to the logarithm of its hydrodynamic volume, which can be then related to its molecular weight.[1] The polydispersity, M_w/M_n, of each polymer is used as a measure of the molecular weight distribution, where M_w is the weight-average molecular weight and M_n is the number-average molecular weight. A polydispersity of $M_w/M_n = 2$ represents the most probable distribution, which is expected in final polymers obtained from conventional free-radical polymerization.[1] A polydispersity of $M_w/M_n = 1$ is approached by "living" polymerization.[1]

The selection of a suitable GPC eluent for the polymer of interest is necessary to ensure proper size separation. For example, N,N-dimethylformamide (DMF) is widely used as a GPC eluent for the characterization of polar polymers, but does not provide a suitable separation for PS because DMF does not sufficiently solubilize PS.[60] Further, salts, such as LiBr, are often added to DMF to suppress polymer-solvent and polymer-substrate interactions that are typically observed in polymers with ionic functional groups. [60,61]

GPC was performed on one of two systems at the University of Texas. Quantitative GPC was performed using a GPC system equipped with a Waters 515 HPLC

solvent pump, two PLgel mixed-C columns (5 μm bead size, Polymer Laboratories Inc.) connected in series, an online interferometric refractometer (Optilab DSP, Wyatt Technology Corp.), and a multiangle laser light scattering (MALLS) detector (λ = 690 nm, DAWN-EOS, Wyatt Technology Corp.). Either THF at 40 ^{o}C or DMF with 0.05 M LiBr at 60 ^{o}C was used as the mobile phase at a flow rate of 1.0 mL/min, depending on the polymer of interest. Specifically, all PHD-containing polymers were characterized in DMF + LiBr, whereas all other polymers investigated in this work were characterized in THF. The combination of light scattering and refractive index data allows for the quantitative determination of the absolute molecular weight and molecular weight distribution if either the total polymer mass injected or the specific refractive index is known.[62] The specific refractive index can be measured using the interferometric refractometer from solutions of known polymer concentrations in the same solvent.

Alternatively, GPC was performed using a Waters HPLC system consisting of HR-1, HR-3, and HR-5E Styragel columns arranged in series, a 1515 pump, and a 2414 RI detector, with DMF (0.01 M LiBr) as the eluent at 40 ^{o}C. Molecular weight data that were obtained relative to PS standards were translated to PHD-equivalent molecular weights using PHD statistical copolymers that were previously characterized on the combined refractive index/light scattering system. The relationship between the absolute number-average molecular weight for PHD statistical copolymers and the polystyrene-equivalent number-average molecular weight, as determined in DMF with 0.01 M LiBr, is shown in Figure 2.9. A linear relationship was regressed between absolute and polystyrene-equivalent molecular weights, with slope = 0.372 and intercept = -143 (R = 0.994). Effectively, the polystyrene-equivalent molecular weight is three times larger than the absolute molecular weight of PHD. We note that the fit is only reliable for polymers of comparable polydispersities. As such, measurements from the second GPC

technique were used only to estimate the molecular weight of PHD copolymers. All quantitative molecular weights and polydispersities of PHD reported in this document were obtained using the first setup.

Nuclear Magnetic Resonance (^{1}H NMR)

^{1}H NMR spectroscopy is used to distinguish between protons in different bonding environments. Protons specific to each monomer type can be observed and quantitatively compared to extract relative compositions. In this way, the relative concentrations of all monomers in a statistical and/or block copolymer containing PHD can be determined. ^{1}H NMR on all samples was performed in a deuterated solvent on a Varian Unity+ 300 MHz NMR spectrometer. Characterization of PHD statistical copolymers was performed in deuterated methanol. Characterization of block copolymers containing PHD statistical copolymers was performed in deuterated N,N-dimethylformamide (DMF). Resonances were integrated to determine the polymer molar compositions. The ^{1}H NMR spectra for PHD and for the block copolymers investigated are shown in Chapters 3 and 4.

Fourier Transform-Infrared Spectroscopy (FTIR)

Fourier transform-infrared spectroscopy is used to detect different chemical bonding environments based on the vibrational characterisics associated with specific bonds upon infrared irradiation. The stretching or bending of a specific bond absorbs the incident irradiation at characteristic energies. Accordingly, FTIR can therefore be used for chemical identification as well as for probing chemical changes within a sample. FTIR measurements were performed on polymer samples cast onto Si test wafers from THF, using a dry-air purged Nicolet Magna-IR 860 spectrometer equipped with an MCT detector operating at room temperature. All spectra were recorded for 500 scans at a resolution of 2 cm^{-1}. A spectrum from a clean Si test wafer was used for background correction.

Small-angle X-ray Scattering (SAXS)

Small-angle x-ray scattering is a non-invasive technique for probing the nanostructures of microphase-separated block copolymers. We used this technique to investigate the solid-state structures and the swollen structures of PHD-containing block copolymers. Bragg's law (Equation 2.11) provides the governing relation between the radiation wavelength (λ), the scattering angle (θ), and the characteristic spacing between lattice planes with Miller indices hkl (d_{hkl}):[63]

$$n\lambda = 2d_{hkl}\sin\theta \qquad \text{(Equation 2.11)}$$

In x-ray scattering, the scattered intensity is collected as a function of scattering angles, which can be expressed as a function of reciprocal lattice plane spacing, q. The inverse lattice spacing is related to the real lattice spacing through Equation 2.12:[63]

$$q = \frac{2\pi}{d_{hkl}} \qquad \text{(Equation 2.12)}$$

Since the periodicity of the block copolymer nanostructures are on the order of tens of nanometers, scattering occurs at angles less than $2\theta = 2^{o}$.

The intensity of the scattered x-rays, I, at q is proportional to the product of the form factor, F(q), and the structure factor, S(q), as shown in Equation 2.13:[63]

$$I(q) \propto S(q) \cdot F(q) \qquad \text{(Equation 2.13)}$$

The structure factor describes scattering from characteristic (hkl) planes that are present in a particular lattice type. The primary peak is denoted q*, with q* providing the characteristic lattice spacing via Equation 2.12. Lamellar samples exhibit higher-order reflections at q/q* = 1, 2, 3, 4, etc.[64] The hexagonal lattice exhibits reflections at q/q* = 1, √3, √4, √7, √9, etc..[64] A body-centered-cubic lattice exhibits reflections at q/q* = 1, √2, √3, etc..[64] SAXS traces therefore provide unique fingerprints for the particular lattice type of microphase-separated block copolymers.[64] Examples of scattering profiles from block copolymers of different morphologies are shown in Figure 2.10.[65] The intensities

of the scattering profiles of lamellar and cylinder-forming block copolymers are corrected (e.g., q^2I for lamellae, qI for cylinders) for intensity decay associated with the shape of the form factors for lamellae (Equation 2.19) and cylinders (Equation 2.18), respectively.[66]

From the position of the primary peak (q*), the radii of spheres (R_s) or cylinders (R_c), or the thickness of the lamellae (t_L) can be determined geometrically, given the volume fraction of one of the blocks (v). The geometrically-based equations for determining the sphere (Equation 2.14) and cylinder radii (Equation 2.15) and the lamellae thicknesses (Equation 2.16) are given below.[64]

$$R_s = \frac{2\pi}{q^*} \cdot \left(\frac{3\sqrt{2}}{4\pi} v \right)^{1/3} \qquad \text{(Equation 2.14)}$$

$$R_c = \frac{2\pi}{q^*} \cdot \left(\frac{2}{\pi \cdot \sqrt{3}} v \right)^{1/2} \qquad \text{(Equation 2.15)}$$

$$t_L = \frac{2\pi}{q^*} \cdot v \qquad \text{(Equation 2.16)}$$

The form factor describes scattering from individual spherical, cylindrical, or lamellar entities. The form factor is typically determined given the spherical or cylindrical radius (Equation 2.14, Equation 2.15) or lamella thickness (Equation 2.16). Form factor curves can be calculated for spheres (Equation 2.17), cylinders (Equation 2.18), and lamellae (Equation 2.19), given the equations below:[66]

$$F(q) \propto \frac{9}{(q \cdot R_s)^3} \left(\sin(q \cdot R_s) - (q \cdot R_s) \cdot \cos(q \cdot R_s)\right)^2 \qquad \text{(Equation 2.17)}$$

$$F(q) \propto \frac{1}{q} \left(\frac{2 \cdot J_1(q \cdot R_c)}{q \cdot R_c} \right)^2 \qquad \text{(Equation 2.18)}$$

$$F(q) \propto \frac{1}{q^2} \left(\frac{\sin\left(\frac{q \cdot t_L}{2} \right)}{\frac{q \cdot t_L}{2}} \right)^2 \qquad \text{(Equation 2.19)}$$

Where $J_1(x)$ is the first-degree Bessel function of the first kind.

SAXS was performed in a long-range sample chamber, and scattered photons were collected on a 2D multiwire gas-filled detector (Molecular Metrology, Inc.). X-rays were produced by a rotating copper anode x-ray generator (Bruker Nonius; $\lambda = 1.5406$ Å) operating at 3.0 kW. Zero angle was calibrated with silver behenate ($CH_3(CH_2)_{20}COOAg$). SAXS profiles on solid-state samples were acquired for either 1 h or 2 h. SAXS experiments on the swollen block copolymer samples were performed using a liquid cell (Molecular Metrology, Inc.), with individual profiles acquired for 1-6 h.

CONCLUSIONS

In this chapter, we provided an overview of the theories, experimental details, and characterization techniques associated with our work. Controlled polymerization techniques, including ATRP and RAFT, will be explored for the copolymerization of HEMA and DMAEMA, and of block copolymers containing PHD in Chapters 3 and 4. Over the course of these chapters, DSC, GC, GPC, 1H NMR, FT-IR, and SAXS are used to characterize the polymers of interest. In Chapter 5, we explore block copolymers containing PHD for use as model ionic hydrogels. In Chapter 6, we consider the temperature response of PHD-containing block copolymers hydrogels, which is analogous to the LCST behavior of PHD statistical copolymers in solution.

FIGURES

Initiation

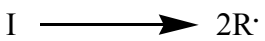

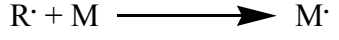

Propagation

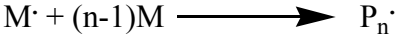

Termination

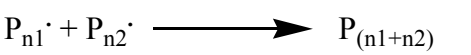

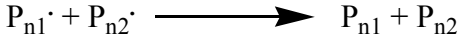

Figure 2.1. Reaction steps associated with conventional free-radical polymerization. I represents the initiator, R· represents a radical generated by either thermal or photo decomposition of I, M represents a monomer, M· represents the radical after the addition of the first monomer, P_n· represents the polymer radical after subsequent (n-1) monomer additions to M·, and P_{n1} and P_{n2} are two polymer radicals of arbitrary lengths n_1 and n_2.

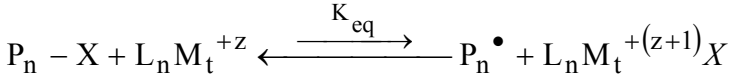

Figure 2.2. ATRP equilibrium between the active and dormant (deactivated) polymer radicals, where P_n-X is a deactivated polymer radical, X is a halide, L_nM_t is a metal-ligand complex in a +z oxidation state, P_n· is an activated polymer radical, and K_{eq} is the equilibrium rate constant.

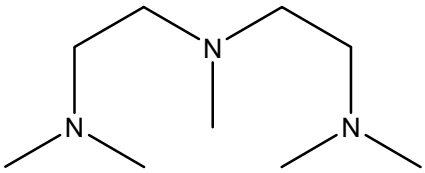

Figure 2.3. Chemical Structure of N,N,N',N",N"-pentamethyldiethylenetriamine, PMDETA.

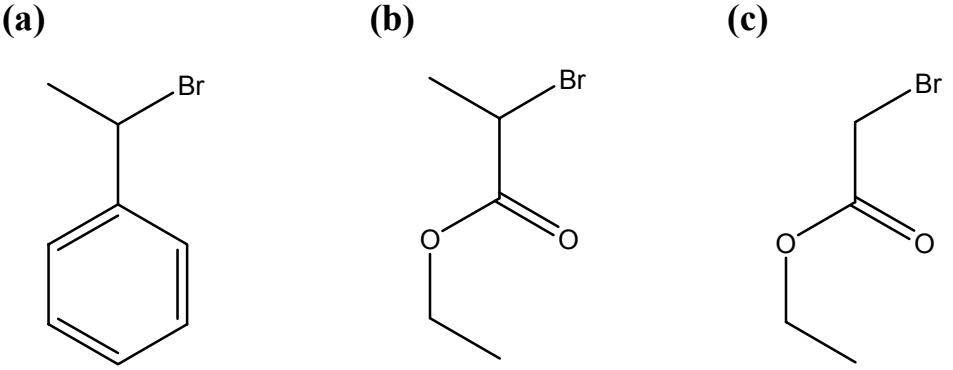

Figure 2.4. Chemical structures of (a) 1-bromoethylbenzene, (b) ethyl α-bromoisobutyrate (EB*i*B), and (c) ethyl α-bromopropionate (EBP).

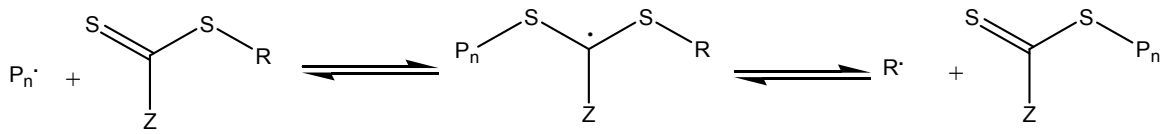

Figure 2.5. RAFT equilibrium, where $P_n\cdot$ is an activated polymer radical, Z is a stabilizing group for the chain transfer agent, Z-C(=S)-S-R, and R is a leaving group.

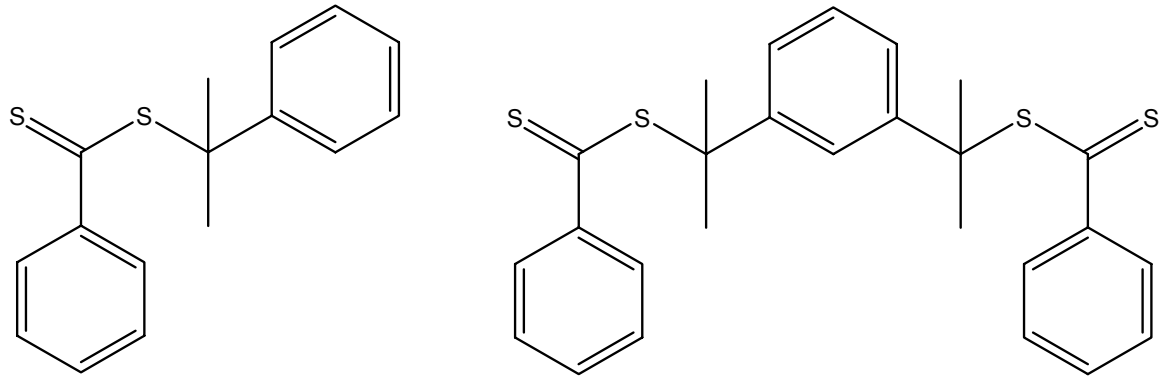

Figure 2.6. Chemical structures of cumyl dithiobenzoate (CDB, left) and 1,3-bis(2-(thiobenzoylthio)prop-2-yl)benzene (TBTPB, right).

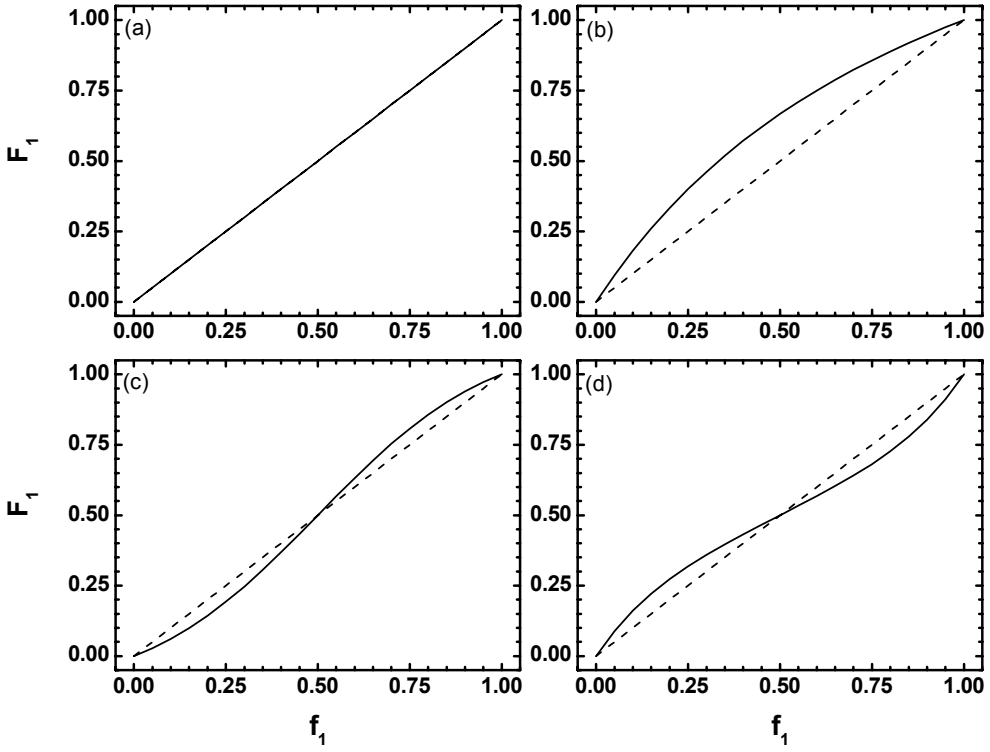

Figure 2.7. The instantaneous polymer composition (F_1), plotted as a function of the instantaneous monomer composition (f_1) in the copolymerization of monomers M_1 and M_2, as predicted by the Skeist Equation for the following cases: (a) $r_1 = r_2 = 1$; (b) $r_1 = 2$, $r_2 = 0.5$; (c) $r_1 = r_2 = 2$; (d) $r_1 = r_2 = 0.5$. The dashed line in each graph corresponds to the 45º line where $F_1 = f_1$, which occurs when both monomer reactivity ratios are unity.

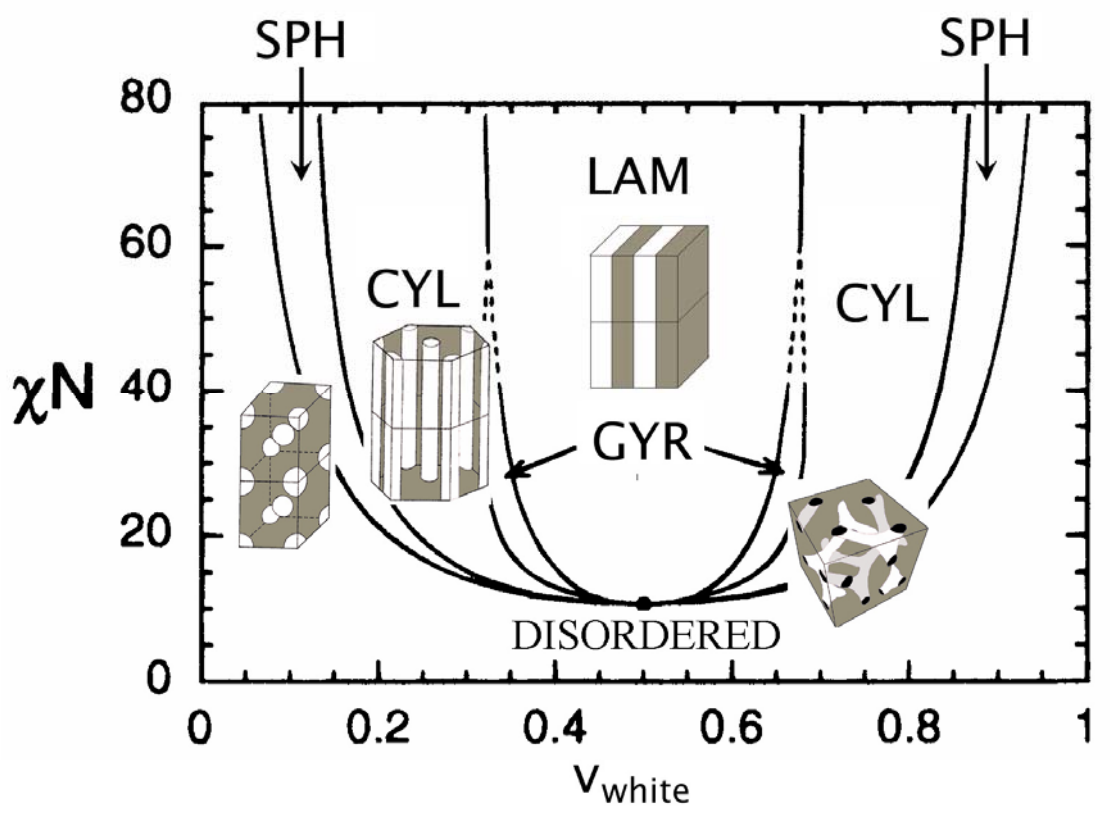

Figure 2.8. Theoretical phase diagram for diblock copolymers in terms of the volume fraction of the white block, v_{white}, and the block copolymer segregation strength, χN, as predicted by self-consistent field theory.[36]

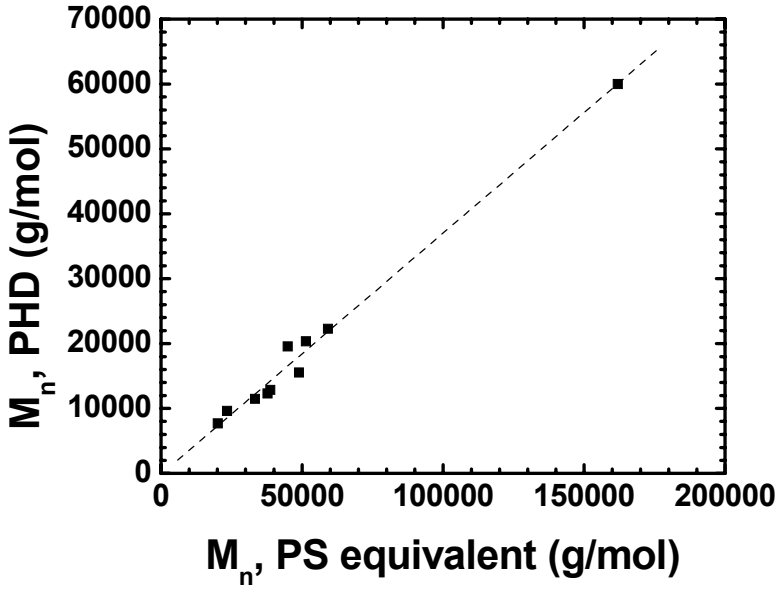

Figure 2.9. Absolute number-average molecular weight of PHD, shown as a function of the polystyrene- (PS) equivalent number-average molecular weight, collected in DMF with 0.01 M LiBr at 40°C. The dashed line represents a linear fit to the data, with slope = 0.372 and intercept = -143 (R = 0.994).

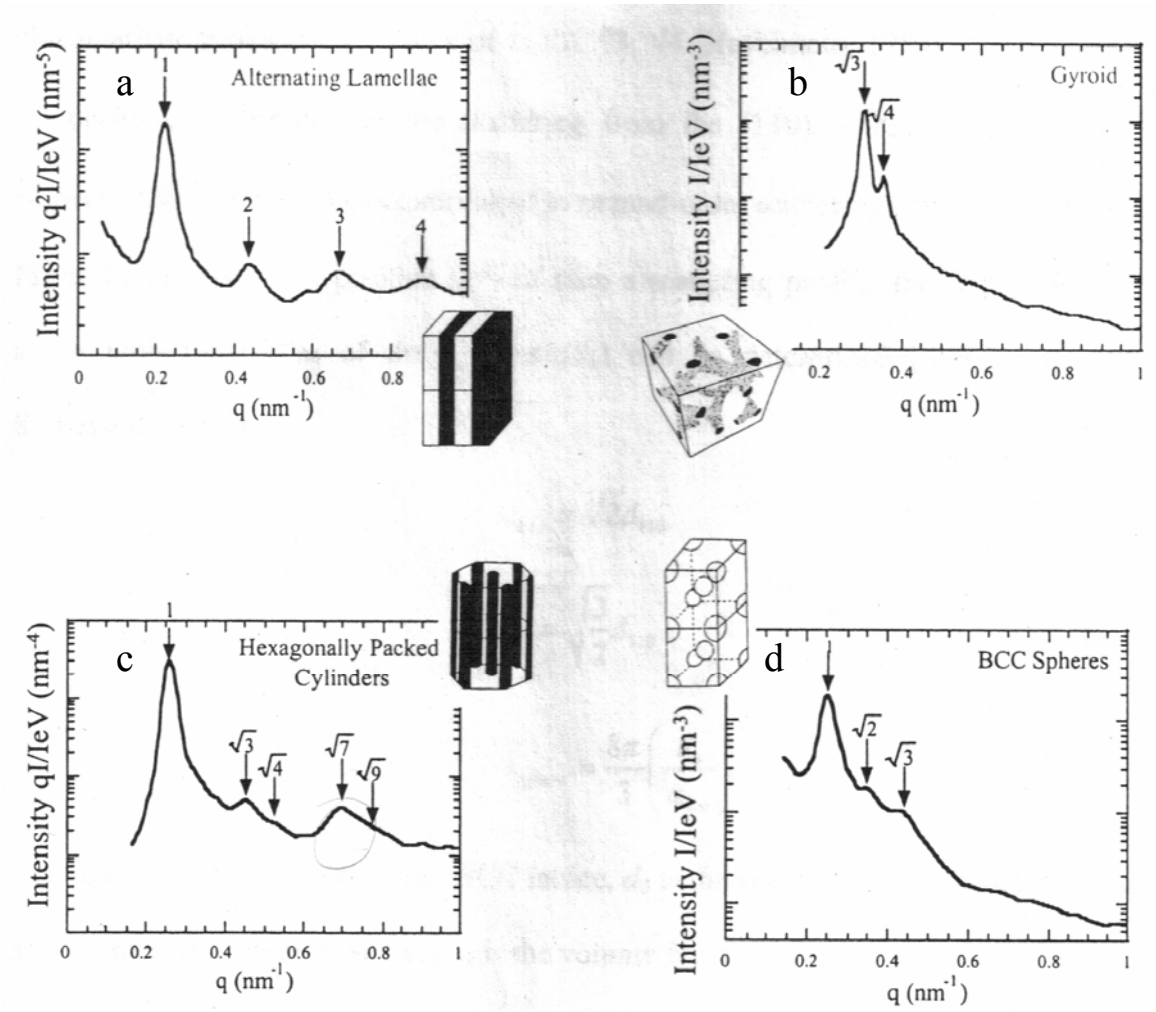

Figure 2.10. Representative SAXS profiles for block copolymers exhibiting alternating lamellae (a), bicontinuous cubic gyroid (b), hexagonally-packed cylinders (c), and spheres on a body-centered cubic-lattice (d). Higher-order peaks in the SAXS profiles are labeled for clarity.

REFERENCES

1. Odian, G., *Principles of Polymerization*. 4th ed.; Wiley-Interscience: New York, 2004.

2. Matyjaszewski, K., General Concepts and History of Living Radical Polymerization. In *Handbook of Radical Polymerization*, Matyjaszewski, K.; Davis, T. P., Eds. Wiley-Interscience: New York, 2002; pp 361-406.

3. Moad, G.; Rizzardo, E.; Thang, S. H. *Australian Journal of Chemistry* **2005,** 58, 379-410.

4. Matyjaszewski, K.; Xia, J., Fundamentals of Atom Transfer Radical Polymerization. In *Handbook of Radical Polymerization*, Matyjaszewski, K.; Davis, T. P., Eds. Wiley-Interscience: New York, 2002; pp 523-628.

5. Bielawski, C. W.; Louie, J.; Grubbs, R. H. *Journal of the American Chemical Society* **2000,** 122, 12872-12873.

6. Ando, T.; Kamigaito, M.; Sawamoto, M. *Tetrahedron* **1997,** 53, 15445-15457.

7. Matyjaszewski, K.; Xia, J. *Chemical Reviews* **2001,** 101, 2921-2990.

8. Tang, W.; Matyjaszewski, K. *Macromolecules* **2006,** 39, 4953-4959.

9. Tsarevsky, N. V.; Pintauer, T.; Matyjaszewski, K. *Macromolecules* **2004,** 37, 9768-9778.

10. Matyjaszewski, K.; Nanda, A. K.; Tang, W. *Macromolecules* **2005,** 38, 2015-2018.

11. Kajiwara, A.; Matyjaszewski, K.; Kamachi, M. *Macromolecules* **1998,** 31, 5695-5701.

12. Matyjaszewski, K.; Shipp, D. A.; Wang, J.-L.; Grimaud, T.; Patten, T. E. *Macromolecules* **1998,** 31, 6836-6840.

13. Schellekens, M. A. J.; de Wit, F.; Klumperman, B. *Macromolecules* **2001,** 34, 7961-7966.

14. Matyjaszewski, K.; Patten, T. E.; Xia, J. *Journal of the American Chemical Society* **1997,** 119, 674-680.

15. Fukuda, T.; Goto, A.; Tsujii, Y., Kinetics of Living Radical Polymerization. In *Handbook of Radical Polymerization*, Matyjaszewski, K.; Davis, T. P., Eds. Wiley-Interscience: New York, 2002; pp 407-462.

16. Fischer, H. *Journal of Polymer Science, Part A: Polymer Chemistry* **1999,** 37, 1885-1901.

17. Zhang, H.; Klumperman, B.; Ming, W.; Fischer, H.; van der Linde, R. *Macromolecules* **2001,** 34, 6169-6173.

18. Snijder, A.; Klumperman, B.; van der Linde, R. *Macromolecules* **2002,** 35, 4785-4790.

19. Cai-yuan, P.; Chun-yan, H., Synthesis and Characterizations of Block Copolymers Prepared via Controlled Radical Polymerization Methods. In *Developments in Block Copolymer Science and Technology*, Hamley, I. W., Ed. John Wiley & Sons: Chichester, 2004; pp 71-126.

20. Teodorescu, M.; Matyjaszewski, K. *Macromolecules* **1999,** 32, 4826-4831.

21. Tsarevsky, N. V.; Matyjaszewski, K. *Chemical Reviews* **2007,** 107, 2270-2299.

22. Krasia, T. C.; Patrickios, C. S. *Macromolecules* **2006,** 39, 2467-2473.

23. Moad, G.; Chiefari, J.; Chong, Y. K.; Krstina, J.; Mayadunne, R. T. A.; Postma, A.; Rizzardo, E.; Thang, S. H. *Polymer International* **2000,** 49, 993-1001.

24. Barner-Kowollik, C.; Quinn, J. F.; Morsley, D. R.; Davis, T. P. *Journal of Polymer Science, Part A: Polymer Chemistry* **2001,** 39, 1353-1365.

25. Lowe, A. B.; McCormick, C. L. *Progress in Polymer Science* **2007,** 32, 283-351.

26. Coote, M. L.; Davis, T. P., Copolymerization Kinetics. In *Handbook of Radical Polymerization*, Matyjaszewski, K.; Davis, T. P., Eds. Wiley-Interscience: New York, 2002; pp 263-300.

27. Skeist, I. *Journal of the American Chemical Society* **1946,** 68, 1781-1784.

28. Czerwinski, W. K. *Polymer* **1997,** 39, 183-187.

29. Tidwell, P. W.; Mortimer, G. A. *Journal of Polymer Science, Part A: General Papers* **1965,** 3, 369-387.

30. Fineman, M.; Ross, S. D. *Journal of Polymer Science* **1950,** 5, 259-262.

31. Kelen, T.; Tudos, F. *Journal of Macromolecular Science, Chemistry* **1975,** A9, 1-27.

32. Deb, P. C. *Polymer* **2007,** 48, 4932-4935.

33. Mao, R.; Huglin, M. B. *Polymer* **1994,** 35, 3525-9.

34. Hill, D. J. T.; Lang, A. P.; O'Donnell, J. H.; O'Sullivan, P. W. *European Polymer Journal* **1989,** 25, 911-15.

35. Leibler, L. *Macromolecules* **1980,** 13, 1602-17.

36. Matsen, M. W.; Bates, F. S. *Macromolecules* **1996,** 29, 1091-1098.

37. Hamley, I. W., Introduction to Block Copolymers. In *Developments in Block Copolymer Science and Technology*, Hamley, I. W., Ed. John Wiley & Sons: Chichester, 2004; pp 1-30.

38. Hanley, K. J.; Lodge, T. P.; Huang, C.-I. *Macromolecules* **2000,** 33, 5918-5931.

39. Lodge, T. P.; Pudil, B.; Hanley, K. J. *Macromolecules* **2002,** 35, 4707-4717.

40. Bucholz, T. L.; Loo, Y.-L. *Macromolecules* **2006,** 39, 6075-6080.

41. Park, M. J.; Bang, J.; Harada, T.; Char, K.; Lodge, T. P. *Macromolecules* **2004,** 37, 9064-9075.

42. Bang, J.; Lodge, T. P. *Journal of Physical Chemistry B* **2003,** 107, 12071-12081.

43. Bell, C. L. P., N.A. *Advances in Polymer Science* **1994,** 122, 129-173.

44. Flory, P. J.; Rehner, J., Jr. *Journal of Chemical Physics* **1943,** 11, 521-6.

45. Brannon-Peppas, L.; Peppas, N. A. *Polymer Bulletin* **1988,** 20, 285-9.

46. Young, R. J.; Lovell, P. A., *Introduction to Polymers*. 2nd ed.; Chapman & Hall: London, 1991.

47. Nykaenen, A.; Nuopponen, M.; Laukkanen, A.; Hirvonen, S.-P.; Rytelae, M.; Turunen, O.; Tenhu, H.; Mezzenga, R.; Ikkala, O.; Ruokolainen, J. *Macromolecules* **2007,** 40, 5827-5834.

48. Cho, S. H.; Jhon, M. S.; Yuk, S. H.; Lee, H. B. *Journal of Polymer Science, Part B: Polymer Physics* **1997,** 35, 595-598.

49. Park, S. Y.; Cho, S. H.; Yuk, S. H.; Jhon, M. S. *European Polymer Journal* **2001,** 37, 1785-1790.

50. Guice, K. B.; Loo, Y.-L. *Macromolecules* **2007,** 40, 9053 -9058.

51. Polymer Handbook, 4th Ed. In Brandrup, J.; Immergut, E. H.; Grulke, E. A., Eds. Wiley-Interscience: New York, 1999, VI-203.

52. Gomez Ribelles, J. L.; Monleon Pradas, M.; Gallego Ferrer, G.; Peidro Torres, N.; Perez Gimenez, V.; Pissis, P.; Kyritsis, A. *Journal of Polymer Science, Part B: Polymer Physics* **1999,** 37, 1587-1599.

53. Liu, W.; Nakano, T.; Okamoto, Y. *Polymer* **2000,** 41, 4467-4472.

54. Weaver, J. V. M.; Bannister, I.; Robinson, K. L.; Bories-Azeau, X.; Armes, S. P.; Smallridge, M.; McKenna, P. *Macromolecules* **2004,** 37, 2395-2403.

55. Guice, K. B.; Loo, Y.-L. *Macromolecules* **2006,** 39, 2474-2480.

56. Teoh, R. L.; Guice, K. B.; Loo, Y.-L. *Macromolecules* **2006,** 39, 8609-8615.

57. Oae, S. Y., T.; Okabe, T. . *Tetrahedron* **1972,** 28, 3203-3216.

58. Becke, F. H., H., *Badische Anilin & Soda-Fabrik Aktiengesellschaft*. Germany, 1968.

59. Asgarzadeh, F. B., E.; Chaumont, P. *Polym. Prepr. (Am. Chem. Soc., Div. Polym. Chem.)* **1999,** 40, 899-900.

60. Dubin, P. L.; Koontz, S.; Wright, K. L., III. *Journal of Polymer Science, Polymer Chemistry Edition* **1977,** 15, 2047-2057.

61. Dias, M. L.; Mano, E. B.; Azuma, C. *European Polymer Journal* **1997,** 33, 559-564.

62. Podzimek, S. *Journal of Applied Polymer Science* **1994**, 54, 91-103.

63. Alexander, L., *X-Ray Diffraction Methods in Polymer Science* Wiley-Interscience: New York, 1985.

64. Shibayama, M.; Hashimoto, T.; Kawai, H. *Macromolecules* **1983,** 16, 16-28.

65. Loo, Y.-L. Controlled polymer crystallization through block copolymer self-assembly, Ph.D. Dissertation, Princeton University, Princeton, N.J. **2001**, p. 42.

66. Porod, G., The Principles of Diffraction, Section 1, General Theory. In *Small-Angle X-ray Scattering*, Glatter, O., Kratky, O., Ed. Academic Press: London, 1982, pp. 17-51.

Chapter 3: Controlled copolymerization of HEMA and DMAEMA

INTRODUCTION

DMAEMA-containing polymers are useful for a wide range of applications, including lenses,[1] nanofiltration systems,[2,3] tissue scaffolds,[4] and drug delivery,[5,6,7,8] due to the fact that DMAEMA is responsive to pH and temperature.[8,9] Specifically, DMAEMA is protonated below its pKa (of 7.5 in its polymeric form),[10] and poly(DMAEMA) also exhibits an LCST in water near 50°C.[9,11] Poly(DMAEMA) and other DMAEMA-containing copolymers have thus been investigated both in solution[9,11-13] and as components within crosslinked hydrogels.[1-7] The synthesis of poly(DMAEMA) has been accomplished with controlled molecular weights and with narrow molecular weight distributions using a variety of controlled free-radical polymerization techniques.[9,14-20] Specifically, ATRP has been demonstrated as a useful controlled free-radical polymerization scheme for the synthesis of poly(DMAEMA) with narrow molecular weight distributions ($M_w/M_n < 1.08$).[17,18,19,20]

It is often useful to copolymerize DMAEMA with other monomers to tune the response of the material.[8,4,18] One monomer of interest is HEMA, which is biocompatible and exhibits moderate swelling in water in its polymeric form.[21] Several investigators have sought to combine the hydrophilicity of HEMA with the environmental-responsiveness of DMAEMA for bioapplications, such as scaffolds for tissue growth and hydrogels for pH-triggered drug delivery.[1,7,5,4,9,22] Bulk free-radical copolymerization of HEMA and DMAEMA in the presence of a crosslinking agent results in cationic hydrogel networks, in which the extent of swelling at any pH is generally controlled by the DMAEMA content.[4,8] While the utility of combining the attributes of HEMA and DMAEMA to tune the response of the final materials has been demonstrated, these

materials are inherently heterogeneous in crosslink density[23] and comonomer distribution due to large differences in monomer reactivity.[24] A better understanding of the dependence of polymer properties on composition in PHD requires control over these heterogeneities.

In this chapter, we identified polymerization schemes in which the comonomer distribution in PHD copolymers can be effectively controlled. Because the reactivity ratios of HEMA and DMAEMA are solvent dependent,[24,25] compositionally uniform PHD statistical copolymers can be synthesized if the copolymerization of HEMA and DMAEMA is carried out in an appropriate solvent and at an appropriate monomer feed composition.

AZEOTROPIC COPOLYMERIZATION OF PHD IN DMF.

The monomer sequence distribution along a polymer chain is related to the reactivity ratios of the comonomers.[26] These reactivity ratios describe the probability with which a polymer radical that is terminated with a monomer of one type adds a similar monomer instead of a dissimilar monomer. Ideally, the reactivity ratios of both monomers are unity, in which case the polymer composition at any point during the copolymerization is equivalent to the monomer feed composition.[26] In this scenario, statistical copolymers can be synthesized from any monomer feed composition.[26] The terminal-model reactivity ratios for our monomers of interest, r_H and r_D, have been reported for bulk copolymerization of HEMA and DMAEMA ($r_H = 1.63$; $r_D = 0.45$),[24] as well as for their copolymerization in water ($r_H = 1.32$; $r_D = 0.78$)[25] and in N,N-dimethylformamide (DMF; $r_H = 0.75$; $r_D = 0.36$).[25] In bulk copolymerization and copolymerization in water, $r_H > 1$ while $r_D < 1$. Correspondingly, the addition of HEMA monomer to all polymer radicals is more probable than the addition of DMAEMA. This scenario results in considerable deviation between the DMAEMA feed composition, $f_{D,o}$,

and the instantaneous DMAEMA composition in the copolymer, F_D. Even when the copolymerizations are carried out to low and moderate conversions, drifts in the instantaneous polymer composition are expected due to the different extents of depletion of HEMA and DMAEMA. It is therefore difficult to maintain compositional homogeneity when copolymerization of HEMA and DMAEMA is carried out in the bulk or in water without continuously monitoring and maintaining the instantaneous monomer composition, f_D, during the reaction. As a consequence, the resulting copolymers are initially enhanced in HEMA and enriched in DMAEMA in the tail.

The reactivity ratios of HEMA and DMAEMA in DMF are both less than one. Given the reactivity ratios, we predicted the instantaneous polymer composition as a function of the instantaneous monomer composition using the Skeist equation (Equation 2.6), which is shown in Figure 3.1 (solid curve).[26] The line $F_D = f_D$ is also shown (dashed line) in the figure for reference. There exists a single point for HEMA and DMAEMA copolymerization in DMF where the instantaneous polymer composition is equal to the instantaneous monomer composition. This single composition is known as the compositional azeotrope, which occurs at $f_D = F_D = 0.28$ in DMF.[25]

We investigated the copolymerization of HEMA and DMAEMA in DMF at the compositional azeotrope. Copolymerizations were carried out by ATRP, initiated with either EB*i*B or with a PS macroinitiator (M_n = 6500 g/mol, M_w/M_n = 1.02), at a DMAEMA feed composition of $f_{D,o} = 0.28$. The PS macroinitiator was used in some of the experiments in order to facilitate collection and cleanup of low molecular weight PHD samples. Aliquots were collected during each polymerization, and the monomer conversions and polymer compositions were determined by GC (Figure 3.2) and ^{1}H NMR (Figure 3.3), respectively. Representative GC traces collected during a copolymerization of HEMA and DMAEMA ($f_{D,o} = 0.28$) at successive time points of 0

hr, 2 hr, and 6 hr are shown in Figure 3.2. The elution times of HEMA, DMAEMA, and 1,2,4-trimethoxybenzene (non-reactive internal standard) are 2.4 min, 2.9 min, and 5.9 min, respectively. The traces for each aliquot are normalized against the peak intensity of 1,2,4-trimethoxybenzene. We observe decreases in both the HEMA and the DMAEMA peak intensities, relative to that of 1,2,4-trimethoxybenzene, with increasing reaction time. To obtain the monomer conversion, we compared the normalized integrated intensities of the monomers with those obtained prior to the initiation of the copolymerization.

A representative ^{1}H NMR spectrum of PHD in deuterated methanol is shown in Figure 3.3. Peaks **A** (δ = 4.04 ppm) are characteristic of the α-hydrogens in the ester groups of both HEMA and DMAEMA (2H each); peak **B** (δ = 3.74 ppm; 2H) is characteristic of the ethyl hydrogens in HEMA; peak **C** (δ = 2.62 ppm; 2H) is characteristic of the ethyl hydrogens in DMAEMA, peak **D** (δ = 2.30 ppm; 6H) is characteristic of the hydrogens in the methyl groups of the tertiary amine of DMAEMA, and peaks **E** and **F** (δ = 0.89-1.94 ppm) are backbone hydrogens. The peak areas of methacrylate (peaks **A**), HEMA (peak **B**), and DMAEMA (peaks **C** and **D**) were used to determine the final polymer composition. We note that ^{1}H NMR analysis provides the average polymer composition ($\overline{F_D}$), whereas the Skeist equation predicts the instantaneous polymer composition, F_D. At the azeotrope, the average polymer composition should equal the instantaneous composition, which is also equal to the monomer feed composition, $f_{D,o}$. The average polymer composition for this PHD copolymer, as calculated from the ^{1}H NMR spectrum, is $\overline{F_D}$ = 0.278.

For simplicity, we have plotted the average polymer composition, as determined by ^{1}H NMR, as a function of monomer conversion for all the aliquots collected during the copolymerizations of HEMA and DMAEMA ($f_{D,o}$ = 0.28), which were initiated with

EB*i*B (■) or with the polystyrene macroinitiator (●), in Figure 3.4. Since both the copolymerizations were carried out at the azeotrope, compositional uniformity along the polymer chains is expected. That $\overline{F_D}$ is constant at 0.28 ± 0.01 at any given point during the course of both the reactions verifies that there is little to no compositional drift along the polymer chain, whether the polymerization is initiated with EB*i*B, or with a polystyrene macroinitiator.

Accordingly, polymerizations at feed compositions other than the azeotropic composition are expected to produce significant compositional drifts along the polymer chain. To illustrate this, we carried out a PHD synthesis from the same polystyrene macroinitiator at $f_{D,o} = 0.75$. Aliquots were taken at several points during the reaction, and we determined the average polymer compositions for each aliquot by ^{1}H NMR. The average DMAEMA molar fractions within PHD are plotted against the total monomer conversion in Figure 3.4 (▲). At early times or low conversions, PHD is enhanced in HEMA relative to the initial monomer composition ($F_D < f_{D,o}$). As the reaction progresses, HEMA monomers are depleted faster than DMAEMA monomers so the tail of PHD is enhanced in DMAEMA (relative to initial monomer composition). For this particular feed composition, the Skeist equation predicts an initial instantaneous polymer composition of $F_D = 0.625$. This prediction is consistent with our initial experimental data point. In the limit of complete monomer conversion, $\overline{F_D}$ should equal $f_{D,o}$ ($\overline{F_D} = f_{D,o} = 0.75$). Since the Skeist equation only predicts the instantaneous polymer composition, we integrated the instantaneous polymer composition to estimate the average polymer composition as a function of monomer conversion. The dashed lines in Figure 3.4 represent the average polymer composition, predicted by the Skeist equation with reactivities of $r_H = 0.75$ and $r_D = 0.36$, at the azeotrope, and at $f_{D,o} = 0.75$, respectively. Our experimental results agree well with the values predicted by the Skeist

equation and implicate the importance of polymerization at the azeotrope to eliminate compositional heterogeneity along the polymer chain. Copolymerization outside the azeotrope, such as that at $f_{D,o}$ = 0.75, results in a gradient copolymer, rather than a statistical copolymer, that is enriched in HEMA at the onset, and in DMAEMA in the tail.

DETERMINATION OF REACTIVITY RATIOS IN OTHER SOLVENTS.

Copolymerization of HEMA and DMAEMA in DMF at the azeotropic composition results in statistical PHD copolymers with a controlled monomer composition. Polymerizations at any compositions other than the azeotropic composition, however, result in significant drifts in the composition along the polymer chain. In order to find suitable polymerization schemes for the synthesis of PHD statistical copolymers at compositions other than the azeotropic composition in DMF, we determined the reactivity ratios of HEMA and DMAEMA during their copolymerization in four other solvents: isopropanol (IPA), tetrahydrofuran (THF), acetonitrile (ACN), and dimethyl sulfoxide (DMSO). While it is not generally true that the reactivity ratios are significantly influenced by solvent choice, the reactivity ratios of HEMA and DMAEMA,[24,25] are solvent dependent. Generally, reactivity ratios are more likely to be solvent dependent in the cases of monomers containing polar functional groups.[27-31]

Copolymerizations of HEMA and DMAEMA at varying monomer feed compositions were carried out by ATRP in IPA, THF, ACN, and DMSO. Aliquots were collected throughout each copolymerization for the determination of monomer conversion (by GC) and average polymer composition (by ^{1}H NMR). Starting with an assumption that the reactivity ratios of HEMA and DMAEMA are unity, and given the monomer feed composition and monomer conversion data, theoretical values of the average polymer composition can be determined as a function of monomer conversion. We minimized the sum of the square errors between the theoretical and the

experimentally-obtained polymer compositions to obtain estimates of r_H and r_D in each solvent. This technique is similar to the nonlinear least-squares regression method proposed by Mortimer and Tidwell.[32] The method of Mortimer and Tidwell was originally applied to the determination of reactivity ratios from a large set polymerizations carried out only to low conversions, given the assumption that the average polymer compositions at these instances match the instantaneous polymer compositions.[32] Having integrated the Skeist equation[26] for the average polymer composition, however, we were able to perform regressions from data obtained over a wider range of monomer conversions and monomer feed compositions in the regression of the reactivity ratios.[33] Although it has been suggested that the reactivity ratios obtained by least-squares regression might be dependent on the initial estimates,[32] we obtained the same values for r_H and r_D for each solvent choice we examined that are independent of the numerous initial conditions explored.

Monomer conversion and the average polymer composition for PHD synthesized in IPA at several monomer feed compositions are shown in Figure 3.5. Each point (▼,◆,●,▲,■) represents an aliquot collected during the copolymerizations. The copolymerizations were performed at monomer feed compositions of $f_{D,o}$ = 0.723 (▼), 0.600 (◆), 0.474 (●), 0.289 (▲), and 0.192 (■). The dotted lines represent the monomer feed composition for each experiment. The solid curves in Figure 3.5 represent the theoretical average polymer composition, predicted by integrating the Skeist equation for each copolymerization. If, during the course of the copolymerization, there is no deviation between the average polymer composition and the monomer feed composition (as in the case when $r_H = r_D = 1$), the solid curves should coincide with the dashed lines. Using least-squares regression, r_H and r_D were determined to be 1.27 and 0.800 in IPA, respectively.

For comparison, the reactivity ratios were also calculated according to the methods proposed by Fineman and Ross,[34] and Kelen and Tudos.[35] Both the Fineman and Ross and the Kelen and Tudos methods approximate the reactivity ratios by fitting initial monomer and low-conversion polymer composition data to linearized forms of the Skeist equation.[34,35] Because these methods were only derived for the limit of low monomer conversion,[35] we only used the data obtained at low conversion (i.e., the first aliquot during each of the copolymerizations in Figure 3.5) for determination of reactivity ratios. The reactivity ratios calculated by all three methods are shown in Table 3.1. The values obtained using the methods of Fineman and Ross, and Kelen and Tudos are similar to those determined by least-squares regression. We believe that the least-squares regression technique is the most reliable, since more data (obtained at higher conversions and at various monomer feed compositions) were used to determine r_H and r_D.

We also determined r_H and r_D in THF, ACN, and DMSO in a similar fashion; the calculated reactivity ratios are summarized in Table 3.1. To demonstrate the effect of solvent selection on r_H and r_D, we have plotted the least-squares regressed values in Figure 3.6, along with previously reported values for r_H and r_D in the bulk,[24] in water,[25] and in DMF.[25] We have drawn 95% joint confidence regions around the reactivity ratios in IPA, THF, ACN, and DMSO, as determined using the method of Tidwell and Mortimer.[32] We have also plotted the predicted instantaneous polymer composition as a function of the instantaneous monomer composition for the copolymerization of HEMA and DMAEMA in IPA, THF, ACN, and DMSO in Figures 3.7a-d (solid curves). The predicted instantaneous polymer composition was calculated from the Skeist equation[26] given the values of r_H and r_D regressed for each solvent. The dashed line in each plot is the 45º line that represents the case of $F_D = f_D$. The Skeist equation should predict exactly this line if both reactivity ratios are unity. The difference between the solid curve

and the dashed line thus represents deviations between the instantaneous monomer composition and the instantaneous polymer composition. In IPA (r_H = 1.27 and r_D = 0.800; Figure 3.7a) and in THF (r_H = 1.46 and r_D = 0.926; Figure 3.7b), r_H is greater than unity, whereas r_D is less than unity. The addition of HEMA is thus favored over the addition of DMAEMA to all polymer radicals. A gradient copolymer that is initially enhanced in HEMA will result during the copolymerization of HEMA and DMAEMA in IPA or THF. Given the calculated reactivity ratios, we predict a greater than 4% deviation between the instantaneous monomer composition and the instantaneous polymer composition over 50% of the entire composition range when copolymerizations take place in either IPA or THF. This deviation is apparent in Figures 3.7a and 3.7b, where considerable differences between F_D and f_D are observed in both solvents. The calculated r_H and r_D in ACN are 1.01 and 0.641, respectively. As shown in Figure 3.7c, HEMA is preferentially added at high f_D. At low f_D (≈0.01-0.05), the solid curve coincides with the 45^o line, suggesting minimal deviation between f_D and F_D. Our 95% confidence interval does not preclude the presence of an azeotrope at $f_D > 0.95$.

The calculated reactivity ratios in DMSO are r_H = 1.08 and r_D = 1.12. The Skeist equation predicts an azeotropic composition in DMSO at f_D = 0.391. In general, however, the reactivity ratios in DMSO are both close to unity. There is therefore very little deviation between the instantaneous monomer composition and the instantaneous polymer composition over the entire range of f_D, as shown in Figure 3.7d. Accordingly, DMSO is an ideal solvent choice for the copolymerization of HEMA and DMAEMA over the full range of composition.

As verification, we carried out two additional copolymerizations of HEMA and DMAEMA in DMSO at initial monomer compositions $f_{D,o}$ = 0.75 and 0.50, respectively, and multiple aliquots for each copolymerization were collected and analyzed as

previously described. The average polymer composition is presented as a function of monomer conversion for the copolymerizations at $f_{D,o} = 0.75$ (▲) and $f_{D,o} = 0.50$ (■) in Figure 3.8. The solid curves in Figure 3.8 represent the theoretical average polymer composition for each copolymerization, as predicted by integrating the Skeist equation. For both copolymerizations, there is negligible drift in average polymer composition with increasing monomer conversion, and the average polymer compositions agree with the theoretical polymer compositions (e.g., $\overline{F_D} \approx F_D$) for every aliquot. In particular, the drift in polymer composition at $f_{D,o} = 0.75$ is significantly less when HEMA and DMAEMA copolymerization takes place in DMSO rather than in DMF (Figure 3.4). We also note that the difference between the initial monomer composition, $f_{D,o}$ and the average polymer composition, $\overline{F_D}$, is less than 1.5 mol% for all collected samples, which is within the error of ^{1}H NMR. PHD copolymers synthesized in DMSO are therefore compositionally uniform. All compositionally-uniform PHD copolymers will henceforth be referred to as PHD_F, where F represents average (or instantaneous) DMAEMA composition, in mol% of the copolymer.

The role of solvent on the reactivity ratios of polar monomers is qualitatively described by the bootstrap effect,[29,30] which surmises polarity-induced differences in the local monomer concentration.[28,31] This model, however, does not provide a prescriptive guide to the selection of the appropriate solvent for producing random copolymers of uniform compositions. During the copolymerization of HEMA and DMAEMA, we noted an interesting correlation between the solubility parameter of the solvent and the extracted reactivity ratios. In particular, we observe that $r_H \approx 1$ when the solubility parameter of the solvent (δ) closely matches the solubility parameter of poly(HEMA), $\delta_{HEMA} = 13.2$ $(cal/cm^3)^{1/2}$.[36] For discussion, we have listed the solubility parameters of the solvents,[37] along with the square of the solubility parameter difference, $(\delta - \delta_{HEMA})^2$,

which is proportional to the contact energy of the solvent and poly(HEMA),[38] in Table 3.1. We observe that $r_H \approx 1$ when $(\delta - \delta_{HEMA})^2$ is small (< 2). With increasing $(\delta - \delta_{HEMA})^2$, however, r_H increases. This trend is consistent with what had been proposed by the bootstrap effect.[29,30] When the solvent-polymer contact energy is high, the local environment of the growing chain is likely enhanced in HEMA monomer. The propensity for the growing radical to add a HEMA monomer is thus high ($r_H > 1$). On the other hand, when the solvent-polymer contact energy is minimal, the local environment is not enhanced in HEMA, so r_H is approximately 1. Our discussion here does not take DMAEMA into account. While we acknowledge that the presence of DMAEMA necessarily changes the local environment, we were not able to find the solubility parameter of DMAEMA in the literature for this comparison. But we speculate the effect to be small given that DMAEMA is not capable of hydrogen bonding (or any other specific interactions), except in water.[10]

KINETICS OF AZEOTROPIC COPOLYMERIZATION IN DMF.

In order to synthesize statistical PHD copolymers with target molecular weights and with narrow molecular weight distributions, there needed to be some understanding of the kinetics of the copolymerization of HEMA and DMAEMA. To examine the kinetics of copolymerization in DMF, HEMA and DMAEMA were copolymerized at the compositional azeotrope with EB*i*B as the initiator, and with a total monomer to initiator ratio of 300:1. We also chose to use a mixed halide system consisting of a bromine initiator (EB*i*B) and a CuCl catalyst. The use of mixed halides to better control ATRP polymerizations was first reported for the synthesis of poly(methyl methacrylate), PMMA.[39] In particular, EB*i*B increases the rate of initiation relative to its chlorine counterpart, ethyl-2-chloroisobutyrate, while CuCl slows propagation compared to CuBr.[39,40] There is therefore consensus that the use of such mixed halide systems results

in faster initiation but better controlled propagation,[39] which in turn improves control over molecular weights, and generally leads to narrower molecular weight distributions. It follows that mixed halide systems are especially effective for the polymerization of monomers with high propagation constants, such as HEMA.[41] In our copolymerization, $CuBr_2$ was added at the onset of the copolymerization to help maintain a decent rate of radical deactivation and to effectively suppress the rate of radical termination.[42] The molar ratio of CuCl to $CuBr_2$ to EB*i*B was 20:1:21.

The kinetics of copolymerization of HEMA and DMAEMA are shown in Figure 3.9 (■). The copolymerization kinetics do not obey classical first-order ATRP kinetics,[43] nor do they proceed with a $t^{2/3}$ dependence, as suggested by the persistent radical effect theory.[44,45] Rather, our copolymerization kinetics data appear to be described by a $t^{1/3}$ dependence (see Equation 2.5), similar to that proposed by Snijder et al.[46]

The classical first-order ATRP kinetics assume a constant radical concentration and appears to only be valid when the overall radical concentration is sufficiently low.[43] Consequently, such kinetics have been observed in polymerizations where the free radical is largely dormant (capped by metal ligand complex), or when the Cu^I catalyst concentration is sufficiently low and the Cu^{II} concentration is sufficiently high.[43] Fischer's persistent radical effect theory,[44,45] which predicts $t^{2/3}$ dependence, is valid when the polymerization undergoes termination that slowly result in a build-up of halogen atoms in solution. In both the first-order and $t^{2/3}$ kinetic models, the reaction medium is homogeneous, *i.e.*, the metal-ligand complex is well solubilized. The Snijder model was developed to describe heterogeneous ATRP polymerizations.[46] In particular, this model invokes the notion of a Cu^{II} deactivator ceiling concentration, $[Cu^{II}]_c$, above which excess Cu^{II} will precipitate from the polymerization medium. The kinetics of heterogeneous

polymerizations of methyl methacrylate in the presence of $CuBr/CuBr_2$/PMDETA, for example, obey this model.[46]

Visually, the conditions we used to copolymerize HEMA and DMAEMA resulted in a heterogeneous reaction medium; a trace amount of yellow-green Cu^{II} precipitant was observed at the bottom of the reaction flask shortly after initiation. As such, we are not surprised that our kinetics data are described by the model proposed by Snijder and coworkers, and not by the classical first-order kinetics or the persistent radical effect theory. To fit our data, we simplified Equation 2.5 (the Snijder model) into an expression with two lumped kinetic parameters, A and B (Equation 3.1):

$$\ln\frac{[M]_o}{[M]} = A\left\{\left(Bt + [I]_o^{-3}\right)^{1/3} - [I]_o^{-1}\right\} \qquad \text{(Equation 3.1)}$$

Where $[M]_o$ is the initial molar concentration of monomer (e.g., HEMA and DMAEMA), $[M]$ is the molar concentration of monomer at time t, $[I]_o$ is the initial molar concentration of initiator, and A and B are defined by Equations 3.2 and 3.3, respectively:

$$A = \frac{k_p\left[Cu^{II}\right]_c}{2k_tK_{eq}} \qquad \text{(Equation 3.2)}$$

$$B = 6k_t\left(\frac{K_{eq}}{\left[Cu^{II}\right]_c}\right)^2 \qquad \text{(Equation 3.3)}$$

In Equations 3.2 and 3.3, k_p is the rate constant of propagation, k_t is the rate constant of termination, and K_{eq} is the equilibrium rate constant. Subjecting our data to a best fit of Equation 3.1 yields $A = 8.41\cdot10^{-4}$ $mol\cdot L^{-1}$ and $B = 5.59\cdot10^{4}$ $L^3\cdot mol^{-3}\cdot s^{-1}$ (correlation coefficient = 0.9957). That our data can be described by Equation 3.1 suggests that the assumptions associated with the Snijder model are relevant to the copolymerization of HEMA and DMAEMA in DMF.

We also investigated the kinetics of azeotropic copolymerization of HEMA and DMAEMA with a PS macroinitiator (M_n = 6500 g/mol; M_w/M_n = 1.02), that was previously synthesized by ATRP. Using a macroinitiator, instead of a small-molecule initiator, to initiate the copolymerization of HEMA and DMAEMA enables the synthesis of well-defined block copolymers. The synthesis and characterization of PHD-containing block copolymers are the subject of Chapter 4. The copolymerization kinetics of HEMA and DMAEMA from the PS macroinitiator are shown in Figure 3.9 (●). While the kinetics data are quantitatively similar to that of copolymerization with EB*i*B (■), and the polymerization proceeds with $t^{1/3}$ kinetics, there is a subtle difference between the two polymerizations. In particular, there is an induction period of approximately 30 min during the onset of copolymerization with the PS macroinitiator. The early times data (< 3 hr) are provided in the inset of Figure 3.9. The reaction appears to start off slowly, but subsequently proceeds at the rate with which HEMA and DMAEMA are copolymerized when the reaction is initiated with EB*i*B. We carried out similar polymerizations with a another PS macroinitiator having a different molecular weight (M_n = 3200 g/mol; M_w/M_n = 1.02) and the kinetics data also show an induction period during the early stages of polymerization. Consistent with the kinetics data, we observed a slower color change (from dull teal to bright blue; indication of "controlled" polymerization) after the PS macroinitiator was added to the reaction medium. We speculate that this slow initiation is associated with the solubility of PS in DMF. PS has a solubility parameter[38] of δ_{PS} = 9.0 $(cal/cm^3)^{1/2}$, while DMF has a solubility parameter of δ_{DMF} = 12.1 $(cal/cm^3)^{1/2}$.[37] One can therefore imagine that the active chain ends are buried in the rather collapsed coils of polystyrene in DMF. The delayed initiation is thus likely to be related to the time needed for the first monomers to access the active chain ends. We note that other groups have also reported slow initiation from macroinitiators;[47,48] although explanations for such

phenomenon were not provided. We stress that this slow initiation from the PS macroinitiator does not impact our ability to control the composition or the molecular weight distribution of the resulting copolymers.

Polymers collected during the azeotropic copolymerizations initiated with EB*i*B and with the PS macroinitiators, were analyzed by GPC with DMF (+ 0.05 M LiBr) as eluent. LiBr was added to suppress polymer-solvent and polymer-substrate interactions that are typically observed in polymers with ionic functional groups.[49,50] GPC traces for each of the aliquot collected during the polymerizations are shown in Figure 3.10. Figures 3.10a and 3.10b contain the GPC traces of aliquots collected during the copolymerization of HEMA and DMAEMA with EB*i*B, and that with a PS (M_n = 6500 kg/mol) macroinitiator, respectively. Characteristic of ATRP, the GPC traces are narrow, symmetric, and monomodal. As the reactions progress, the peaks shift to smaller elution volumes, indicating a time-dependent increase in molecular weight during both copolymerizations.

We determined the absolute number-average molecular weight of our PS macroinitiator (M_n = 6500 g/mol; M_w/M_n = 1.02) using GPC with THF as the eluent. For comparison, we also analyzed the same PS macroinitiator by GPC with DMF and 0.05 M LiBr as the eluent. In this case, the PS macroinitiator elutes at a much higher elution volume (18.15 mL). In fact, the PS macroinitiator peak overlaps with the solvent peak in the GPC trace (far right) in Figure 3.10b despite real differences in molecular weights between the two. Though peculiar at first glance, this phenomenon has previously been reported by Dubin and coworkers where low molecular weight PS samples (< 4000 g/mol) elute at the same volume as polar small molecules when GPC is performed in DMF.[50] The presence of salt (0.1 M LiBr) shifts the PS peak to even higher elution volumes.[50] This "salting out" phenomenon observed with PS is caused by a reduction in

the solubility of the polymer in the eluent, which is manifested by a decrease in the effective hydrodynamic volume so that a higher elution volume is measured.[50] As a reference, we also measured a PS standard of a slightly higher absolute molecular weight (M_n = 7800 g/mol, M_w/M_n = 1.05) under the same conditions. This PS standard also elutes near the solvent peak, at 17.95 mL.

The number-average molecular weights for PHD aliquots collected during both copolymerizations with $f_{D,o}$ = 0.28 (■,●) are compiled in Figure 3.11. The absolute number-average molecular weights for the polymers collected during the copolymerization with EB*i*B (■) were extracted from GPC data using a dn/dc of 0.1009 (± 0.0067; measured independently with an interferometric refractometer from five concentrations of PHD_{28} in DMF with 0.05 M LiBr). The absolute number-average molecular weights of PHD_{28} in copolymerizations initiated by the PS macroinitiator (●) were obtained with compositions from ^{1}H NMR analysis, given an absolute M_n for the PS macroinitiator. In both polymerizations, the molecular weight increases linearly with total monomer conversion. Additionally, the increase in molecular weights in both polymerizations appear to be well described by a single fit (dashed line is fit to both sets of molecular weight data). Both features are characteristic of ATRP polymerization and indicate controlled reactions. We note, however, that the molecular weight at any given conversion is higher than the theoretical molecular weight predicted by the initial monomer and initiator concentrations (solid line). We also carried out copolymerizations at a different total monomer to initiator molar ratio ($[M]_o:[I]_o$ = 150:1 instead of 300:1). The polymer molecular weights in this case are also higher than the theoretical molecular weights, but they are well described by the same fit (dashed line) when we account for the different monomer to initiator ratio used. Higher than expected molecular weights during ATRP polymerizations are not uncommon, and have been observed by many

others.[51,18] While we do not have a clear explanation for this observation, we suspect that pronounced termination at early reaction times might be responsible. While pronounced termination should result in increased polydispersity, the polydispersities of the PHD copolymers collected over the course of the copolymerizations are generally less than 1.2. One possible explanation for this discrepancy is that lower molecular weight PHD copolymers, which might result from pronounced termination at early reaction times, are selectively removed during dialysis of the polymerization medium against THF.

The degree of termination for the PHD copolymerizations that were carried out in DMF appears to be independent of the types of initiator used (whether EB*i*B, or PS macroinitiator) and monomer to initiator ratios (whether $[M]_o:[I]_o$ = 150:1, or 300:1). As such, well-defined PHD_{28} copolymers of desired molecular weights can still be tailor-made, given the information in Figure 3.11.

The molecular weight distributions (□,○) for each of the aliquot collected during both polymerizations remain narrow (< 1.2 for copolymers from EB*i*B and ≈ 1.15 for the block copolymers from the PS macroinitiator), indicating that the polymerizations were well-controlled throughout. The final sample collected in the copolymerization of HEMA and DMAEMA from the PS macroinitiator, however, exhibits a higher polydispersity (M_w/M_n = 1.33) compared to the other aliquots. Since this particular aliquot was collected after > 24 hour reaction, we suspect a gradual loss in the metal-ligand complex activity to be responsible for the slight increase in its molecular weight distribution. A gradual loss in metal-ligand complex activity might be associated with a loss of Cu^{II} from solution, which is in agreement with the Snijder model.[46]

KINETICS OF COPOLYMERIZATION OF HEMA AND DMAEMA IN DMSO.

We were also interested in determining the kinetics of the copolymerization of HEMA and DMAEMA in DMSO, as DMSO is the more versatile polymerization

medium for the synthesis of PHD statistical copolymers. It has been previously reported that DMSO can coordinate with both Cu^{I} and Cu^{II}, and that these interactions can complicate the polymerization kinetics and the controllability of reactions performed in DMSO.[17] Accordingly, we used a mixed halide system to improve control over our copolymerization. We also performed the copolymerizations with a low concentration of CuCl and a high concentration of $CuCl_2$ (CuCl : $CuCl_2$: EB*i*B = 1:12:10) to suppress early termination reactions during the copolymerization, with the hope of synthesizing PHD statistical copolymers with controlled molecular weights.

We carried out copolymerizations of HEMA and DMAEMA in DMSO at $f_{D,o}$ = 0.75 and $f_{D,o}$ = 0.50 with a total monomer to initiator ratio of 300:1 and tracked the copolymerization kinetics; data from both copolymerizations ($f_{D,o}$ = 0.75, ▲; $f_{D,o}$ = 0.50, ■) are shown in Figure 3.12. Just as we had observed for copolymerizations at the compositional azeotrope in DMF, the kinetics of copolymerizations of HEMA and DMAEMA by ATRP in DMSO do not follow the classical first-order kinetics that is attributed to living polymerizations.[43] Instead, these copolymerizations follow the $t^{1/3}$ model proposed by Snijder and coworkers (Equation 2.5; In Figure 3.12, $f_{D,o}$ = 0.75 is represented by dashed curve and $f_{D,o}$ = 0.50 is represented by a solid curve).[46] In general, we also observe that the copolymerizations are faster with decreasing $f_{D,o}$. To quantify, we compared the rate constants of propagation, k_p, for copolymerizations in DMSO at $f_{D,o}$ = 0.75 and $f_{D,o}$ = 0.50, assuming that the ATRP equilibrium constant, K_{eq}, and the ceiling Cu^{II} concentration, $[Cu^{II}]_c$, are independent of the monomer feed composition. Given these assumptions, the ratio of the rate constants of propagation is equal to the ratio of the products of the lumped parameters A (Equation 3.2) and B (Equation 3.3) for each copolymerization. We found k_p at $f_{D,o}$ = 0.50 to be 1.5 times greater than that at $f_{D,o}$ = 0.75. It has been previously observed that the rate of polymerization of HEMA is

considerably faster than the rate of polymerization of DMAEMA, when the homopolymerizations take place under similar conditions.[18] It is therefore not surprising that the overall rate of copolymerization is related to the feed composition, and is suppressed with decreasing DMAEMA in the monomer feed.

The PHD copolymers synthesized in DMSO were also analyzed by GPC with DMF (+ 0.05 M LiBr) as the eluent. GPC traces for each collected aliquot during the copolymerizations at $f_{D,o} = 0.75$ and at $f_{D,o} = 0.50$ are shown in Figures 3.13a and 3.13b, respectively. All the GPC traces are narrow and monomodal; the peaks shift to smaller elution volumes with increasing monomer conversion. The extracted molecular weight distributions for the copolymers are plotted as a function of total monomer conversion in Figure 3.14. The molecular weight distributions remained narrow (< 1.11), even at high monomer conversions (x = 0.637). The molecular weight distributions are generally narrower than those we previously reported during copolymerizations in DMF, which were carried out with a higher Cu^{I} concentration and a lower initial Cu^{II} concentration. We speculate that a reduction in Cu^{I} concentration and an increase in initial Cu^{II} concentration results in better control over the copolymerization of HEMA and DMAEMA.

The absolute number-average molecular weights for the PHD copolymers collected during both copolymerizations are also plotted in Figure 3.14. During both copolymerizations, the molecular weights increased linearly with total monomer conversion. For reference, we have also plotted the theoretical molecular weight, as predicted by the monomer to initiator ratio in Figure 3.14 (solid line). The molecular weights appear to agree with the theoretical molecular weights, which points to the "livingness" of this polymerization.[42] Previously, we observed deviations between the theoretical and experimental molecular weights during copolymerizations of HEMA and

DMAEMA in DMF. This observation was largely independent of the type of initiator (PS macroinitiator or EB*i*B) and the monomer to initiator molar ratio, and we attributed the difference between the experimentally obtained and the theoretically predicted molecular weights to early termination. By decreasing the Cu^{I} concentration and increasing the Cu^{II} concentration correspondingly, we were able to suppress the early termination reactions and synthesize PHD statistical copolymers of target molecular weights.

EFFECT OF PHD COMPOSITION ON FINAL POLYMER PROPERTIES.

Glass Transition Temperature.

We measured the glass transition temperatures (T_g) of PHD synthesized by ATRP at the azeotropic composition in DMF and at multiple compositions in DMSO by DSC. The samples were heated twice; the first heat ensured uniform thermal contact between the sample and the pan and we only extracted the glass transition temperature from the second heat. The DSC thermograms of each PHD statistical copolymer show a single step change in enthalpy indicating a glass transition.[52] We also determined the glass transition temperatures of poly(DMAEMA) and poly(HEMA) homopolymers. All the extracted T_gs are plotted against the weight fraction of DMAEMA, w_D, within the random copolymer in Figure 3.15. The glass transition temperature decreases with increasing DMAEMA content, and the trend appears to be qualitatively described by the Fox equation[53] (dashed line; based on Equation 3.4):

$$\frac{1}{T_g} = \frac{w_D}{T_{g,D}} + \frac{1 - w_D}{T_{g,H}} \qquad \text{(Equation 3.4)}$$

Where $T_{g,D}$ and $T_{g,H}$ are the glass transition temperatures of poly(DMAEMA) and poly(HEMA) in Kelvins, respectively.

That the Fox equation adequately describes the increase in T_g we observe in our polymers is unexpected, given that HEMA is capable of hydrogen bonding.[24] Contrary to what has been proposed for HEMA-containing systems,[24] our observations suggest that the specific interactions do not dominate the physical properties in our PHD copolymers.

Lower Critical Solution Behavior.

DMAEMA-containing polymers are known to exhibit a lower critical solution temperature (LCST) in water which results from a hydrophilic-to-hydrophobic transition with increasing temperature.[11,54] The LCST of poly(DMAEMA) has been demonstrated to occur around 50 °C.[11] Further, it has been demonstrated that copolymerization of DMAEMA with other monomers can alter the LCST of the final polymer. Generally, copolymerization with hydrophilic monomers elevates the LCST of the final polymer by increasing the hydrophilicity at higher temperatures, relative to poly(DMAEMA).[9] Alternatively, copolymerization with hydrophobic monomers decreases the LCST of the final polymer.[9, 12] In conjunction with the Genzer group at North Carolina State University, we explored the LCST behavior of PHD copolymers of similar molecular weights ($M_n \approx$ 15-25 kg/mol) and narrow molecular weight distributions ($M_w/M_n < 1.2$), all prepared by ATRP.

The solution behaviors of these PHD copolymers are shown in terms of the normalized transmittance of light through dilute solutions as a function of temperature in Figure 3.16. We also synthesized poly(DMAEMA) of comparable molecular weight (Mn = 19 kg/mol, Mw/Mn = 1.15) and examined its solution behavior (○) to serve as a point of reference in Figure 3.16. The lower critical solution temperature for poly(DMAEMA), extracted as the midpoint in the transmittance curve, was determined to be 36 °C. Relative to the observed LCST of poly(DMAEMA), the LCST of PHD copolymers decreases with decreasing DMAEMA content. The observed LCSTs for PHD_{75}, and

PHD_{50} similar molecular weights are 29 °C, 27 °C, and 22 °C, respectively. Further, we note that neither poly(HEMA) nor PHD_{28} are soluble in deionized water. Whereas poly(DMAEMA) is soluble in water under ambient conditions,[11] poly(HEMA) is capable of swelling in water but is not soluble due to the methyl group located off of its polymer backbone.[55] The observed solution behavior of PHD statistical copolymers are consistent with what is expected for the copolymerization of DMAEMA with monomers that are not soluble in water in their polymeric form.[9]

CONCLUSIONS

In this chapter, we demonstrated that PHD statistical copolymers with uniform composition distributions can be synthesized by the selection of an appropriate polymerization medium. Specifically, PHD statistical copolymers can be synthesized at the compositional azeotrope in DMF ($f_{D,o} = 0.28$) or at any composition in DMSO, where the monomer reactivity ratios of HEMA and DMAEMA are near unity. We also demonstrated that the kinetics of copolymerization of HEMA and DMAEMA follow a $t^{1/3}$ power law, and that the molecular weight and molecular weight distribution of PHD statistical copolymers synthesized in DMF or in DMSO can be well-controlled through the use of highly optimized ATRP schemes. In particular, the use of a high initial concentration of Cu^{II} and a low initial concentration of Cu^{I} was demonstrated to produce PHD statistical copolymers with molecular weights that correspond to their predicted molecular weights. PS macroinitiators can also be used to effectively initiate the copolymerization of HEMA and DMAEMA in DMF. As we will see in Chapter 4, this strategy can also be used to synthesize a diverse selection of PHD-containing block copolymers.

We have developed a model system for investigating the effects of polymer composition on the properties of copolymers. In this chapter, we demonstrated that the

composition of PHD statistical copolymers can influence both the glass transition temperature and the LCST of the statistical copolymer. Our synthetic methodology provides a useful route to the design and controlled synthesis of PHD copolymers and PHD-containing block copolymers.

TABLES

Table 3.1. Solubility Parameters (δ) of Solvents and Reactivity Ratios of HEMA and DMAEMA (r_H and r_D) Calculated by Various Methods.

Solvent	**Solubility Parameter[37]**	**Solubility Parameter Difference**	**Least-Squares Regression**		**Fineman and Ross[34]**		**Kelen and Tudos[35]**	
	δ $(cal/cm^3)^{1/2}$	$(\delta - \delta_{HEMA})^2$	r_H	r_D	r_H	r_D	r_H	r_D
IPA	11.5	2.9	1.27	0.800	1.19	0.783	1.18	0.767
THF	9.1	17	1.46	0.926	1.52	0.857	1.49	0.844
ACN	11.9	1.7	1.01	0.641	1.02	0.681	1.04	0.699
DMSO	14.5	1.7	1.08	1.12	0.976	1.02	1.05	1.09

FIGURES

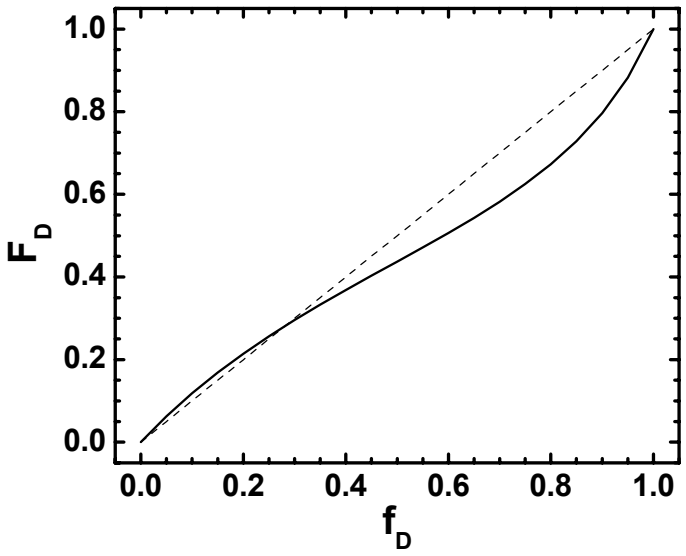

Figure 3.1. Instantaneous polymer composition, F_D, as a function of instantaneous monomer composition, f_D, for the copolymerization of HEMA and DMAEMA in DMF, as predicted by the Skeist equation[26] ($r_H = 0.75$, $r_D = 0.36$).[25] The dashed line in corresponds to the 45º line where the instantaneous polymer composition is equal to that of the instantaneous monomer composition. An azeotrope occurs at $F_D = f_D = 0.28$, wherein the instantaneous polymer composition is equal to the instantaneous monomer composition.

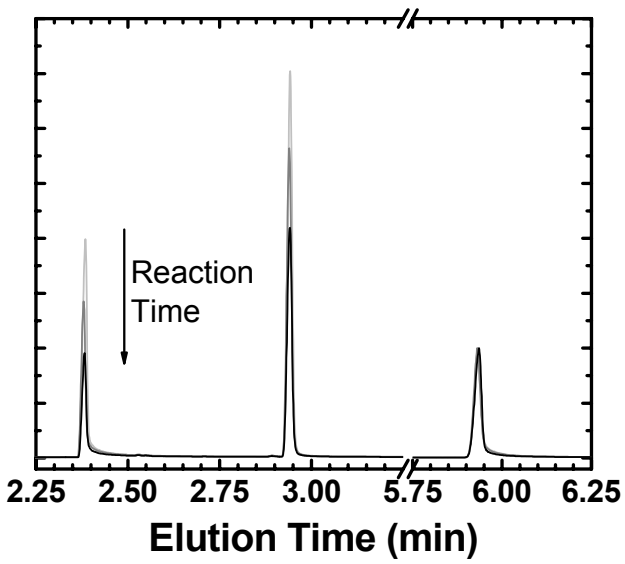

Figure 3.2. Gas chromatography traces from several aliquots collected during the course of a copolymerization of HEMA (elutes at 2.4 min) and DMAEMA (elutes at 2.9 min) at $f_{D,o} = 0.28$. The traces are normalized against the peak intensity of 1,2,4-trimethoxybenzene (internal standard, elutes at 5.9 min). The GC traces were collected at successive time points of 0 hr, 2 hr, and 6 hr. HEMA and DMAEMA peak intensities decrease with increasing reaction time. Monomer conversion was determined by integrating the peak intensities of HEMA and DMAEMA.

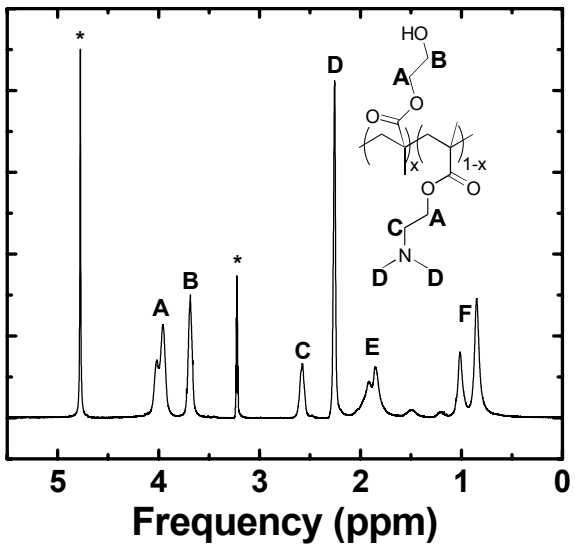

Figure 3.3. ^{1}H NMR spectrum of PHD in deuterated methanol. The proton contributions of PHD are labeled for clarity. The integrated areas of peaks **A**, **B**, **C**, and **D** were used to determine the average polymer composition in each aliquot. * indicates solvent peaks (d-MeOH).

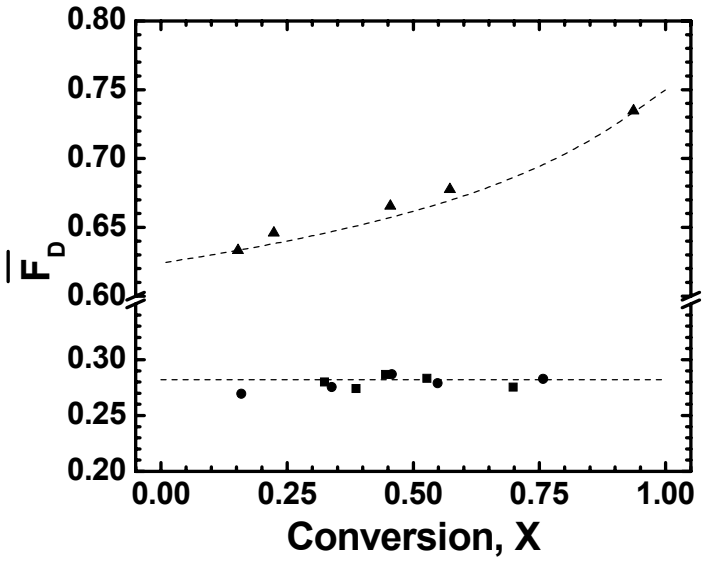

Figure 3.4. Average polymer composition, $\overline{F_D}$, during three separate ATRP of HEMA and DMAEMA: at the azeotrope ($f_{D,o} = 0.28$) with EB*i*B as the initiator (■), at the azeotrope with a PS macroinitiator (●), and off the azeotrope ($f_{D,o} = 0.75$) with the same PS macroinitiator (▲). Dashed curves indicate the time-average polymer composition; we integrated the instantaneous polymer compositions predicted by the Skeist equation to obtain these curves.

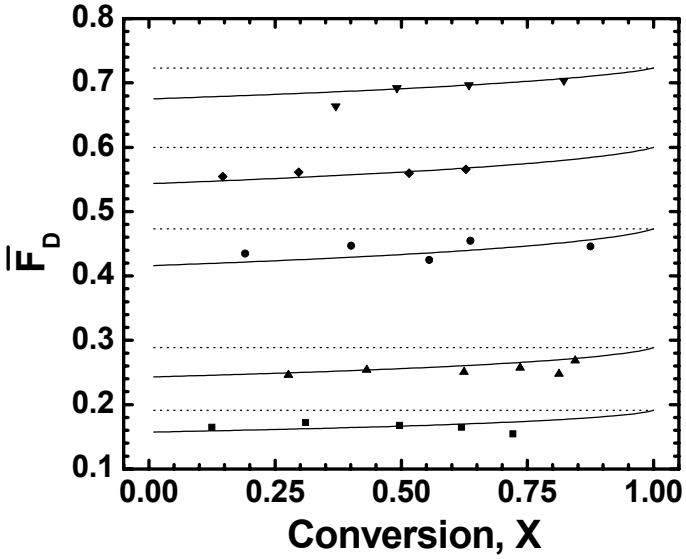

Figure 3.5. Monomer conversion and average polymer composition for copolymerizations of HEMA and DMAEMA in IPA collected from separate ATRP at molar monomer feed compositions, $f_{D,o}$ of 0.723 (▼), 0.600 (◆), 0.474 (●), 0.289 (▲), and 0.192 (■). The dotted lines represent the molar monomer feed compositions for each experiment. The solid curves represent the theoretical average polymer composition, predicted by integrating the Skeist equation with regressed reactivity ratios of $r_H = 1.27$ and $r_D = 0.800$.

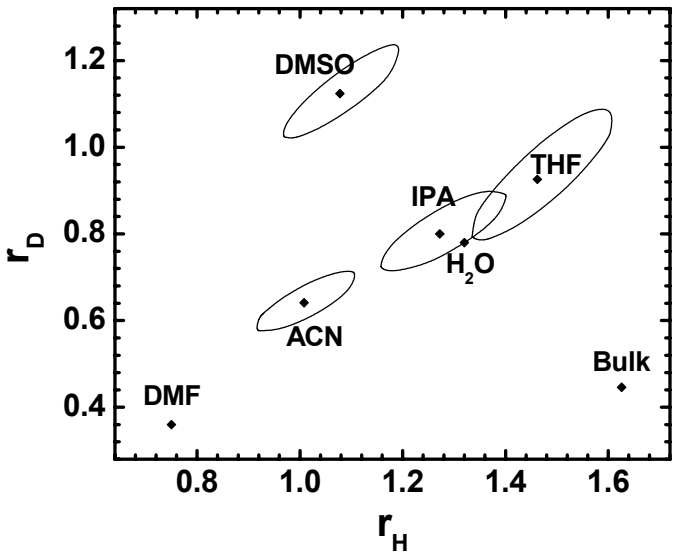

Figure 3.6. Reactivity ratios of HEMA (r_H, x-axis) and DMAEMA (r_D, y-axis), along with 95% joint confidence intervals (ellipses), for IPA, THF, ACN, and DMSO. Previously reported reactivity ratios in the bulk,[24] in water,[25] and in DMF[25] are also shown.

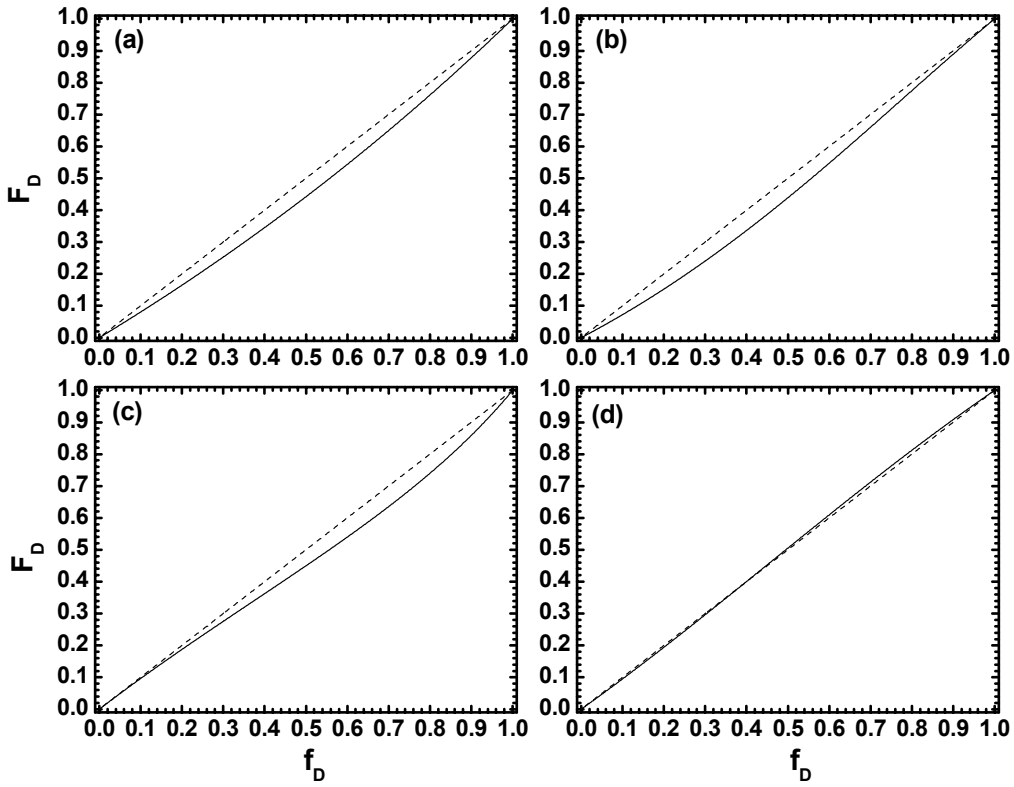

Figure 3.7. Instantaneous polymer compositions, F_D, as a function of the instantaneous monomer composition, f_D, for copolymerization of HEMA and DMAEMA in (a) IPA, (b) THF, (c) ACN, and (d) DMSO. F_D was predicted by the Skeist equation given the regressed reactivity ratios for each solvent. The dashed line in each graph corresponds to the 45º line where the instantaneous polymer composition is equal to the instantaneous monomer composition ($F_D = f_D$), which occurs when both monomer reactivity ratios are unity.

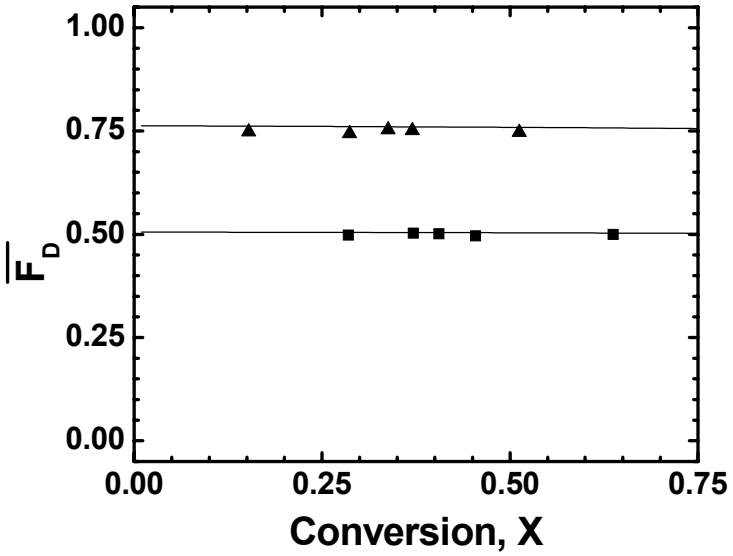

Figure 3.8. Monomer conversion and average polymer composition for copolymerizations of HEMA and DMAEMA in DMSO at molar monomer feed compositions, $f_{D,o}$, of 0.75 (▲) and 0.50 (■). The solid curves represent the theoretical average polymer composition, predicted by integrating the Skeist equation with regressed reactivity ratios of $r_H = 1.08$ and $r_D = 1.12$.

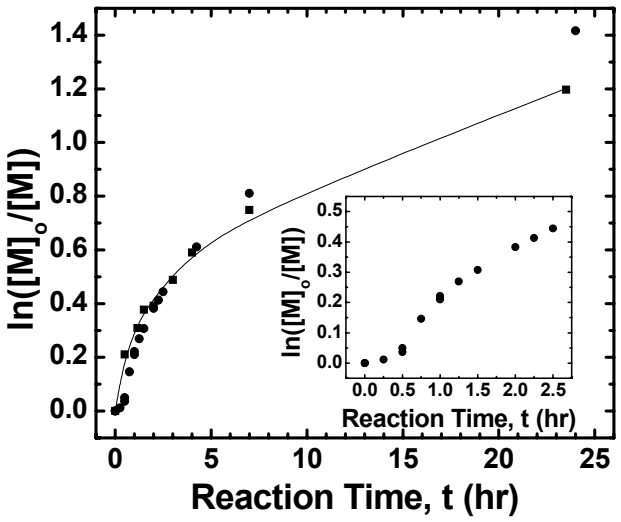

Figure 3.9. The kinetics of copolymerization of HEMA and DMAEMA at the azeotropic composition of $f_{D,o} = 0.28$ with EB*i*B as the initiator (■), and with a PS macroinitiator (●). Inset: polymerization kinetics with a PS macroinitiator at early times (< 3 h).

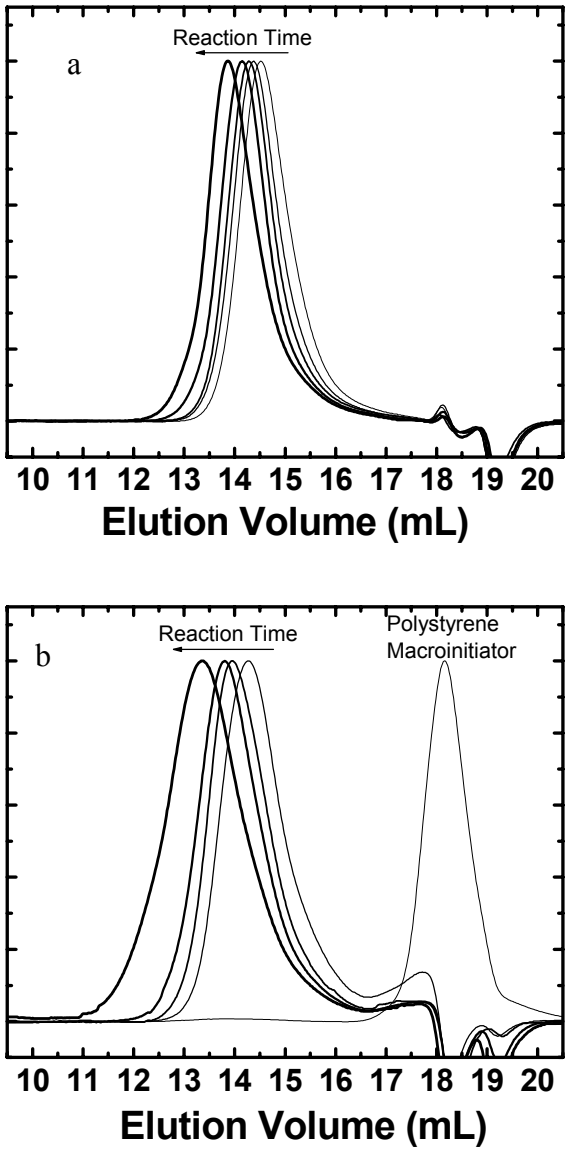

Figure 3.10. GPC traces with DMF (0.05M LiBr) as the eluent at 1 mL/min showing the time-dependent molecular weight distribution during copolymerizations of HEMA and DMAEMA in DMF at $f_{D,o} = 0.28$ that were initiated with (a) EB*i*B or (b) a PS macroinitiator. The GPC trace of the PS macroinitiator is labeled in (b).

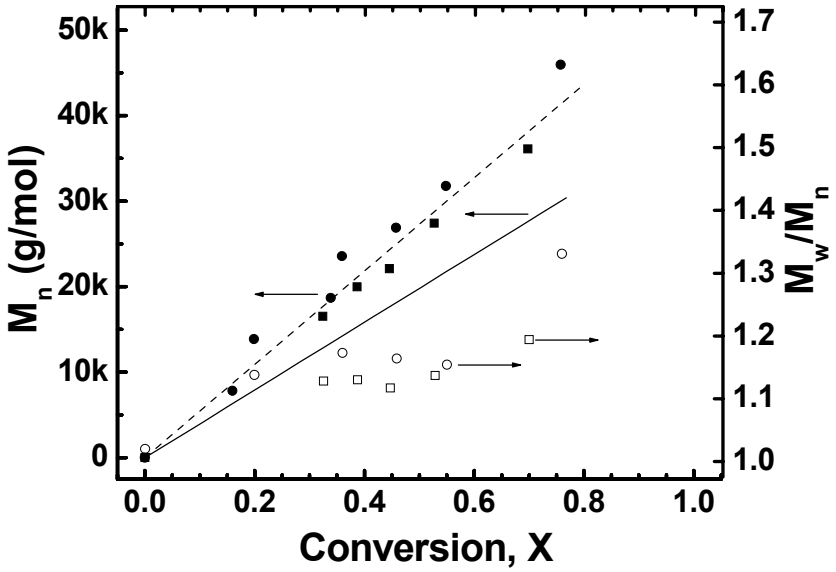

Figure 3.11. The molecular weight of PHD as a function of monomer conversion during the ATRP of HEMA and DMAEMA in DMF at $f_{D,o} = 0.28$ with EB*i*B as the initiator (■,□), and with a PS macroinitiator (●,○), and with a ratio of $[Cu^{I}]_o:[Cu^{II}]_o:[I]_o$ of 20:1:21. The absolute number-average molecular weight of PHD (M_n; ■,●) is plotted on the left axis, and the polydispersity (M_w/M_n; □,○) is plotted on the right axis. The dashed line represents a single fit through both sets of data while solid line represents the theoretical molecular weight given the initial total monomer to initiator ratio (300:1).

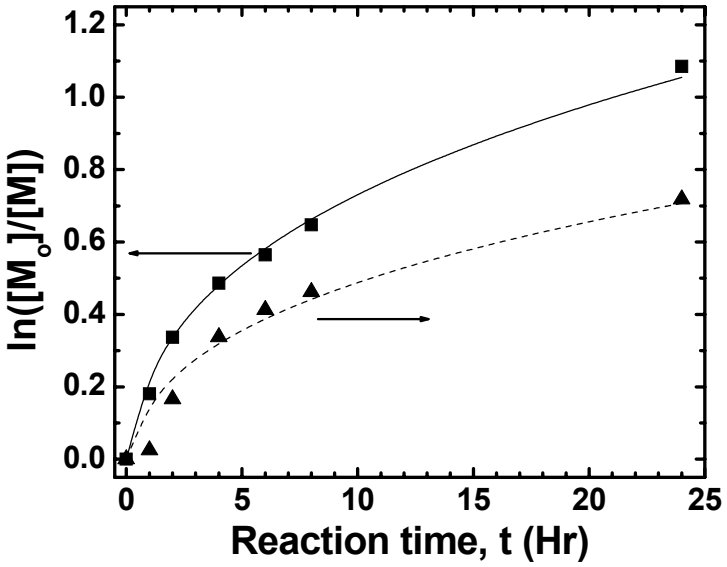

Figure 3.12. The kinetics of atom transfer radical copolymerization of HEMA and DMAEMA in DMSO with $f_{D,o} = 0.50$ (■) and with $f_{D,o} = 0.75$ (▲).

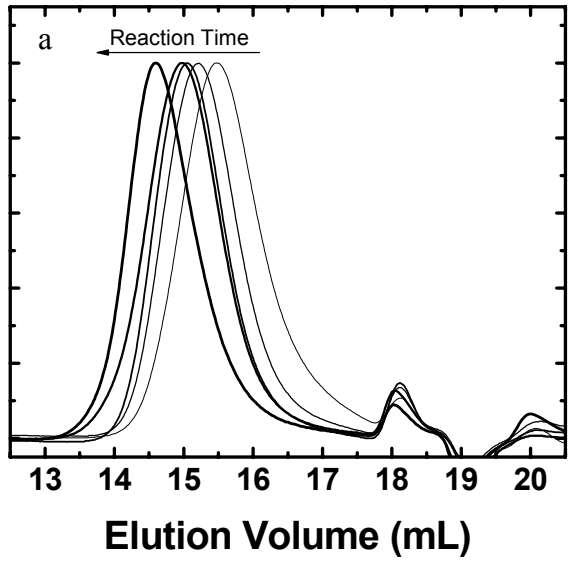

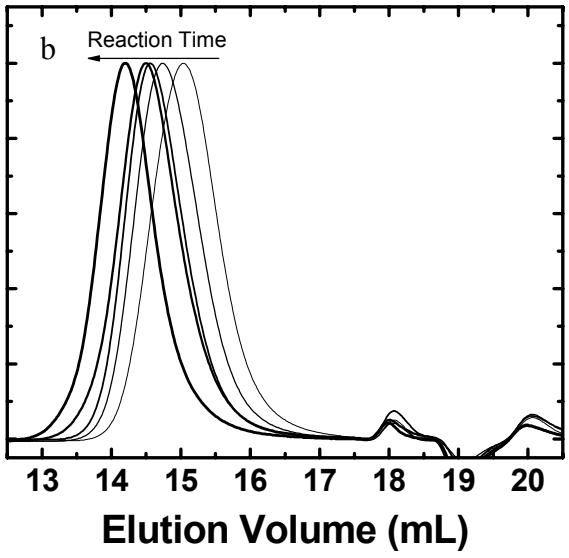

Figure 3.13. GPC traces with DMF (0.05M LiBr) as the eluent at 1 mL/min showing the time-dependent molecular weight distribution during copolymerizations of HEMA and DMAEMA in DMSO with (a) $f_{D,o} = 0.75$ (b) $f_{D,o} = 0.50$.

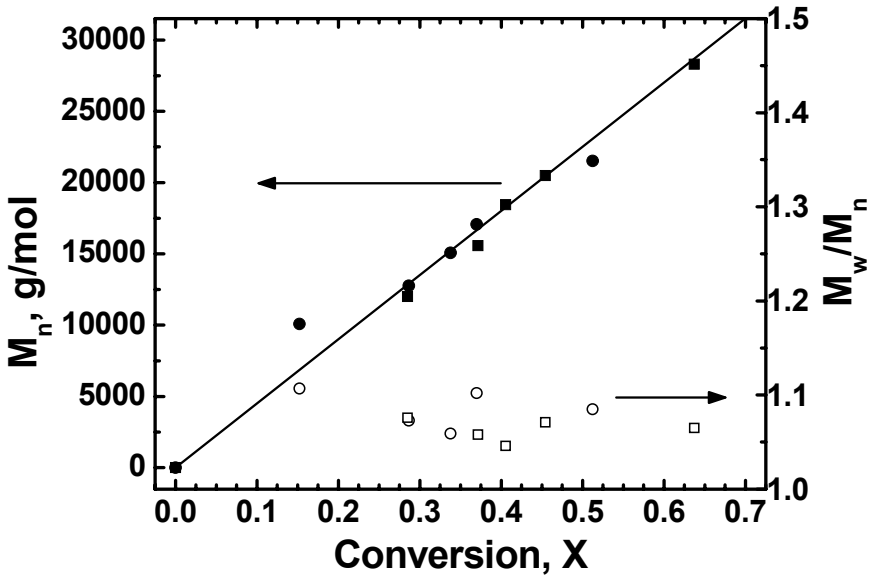

Figure 3.14. The molecular weight of PHD as a function of monomer conversion during ATRP in DMSO at molar monomer feed compositions $f_{D,o}$ of 0.75 (●,○) and $f_{D,o}$ = 0.50 (■,□), and with a ratio of $[Cu^I]_o$:$[Cu^{II}]_o$:$[I]_o$ of 1:12:10. The absolute number-average molecular weight (M_n; ■,●) is plotted on the left axis, and the overall molecular weight distribution (M_w/M_n; □,○) is plotted on the right axis. The solid line represents the theoretical molecular weight, as predicted from the initial total monomer to initiator ratio (300:1).

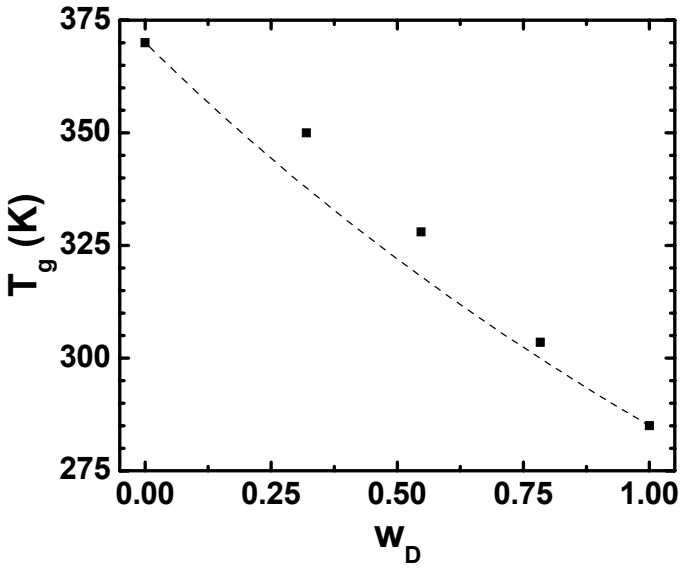

Figure 3.15. The glass transition temperatures of poly(HEMA), poly(DMAEMA), and PHD random copolymers. The dashed curve represents the Fox equation given the glass transition temperatures of the two homopolymers.

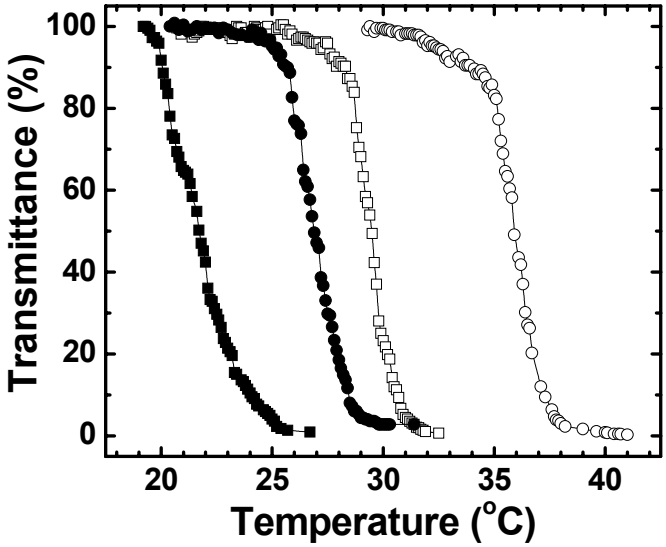

Figure 3.16. Solution behavior as a function of temperature for poly(DMAEMA) (○) and of PHD_{75}, (□), PHD_{63} (●), and PHD_{50} (■). LCSTs were extracted from the midpoint in the transmittance curves.

REFERENCES

1. Dong, L.; Agarwal, A. K.; Beebe, D. J.; Jiang, H. *Nature* **2006,** 442, 551-554.

2. Du, R.; Zhao, J. *Journal of Applied Polymer Science* **2004,** 91, 2721-2728.

3. Yilmaz, Z.; Akkas, P. K.; Sen, M.; Guven, O. *Journal of Applied Polymer Science* **2006,** 102, 6023-6027.

4. Kroupova, J.; Horak, D.; Pachernik, J.; Dvorak, P.; Slouf, M. *Journal of Biomedical Materials Research, Part B: Applied Biomaterials* **2006,** 76B, 315-325.

5. Satish, C. S.; Shivakumar, H. G. *Journal of Macromolecular Science, Part A: Pure and Applied Chemistry* **2007,** 44, 379-387.

6. Traitel, T.; Cohen, Y.; Kost, J. *Biomaterials* **2000,** 21, 1679-1687.

7. Brahim, S.; Narinesingh, D.; Guiseppi-Elie, A. *Biomacromolecules* **2003,** 4, 1224-1231.

8. Brahim, S.; Narinesingh, D.; Guiseppi-Elie, A. *Biomacromolecules* **2003,** 4, 497-503.

9. Fournier, D.; Hoogenboom, R.; Thijs, H. M. L.; Paulus, R. M.; Schubert, U. S. *Macromolecules* **2007,** 40, 915-920.

10. Van de Wetering, P.; Moret, E. E.; Schuurmans-Nieuwenbroek, N. M. E.; Van Steenbergen, M. J.; Hennink, W. E. *Bioconjugate Chemistry* **1999,** 10, 589-597.

11. Cho, S. H.; Jhon, M. S.; Yuk, S. H.; Lee, H. B. *Journal of Polymer Science, Part B: Polymer Physics* **1997,** 35, 595-598.

12. Liu, Q.; Yu, Z.; Ni, P. *Colloid and Polymer Science* **2004,** 282, 387-393.

13. Yuk, S. H.; Cho, S. H.; Lee, S. H. *Macromolecules* **1997,** 30, 6856-6859.

14. Krasia, T. C.; Patrickios, C. S. *Macromolecules* **2006,** 39, 2467-2473.

15. Sahnoun, M.; Charreyre, M.-T.; Veron, L.; Delair, T.; D'Agosto, F. *Journal of Polymer Science, Part A: Polymer Chemistry* **2005,** 43, 3551-3565.

16. Xiong, Q.; Ni, P.; Zhang, F.; Yu, Z. *Polymer Bulletin* **2004,** 53, 1-8.

17. Monge, S.; Darcos, V.; Haddleton, D. M. *Journal of Polymer Science, Part A: Polymer Chemistry* **2004,** 42, 6299-6308.

18. Jin, X.; Shen, Y.; Zhu, S. *Macromolecular Materials and Engineering* **2003,** 288, 925-935.

19. Lee, S. B.; Russell, A. J.; Matyjaszewski, K. *Biomacromolecules* **2003,** 4, 1386-1393.

20. Zhang, X.; Xia, J.; Matyjaszewski, K. *Macromolecules* **1998,** 31, 5167-5169.

21. Kwok, A. Y.; Qiao, G. G.; Solomon, D. H. *Polymer* **2004,** 45, 4017-4027.

22. Traitel, T.; Kost, J.; Lapidot, S. A. *Biotechnology and Bioengineering* **2003,** 84, 20-28.

23. Triftaridou, A. I.; Hadjiyannakou, S. C.; Vamvakaki, M.; Patrickios, C. S. *Macromolecules* **2002,** 35, 2506-2513.

24. Martin-Gomis, L.; Cuervo-Rodriguez, R.; Fernandez-Monreal, M. C.; Madruga, E. L.; Fernandez-Garcia, M. *Journal of Polymer Science, Part A: Polymer Chemistry* **2003,** 41, 2659-2666.

25. Mathew-Krotz, J.; Mahadevan, V. *Macromolecular Chemistry and Physics* **1997,** 198, 1597-1604.

26. Skeist, I. *Journal of the American Chemical Society* **1946,** 68, 1781-1784.

27. Coote, M. L.; Davis, T. P., Copolymerization Kinetics. In *Handbook of Radical Polymerization*, Matyjaszewski, K.; Davis, T. P., Eds. Wiley-Interscience: New York, 2002; pp 263-300.

28. Cowie, J. M. G.; McEwen, I. J.; Yule, D. J. *European Polymer Journal* **2000,** 36, 1795-1803.

29. Klumperman, B.; O'Driscoll, K. F. *Polymer* **1993,** 34, 1032-1037.

30. Klumperman, B.; Kraeger, I. R. *Macromolecules* **1994,** 27, 1529-1534.

31. Fernandez-Monreal, C.; Martinez, G.; Sanchez-Chaves, M.; Madruga, E. L. *Journal of Polymer Science, Part A: Polymer Chemistry* **2001,** 39, 2043-2048.

32. Tidwell, P. W.; Mortimer, G. A. *Journal of Polymer Science, Part A: General Papers* **1965,** 3, 369-387.

33. Czerwinski, W. K. *Polymer* **1997,** 39, 183-187.

34. Fineman, M.; Ross, S. D. *Journal of Polymer Science* **1950,** 5, 259-262.

35. Kelen, T.; Tudos, F. *Journal of Macromolecular Science, Chemistry* **1975,** A9, 1-27.

36. Caykara, T.; Ozyurek, C.; Kantoglu, O.; Guven, O. *Journal of Polymer Science, Part B: Polymer Physics* **2002,** 40, 1995-2003.

37. Polymer Handbook, 4th Ed. In Brandrup, J.; Immergut, E. H.; Grulke, E. A., Eds. Wiley-Interscience: New York, 1999, VI-203.

38. Young, R. J.; Lovell, P. A., *Introduction to Polymers*. 2nd ed.; Chapman & Hall: London, 1991.

39. Matyjaszewski, K.; Shipp, D. A.; Wang, J.-L.; Grimaud, T.; Patten, T. E. *Macromolecules* **1998,** 31, 6836-6840.

40. Schellekens, M. A. J.; de Wit, F.; Klumperman, B. *Macromolecules* **2001,** 34, 7961-7966.

41. Wang, T.-L.; Liu, Y.-Z.; Jeng, B.-C.; Cai, Y.-C. *Journal of Polymer Research* **2005,** 12, 67-75.

42. Matyjaszewski, K.; Xia, J. *Chemical Reviews* **2001,** 101, 2921-2990.

43. Matyjaszewski, K.; Patten, T. E.; Xia, J. *Journal of the American Chemical Society* **1997,** 119, 674-680.

44. Fischer, H. *Journal of Polymer Science, Part A: Polymer Chemistry* **1999,** 37, 1885-1901.

45. Zhang, H.; Klumperman, B.; Ming, W.; Fischer, H.; van der Linde, R. *Macromolecules* **2001,** 34, 6169-6173.

46. Snijder, A.; Klumperman, B.; van der Linde, R. *Macromolecules* **2002,** 35, 4785-4790.

47. Even, M.; Haddleton, D. M.; Kukulj, D. *European Polymer Journal* **2003,** 39, 633-639.

48. Miller, P. J.; Matyjaszewski, K. *Macromolecules* **1999,** 32, 8760-8767.

49. Dias, M. L.; Mano, E. B.; Azuma, C. *European Polymer Journal* **1997,** 33, 559-564.

50. Dubin, P. L.; Koontz, S.; Wright, K. L., III. *Journal of Polymer Science, Polymer Chemistry Edition* **1977,** 15, 2047-2057.

51. Weaver, J. V. M.; Bannister, I.; Robinson, K. L.; Bories-Azeau, X.; Armes, S. P.; Smallridge, M.; McKenna, P. *Macromolecules* **2004,** 37, 2395-2403.

52. Odian, G., *Principles of Polymerization*. 4th ed.; Wiley-Interscience: New York, 2004.

53. Fox, T. G. *Bulletin of the American Physical Society* **1956,** 1, 123.

54. Park, S. Y.; Cho, S. H.; Yuk, S. H.; Jhon, M. S. *European Polymer Journal* **2001,** 37, 1785-1790.

55. Mori, H.; Wakisaka, O.; Hirao, A.; Nakahama, S. *Macromolecular Chemistry and Physics* **1994,** 195, 3213-24.

Chapter 4. Synthesis and characterization of block copolymers containing PHD statistical copolymers

INTRODUCTION

Many applications for DMAEMA-containing polymers, such as lenses,[1] nanofiltration systems,[2,3] tissue scaffolds,[4] and drug delivery systems,[5,6,7,8] require that the polymer is constrained into a crosslinked hydrogel network to prevent solubilization. The most common synthetic method to achieve crosslinked hydrogel networks involves the polymerization of comonomers in the presence of a multifunctional crosslinker.[8] This method results in the formation of chemical crosslinks during the polymerization, thus stabilizing the macroscopic network during subsequent swelling. While this technique is relatively easy to implement, the synthetic simplicity necessarily limits the ability to fabricate designer materials. Further, one of the primary drawbacks of this technique is that the resulting hydrogel is difficult to characterize, so characteristics, such as molecular weight, molecular weight distribution, and polymer composition are unknown.[9] Moreover, crosslinking reactions in traditional hydrogels are generally uncontrolled, leading to significant heterogeneities in crosslink distributions.[10-13] Taken together, the inherent compositional heterogeneities, which make traditional hydrogels difficult to characterize, make the generation of structure-property relationships for hydrogels challenging.[14-16]

An alternative route to the design of hydrogels involves the use of an amphiphilic block copolymers, wherein hydrophobic blocks are incorporated in order to anchor the swelling of hydrophilic polymers, thus rendering the resulting hydrogel insoluble in aqueous environments.[9,17,18,19,20] Upon microphase separation, hydrophobic microdomains can act as physical crosslinks during the swelling of hydrophilic segments.

As a result, amphiphilic block copolymers do not need to be chemically crosslinked. Accordingly, the polymers can be redissolved in a common solvent and characterized at any point in the investigation. In addition, the molecular weight and molecular weight distribution of the swellable component (i.e., the hydrophilic block in amphiphilic block copolymers) can be directly related to the physical characteristics of the final hydrogel (e.g., molecular weight between crosslinks, crosslink distribution), which enables the direct design of hydrogels with specific physical characteristics.[9,17,18,19,20] Well-controlled amphiphilic block copolymers are therefore interesting candidates as model hydrogel systems.

As an added advantage, block copolymer microphase separation[21] can be utilized to assemble amphiphilic block copolymers into well-ordered periodic nanoscale structures, such as alternating lamellae (L), hexagonally-packed cylinders (H), and body-centered cubic lattice of spheres (S), depending on the relative size of each block and the segregation strength.[22] As such, the block copolymer architecture provides a route to achieve structurally-organized model hydrogels.[23-27]

An understanding of the synthesis and characterization of amphiphilic block copolymers is necessary to the successful design of model amphiphilic block copolymer hydrogels. In this chapter, we extend our earlier investigation of PHD statistical copolymers to include amphiphilic block copolymers containing PHD statistical copolymers. Specifically, we discuss the synthetic approaches necessary to design of a variety of PHD-containing amphiphilic diblock and triblock copolymers. We also describe the chemical and structural characterization of the resulting materials. This work will form the basis for making PHD-containing model hydrogels that will be examined in subsequent chapters.

PHD-CONTAINING BLOCK COPOLYMERS WITH POLYSTYRENE.

In Chapter 3, we demonstrated that polystyrene, PS, which was first synthesized by ATRP, can be used as a macroinitiator to initiate the synthesis of PHD statistical copolymers in DMF, at the compositional azeotrope ($\overline{F_D}$ = F_D = 0.28). The resulting material from such sequential polymerization is a block copolymer of PS/PHD_{28}. After addition of HEMA and DMAEMA to the PS macroinitiator (M_n = 6.5 kg/mol, M_w/M_n = 1.02), the resulting GPC profiles shift to lower elution volumes (Figure 3.10b), thus confirming the addition of PHD to the PS macroinitiator. Given the absolute molecular weight of the PS macroinitiator, the number-average molecular weight of the PHD block can be determined from the polymer composition obtained by ^{1}H NMR. A sample ^{1}H NMR spectrum of PS/PHD_{28} is shown in Figure 4.1. Peak **A** (δ = 7.14 ppm, 6.69 ppm; 5H) is characteristic of the aromatic hydrogens of styrene. The molar composition of PS in the diblock copolymer is 0.240 based on the relative areas of peaks **A** (styrene) and **B** (both HEMA and DMAEMA, 2H). Given the molecular weight of the PS macroinitiator (M_n = 6.5 kg/mol by GPC), the molecular weight of the PHD_{28} block was determined to be 27 kg/mol. Integration of unique proton peaks for HEMA and DMAEMA (see Figure 3.3) indicates that the PHD block has an average DMAEMA composition of $\overline{F_D}$ = 0.287 mol%, which is consistent with the copolymerization of HEMA and DMAEMA at the compositional azeotrope in DMF.

We will henceforth refer to this block copolymer as PS/PHD_{28} 6.5/27, where PS is used to denote the presence of a polystyrene block, PHD_{28} denotes the PHD block having an average polymer composition of $\overline{F_D}$ = 0.28, and 6.5 and 27 denote the number-average molecular weights of the PS and PHD_{28} blocks, in kg/mol, respectively. All block copolymers discussed in this thesis will be labeled in a similar fashion. The

polymer characteristics for each of the PHD-containing block copolymer described in this chapter are included in Table 4.1.

We used the same PS macroinitiator to synthesize PS/PHD_{28} 6.5/16, and we used a slightly larger PS macroinitiator (M_n = 6.8 kg/mol, M_w/M_n = 1.05) to synthesize PS/PHD_{28} 6.8/5.8 and PS/PHD_{28} 6.8/27.

PS and PHD are expected to phase separate due to large differences in chemical structures and solubility parameters of the two blocks.[28,29] We chose to assess the solid-state morphologies of two PS/PHD_{28} diblock copolymers, PS/PHD_{28} 6.5/16 and PS/PHD_{28} 6.5/27. PS/PHD_{28} films were cast from solutions of both THF and DMF (0.2 mg/mL) in Teflon dishes, and the solvent was allowed to slowly evaporate under a partially covered Petri dish. Because of its high volatility, THF generally evaporated over the course of 24 hr while DMF (with a higher boiling temperature of 153 ^oC) evaporated over ≈ 6 days. The films were then peeled from the casting dish and dried in a vacuum oven at 40 ^oC for an additional 24 hr. The average film thickness is 0.40 ± 0.05 mm. We calculated the volume fractions of the block copolymers using a published PS density[30] of 1.05 g/cm^3. Separately, we determined the density of PHD_{28}, using a pycnometer with cyclohexane as the nonsolvent, to be 1.20 ± 0.01 g/cm^3, according to ASTM D153-84, Method C.[31] The volume fraction of the PHD_{28} block, v_{PHD}, is reported for each block copolymer in Table 4.1.

SAXS traces for PS/PHD_{28} 6.5/16 (v_{PHD} = 0.688) cast from DMF, and from THF are shown in Figure 4.2a and Figure 4.2b, respectively. In Figure 4.2a, we observe an intense primary peak, followed by a broad bump at approximately q = 0.6 nm^{-1} in the SAXS profile. Given the volume fraction of PS/PHD_{28} 6.5/16 (v_{PHD} = 0.688), we expect this sample to adopt a hexagonally-packed cylindrical morphology (H, with PS cylinders). Accordingly, we placed markers (▼) at q/q* ratios of 1, √3, √4, and √7 for

comparison. The higher-order bump corresponds to $q/q^* = \sqrt{4}$ of the H morphology.[32] For completeness, we have also plotted the form factor curve (dashed line).[33] Since the first form factor minimum coincides with $q/q^* = \sqrt{3}$, the structure factor peak corresponding to this higher-order reflection is suppressed in the overall SAXS trace. Given the primary peak location ($q^* = 0.309$ nm^{-1}) and the volume fraction, we calculated the spacing between the (10) planes to be 20.4 nm and an average cylindrical radius of 6.9 nm. The SAXS trace from the THF-cast film of PS/PHD$_{28}$ 6.5/16 (Figure 4.2b) also shows a narrow and intense primary peak, but with characteristic peaks at $q/q^* = 2, 4, 5$, indicating an alternating lamellar (L) morphology instead of the H morphology.[32] The form factor curve corresponding to L with $v_{PHD} = 0.688$ is provided (dashed line).[33] The third-order reflection is suppressed in this case due to its coincidence with a form factor minimum. Based on the primary peak position ($q^* = 0.226$ nm^{-1}), we estimate the characteristic spacing to be 27.8 nm. Additionally, we note a broader and less intense peak at $q/q^* = \sqrt{7}$, which we indicate in Figure 4.2b with a *. While the $\sqrt{7}$ reflection should not be observed in L, it is characteristic of H.[32] We therefore suspect a coexistence of L and H in this cast film. Yet, the peak at $q/q^* = \sqrt{3}$ ($q = 0.391$ nm^{-1}), also characteristic of H, is absent. Given how narrow the primary peak is ($W_{0.5} = 0.038$ nm^{-1}, where $W_{0.5}$ is the width of the peak at half of its maximum intensity), the lamellae and cylinders, if present, must share the same characteristic spacing, or the same q*. That L and H phases share the same characteristic spacing due to epitaxial phase transformation has previously been reported.[34] We calculated the form factor curve based on the same q* assuming a H morphology.[33] The first minimum in the cylinder form factor curve occurs at $q = 0.407$ nm^{-1}, which is likely the reason why the $\sqrt{3}$ reflection of the H morphology is not observed. Since this specimen has not been thermally annealed above the glass transition temperatures of either of the blocks, the

solid-state morphology is a reflection of the casting conditions. We are therefore not surprised to see coexistence of two neighboring phases in our specimen. We are also not surprised to see differences in morphologies from the two different castings. In fact, the difference in morphologies (H versus L) due to changes in the solvent quality (DMF versus THF) is entirely consistent with solubility parameter arguments. Published solubility parameters, δ_{DMF} = 12.1 $(cal/cm^3)^{1/2}$;[30] δ_{THF} = 9.1 $(cal/cm^3)^{1/2}$;[30] δ_{PS} = 9.0 $(cal/cm^3)^{1/2}$;[28] δ_{PHEMA} = 13.2 $(cal/cm^3)^{1/2}$,[29] indicate that THF is a better solvent for PS than DMF and that DMF is a better solvent for poly(HEMA) compared with THF. Exact comparison with PHD_{28} is difficult because the solubility parameter of the copolymer is not known. As such, the volume occupied by the PS block must be greater when PS/PHD_{28} 6.5/16 is cast from THF compared to DMF.

SAXS traces for PS/PHD_{28} 6.5/27 (v_{PHD} = 0.784) are shown in Figures 4.3a and 4.3b. Figure 4.3a shows the SAXS trace that was acquired on a DMF-cast film, while Figure 4.3b shows the trace acquired on a THF-cast film. The SAXS trace acquired on the DMF-cast film shows a narrow and intense peak followed by a shoulder at $q/q^* = \sqrt{2}$ indicating that PS/PHD_{28} 6.5/27 adopts the a body-centered cubic (BCC) spherical morphology (S).[32] The form factor[33] curve for individual, isolated spheres is also plotted (dashed line). The higher-order structure factor peak at $q/q^* = \sqrt{3}$ is absent because it coincides with a form factor minimum. We also observe a broad bump in the overall SAXS trace between 0.65 – 0.9 nm^{-1} that corresponds to a maximum in the form factor curve. Given the primary peak position (q^* = 0.338 nm^{-1}) and the volume fraction (v_{PHD} = 0.784), we estimate the spacing between (100) planes in the BCC lattice to be 18.6 nm, and an average spherical radius of 7.8 nm. The SAXS trace acquired on the THF-cast film, on the other hand, shows a primary peak and a higher-order peak at $q/q^* = \sqrt{3}$ that is characteristic of the H morphology. The form factor[33] curve for isolated cylinders is

plotted (dashed line); the minima and maxima appear to correspond well with the overall SAXS trace. The primary peak position is q* = 0.247 nm^{-1}, indicating a characteristic spacing of 25.5 nm, with an average cylindrical radius of 7.2 nm. Consistent with PS/PHD_{28} 6.5/16, we observe a shift in the solid-state morphology of PS/PHD_{28} 6.5/27 with different solvents. A similar dependence of the solid-state morphology on the choice of casting solvent has also been previously observed by transmission electron microscopy for PS/poly(HEMA) block copolymers.[35] In that work, the authors suggest that DMF preferentially solvates the poly(HEMA) block, producing structures outside the predicted morphology. We note, however, that DMF castings of both block copolymers produce morphologies that are closer to the expected equilibrium structure predicted by the mean-field theory given the actual volume fractions.[22] To ascertain the equilibrium morphologies for these block copolymers, high-temperature annealing above the glass transition temperatures of both blocks ($T_{g,PS}$[30] = 105°C, $T_{g,PHD28}$[27] = 77°C) is undoubtedly necessary. Our attempts to reach thermal equilibrium, however, were limited by transesterification side reactions that crosslinked the PHD block.[36, 37]

Taken together, the SAXS data collected from the different castings of PS/PHD_{28} 6.5/16 and PS/PHD_{28} 6.5/27 suggest that block copolymers containing PS and PHD_{28} readily microphase separate into well-ordered nanostructures in the solid state. The solid-state structure depends on χN, the volume fraction of each block, and the casting conditions (i.e., solvent quality). The volume fraction can be controlled synthetically by adjusting the relative molecular weights of each block, and the casting conditions provide additional tunability in achieving structures other than that predicted by phase equilibria.

PHD-CONTAINING BLOCK COPOLYMERS WITH POLY(METHYL ACRYLATE).

The macroinitiation strategy that we utilized to synthesize PS/PHD_{28} diblock copolymers can also be used to synthesize a variety of PHD-containing amphiphilic block

copolymers. For example, poly(methyl acrylate), PMA, a hydrophobic polymer with a low glass transition temperature ($T_{g,PMA}$[38] = 12.5°C), can also be used as a macroinitiator to initiate the copolymerization of HEMA and DMAEMA. Moreover, because PMA is soluble in DMSO, it can be used to initiate the polymerizations of HEMA and DMAEMA statistical copolymers over a wide range of compositions. The synthesis of PMA macroinitiators and PMA/PHD diblock copolymers by ATRP resulted in well-controlled polymers with narrow molecular weight distributions. Figure 4.4 shows the GPC traces for a PMA macroinitiator (M_n = 13 kg/mol, M_w/M_n = 1.02; solid line) and PMA/PHD_{75} 13/11 (dashed line). Both GPC traces are narrow and monomodal, and the GPC trace of the diblock copolymer is shifted to a lower elution volume from that of the macroinitiator, indicating an increase in molecular weight. The molecular weight of the PHD block in PMA/PHD_{75} 13/11 can be quantified using ^{1}H NMR (Figure 4.5, proton contributions labeled), given the absolute molecular weight of the PMA 13 macrointiator (M_n = 13 kg/mol). We calculated the molecular weight of the PHD block to be 11 kg/mol (v_{PHD} = 0.44). The composition of DMAEMA in the PHD block for this particular diblock copolymer, as determined by ^{1}H NMR (Figure 4.5), is 75.3 mol%. This composition of DMAEMA in the PHD_{75} block is the same as the monomer feed composition, which is expected for copolymerizations of HEMA and DMAEMA in DMSO given that both the monomer reactivity ratios are near unity.[27] We synthesized and characterized PMA/PHD_{63} 10/9.7, PMA/PHD_{50} 12/15, and PMA/PHD_{28} 8.0/13 in a similar manner. These block copolymers were synthesized with varying F_D of the PHD block, as denoted by the subscripts.

One-dimensional SAXS profiles of PMA/PHD_{75} 13/11, PMA/PHD_{63} 10/9.7, PMA/PHD_{50} 12/15, and PMA/PHD_{28} 8.0/13, collected at room temperature, are shown in Figures 4.6a-d. The SAXS profile of PMA/PHD_{75} 13/11 (Figure 4.6a) exhibits a narrow

and intense primary peak at q* = 0.290 nm^{-1} and higher-order reflections (▼) at q/q* ratios of 2 and 3, consistent with that of an alternating lamellar morphology.[32] The characteristic spacing of the lamellar microstructure is 21.7 nm.

The SAXS profiles of PMA/PHD_{63} 10/9.7 (Figure 4.6b), PMA/PHD_{50} 12/15 (Figure 4.6c), and PMA/PHD_{28} 8.0/13 (Figure 4.6d) exhibit primary peaks at q* = 0.393 nm^{-1}, 0.292 nm^{-1}, and 0.352 nm^{-1}, respectively. Given that the volume fractions of PHD are close to 0.5 (in Table 4.1), the PMA/PHD diblock copolymers examined in this study should all adopt an alternating lamellar morphology. With the exception of the SAXS profile of PMA/PHD_{75} (Figure 4.6a), however, the SAXS profiles of the other diblock copolymers (Figures 4.6b-d) do not exhibit any higher-order reflections. We attribute the absence of higher-order reflections in the SAXS profiles of PMA/PHD_{63} 10/9.7, PMA/PHD_{50} 12/15, and PMA/PHD_{28} 8.0/13 to two factors: that these block copolymers are not particularly strongly segregated and that the electron density contrast between PMA and PHD is low.

Visual inspection of PMA/PHD_{75} 13/11 and PMA/PHD_{63} 10/9.7 indicate that these diblock copolymers flow under their own weight above 110°C, suggesting that the ODTs of these block copolymers are near 110°C. To further qualify the segregation strength of PMA/PHD_{75} 13/11, we monitored the sample by SAXS during temperature ramp experiments. After each temperature ramp, the polymer sample was allowed to equilibrate for 30 min before SAXS was acquired. Figure 4.7a contains the SAXS profiles collected on PMA/PHD_{75} 13/11 during a temperature ramp experiment. The SAXS profile collected at 51°C exhibits a narrow and intense primary peak at q* = 0.295 nm^{-1} ($W_{0.5}$ = 0.057) with a higher-order reflection at q/q* = 2. With increasing temperature, the primary peak position in the SAXS profiles shifts to a larger q*, which is consistent with a decrease in χ with increasing temperature. Moreover, we observe a loss

of the second-order reflection and a significant broadening of the primary peak in the SAXS profiles acquired above 90°C. We quantified the broadening of the primary peak, in terms of $W_{0.5}$ in Figure 4.7b. The breadth of the primary peak at T = 105°C is approximately two times that of the primary peak collected at T = 85°C, which suggests that we were approaching the ODT for PMA/PHD_{75} 13/11 at T = 105°C.[39] By comparison, the ODT of a strongly-segregated lamellar block copolymer comprised of poly(pentafluorostyrene), PPFS, and poly(methyl methacrylate), PMMA, of similar molecular weight (PPFS/PMMA 8.5/14) was determined to be beyond the temperature range of our experimental setup (300°C).[39]

The observations made during temperature ramp experiments on PMA/PHD_{75} 13/11 are reversible. We observed a decrease in $W_{0.5}$, a reappearance of the second-order reflection, and a shift of the primary peak to smaller q with decreasing temperature. We caution, however, that we were only able to observe such reversibility when the temperature ramp experiments are kept below a threshold temperature of 110°C. We attribute this loss of reversibility upon further heating to transesterification side reactions that can crosslink the PHD block.[36,37]

We also performed temperature ramp experiments on PMA/PHD_{28} 8.0/13. The SAXS profiles collected during these temperature ramp experiments did not show any peak broadening below 110°C. The fact that we did not observe broadening in the primary peak for PMA/PHD_{75} 13/11 below the 110°C suggests that the segregation strength of PMA/PHD_{28} 8.0/13 is higher than that of PMA/PHD_{75} 13/11. We also observed notable peak broadening in the primary peak of PMA/PHD_{28} 8.0/13 near 150°C, which is suggestive of an ODT. However, we were unable to redissolve or even swell PMA/PHD_{28} 8.0/13 after the temperature ramp experiment, which suggests that PMA/PHD_{28} 8.0/13 had significantly crosslinked. As a consequence, quantification of

the segregation strength of our PMA/PHD diblock copolymers is not possible. Gomez et al. reported that crosslinking of structurally organized block copolymers results in an increase in the order-disorder temperature of the block copolymer.[40] Assuming that the results reported by Gomez are consistent with our system, the measured ODT near 150°C for PMA/PHD_{28} 8.0/13 represents an upper bound for the ODT of uncrosslinked PMA/PHD_{28} 8.0/13.

Several of our PMA/PHD diblock copolymers also do not exhibit higher-order reflections in their SAXS profiles because the electron density contrast between PMA and PHD is low. The electron density contrast between PMA and PHD also changes significantly with DMAEMA content. The change in electron density contrast with DMAEMA content can be seen by comparing the primary peak intensities of the individual SAXS profiles of the diblock copolymers (Figure 4.6a-d). While PMA/PHD_{75} 13/11 exhibits a narrow and intense primary peak above background, the primary peak intensities of PMA/PHD_{63} 10/9.7, PMA/PHD_{50} 12/15, and PMA/PHD_{28} 8.0/13 acquired for the same amount of time are significantly reduced, with the primary peak in the SAXS profile of PMA/PHD_{50} 12/15 being the weakest. Electron density calculations for the PMA and PHD blocks based on polymer densities (see Table 4.1) and chemical compositions of the PHD block are consistent with our observations. Specifically, PHD_{75} is more electron-rich than PMA; the ratio of the electron densities of PHD_{75} and PMA in PMA/PHD_{75} 13.2/10.6 is 1.044. The ratio of electron densities of PHD and PMA in PMA/PHD_{63} 10.0/9.7, PMA/PHD_{50} 12/15, and PMA/PHD_{28} 8.0/13 are 1.022, 1.005, and 0.9769, respectively. For reference, the same calculations carried out for PS/polyisoprene yield an electron density contrast of 1.121.[41] We thus believe that it is the combination of low segregation strength and weak electron density contrast in

PMA/PHD that has made morphological assessment of neat PMA/PHD_{63} 10/9.7, PMA/PHD_{50} 12/15, and PMA/PHD_{28} 8.0/13 by SAXS difficult.

PHD-CONTAINING BLOCK COPOLYMERS WITH POLY(*TERT*-BUTYL ACRYLATE).

We also used the macrointiation strategy to synthesize PHD-containing block copolymers from poly(*tert*-butyl acrylate), P*t*BA, macroinitiators. P*t*BA is a hydrophobic polymer that is glassy at room temperature, but its glass transition temperature is lower than that of PS. To quantify, we performed DSC on P*t*BA 15 (M_n = 15 kg/mol, M_w/M_n = 1.02). The second-heat DSC thermogram of PtBA is shown in Figure 4.9. The glass transition temperature of P*t*BA, extracted at the midpoint of the step change in heat capacity in the thermogram, is 41°C. Our interest in P*t*BA lies in the fact that it is a hydrophobic polymer with an accessible glass transition temperature below the temperature at which transesterification of PHD copolymers takes place.

Starting with a P*t*BA macroinitiator (M_n = 15 kg/mol, M_w/M_n = 1.02), we synthesized a PHD-containing block copolymer, P*t*BA/PHD_{28} 15/18, at the compositional azeotrope in DMF. GPC traces of P*t*BA/PHD_{28} 15/18 (dashed) and PtBA 15 (solid) are shown in Figure 4.10. The GPC traces of both P*t*BA 15 and P*t*BA/PHD_{28} 15/18 are narrow and monomodal, with P*t*BA/PHD_{28} 15/18 eluting at a lower elution volume than P*t*BA 15. Taken together, these findings suggest that P*t*BA is an effective macroinitiator for the synthesis of PHD_{28} in DMF. The ^{1}H NMR spectrum for P*t*BA/PHD_{28} 15/18 is shown in Figure 4.11. In addition to the peaks associated with PHD statistical copolymers, the ^{1}H NMR spectrum includes a sharp peak at ≈ 1.5 ppm, which is characteristic of the proton contributions of P*t*BA. Given the absolute molecular weight of PtBA 15, we determined the number-average molecular weight of the PHD_{28} block to be 18 kg/mol. P*t*BA/PHD_{28} 15/18 was solvent cast from THF and lightly annealed at 40°C, per previous experiments with PS/PHD_{28} diblock copolymers. The SAXS profile

of the cast sample exhibits a primary peak at q* = 0.208 nm^{-1}, and higher-order peaks at q/q* ratios of 2, 3, and 4 (Figure 4.12). The locations of the higher-order peaks are consistent with the L morphology,[32] with a characteristic spacing of 30.2 nm.

A similar macroinitiation strategy can be used to synthesize BAB triblock copolymers, where A represents a bifunctional macroinitiator and B represents the second block, grown simultaneously from both ends of A. To demonstrate this synthetic procedure, we first synthesized a P*t*BA macroinitatior (M_n = 16 kg/mol, M_w/M_n = 1.05) starting with the bifunctional initiator, 2Me2BrC7D. We then used the purified P*t*BA 16 to initiate the polymerization of PHD_{28} in DMF, resulting in PHD_{28}/P*t*BA/PHD_{28} 8.5/16.1/8.5. GPC traces of P*t*BA 16 (solid) and PHD_{28}/P*t*BA/PHD_{28} 8.5/16.1/8.5 (dashed) are shown in Figure 4.13. Both GPC traces are narrow and monomodal. As in previous cases, the block copolymer elutes at an earlier elution volume than that of the P*t*BA macroinitiator, indicating an increase in molecular weight. The triblock copolymer was solvent cast from THF and lightly annealed. The cast sample exhibits an alternating lamellar morphology,[32] with a SAXS primary peak at q* = 0.265 nm^{-1} and higher order peaks at q/q* ratios of 2, 3, and 4 (Figure 4.14). The characteristic lamellar spacing within PHD_{28}/P*t*BA/PHD_{28} 8.5/16.1/8.5 is 23.7 nm.

As our discussion of P*t*BA/PHD_{28} 15/18 and PHD_{28}/P*t*BA/PHD_{28} 8.5/16/8.5 suggests, the same macroinitiation strategy used to synthesize PS/PHD_{28} diblock copolymers can be used to produce different block copolymers. Moreover, the range of block copolymers that can be produced in this fashion are not limited to diblock copolymers.

PHD-CONTAINING BLOCK COPOLYMERS WITH POLY(E-CAPROLACTONE).

The general ATRP strategy to create block copolymers with a macroinitiator is not limited to macrointiators that were synthesized by ATRP. In fact, our laboratory has

considered the combination of ring-opening polymerization (ROP) and ATRP, by converting a polymer that has been synthesized by ROP into an ATRP macroinitiator.[42] For example, polymerization of ε-caprolactone can be carried out by ROP to produce a poly(ε-caprolactone), PCL,[43, 44] which can be hydroxyl-functionalized upon exposure to acid and then further functionalized into a bromine-terminated PCL macroinitiator for ATRP.[42,43, 44] The synthesis of PCL was carried out in our laboratory by Dr. Sally Peng Li. PCL is a hydrophobic, semicrystalline polymer with a low glass transition temperature ($T_g \approx$ -60°C) and with a melting temperature (T_m) near 60°C.[45] To demonstrate the versatility of ATRP, we successfully synthesized PHD_{28} in DMF using a 9.0 kg/mol PCL macroinitiator (M_w/M_n = 1.06), resulting in PCL/PHD_{28} 9.0/18. GPC traces of PCL 9.0 and of PCL/PHD_{28} 9.0/18 are shown in Figure 4.15. The traces are both narrow and monomodal, and there is a clear shift to lower elution volumes for the diblock copolymer, indicating an increase in molecular weight. The ^{1}H NMR spectrum for PCL/PHD_{28} 9.0/18 is shown in Figure 4.16, and proton contributions from PCL and PHD_{28} are labeled. Given the absolute molecular weight of PCL 9.0 (Mn = 9.0 kg/mol), the molecular weight of the PHD_{28} block was determined to be 18 kg/mol.

PCL/PHD_{28} 9.0/18 was solvent cast from THF and annealed in the vacuum oven at 80°C for 20 h to induce microphase separation. The SAXS profile of PCL/PHD_{28} 9.0/18 is shown in Figure 4.17. The SAXS profile exhibits a narrow primary peak at q* = 0.253 nm^{-1}, and higher-order peaks at the ratios q/q* = √3, √4, √7, and √13, consistent with the H morphology.[32] Given the volume fraction of PHD_{28} (v_{PHD} = 0.653), we expect PCL to occupy discrete cylinders within a PHD_{28} matrix, with an average cylindrical radius of 8.9 nm. We do not observe the presence of PCL crystals in the SAXS profile, which suggests that the crystallization temperature of PCL 9.0 is suppressed due to confinement within the cylindrical domains.[46] Accordingly, we also did not observe any

evidence melting or crystallization in PCL/PHD_{28} 9.0/18 by DSC, when the experiments were performed over the temperature range of 0°C to 90°C with a heating and cooling rate of 5°C/min. The T_m for PCL 9.0 was determined to be 52°C upon heating, whereas The T_c for PCL 9.0 was determined to be 24°C upon cooling, at a rate of 5°C/min. Loo et al. previously reported that confinement of the crystallizable block within discrete nanoscale microdomains can effectively suppress T_c by more than 40°C.[47] Given that PCL/PHD_{28} 9.0/18 has a glassy matrix ($T_{g,PHD28}$ = 77°C) above the T_m of PCL 9.0, if crystallization of PCL were to occur at all, it must occur within the confines of microdomains prescribed by microphase separation.

LIMITATIONS OF BLOCK COPOLYMER SYNTHESIS VIA ATRP.

The use of a macroinitiator to synthesize PHD-containing block copolymers by ATRP has been demonstrated with a variety of macroinitiators (e.g., PS, PMA, P*t*BA, PCL) at the compositional azeotrope in DMF. We also demonstrated that PMA can be used to initiate the polymerization of HEMA and DMAEMA at any composition in DMSO, in which the reactivity ratios of HEMA and DMAEMA are near unity.[27] In order to synthesize block copolymers using the macroinitiation strategy, it is necessary that the macroinitiator is soluble in the polymerization medium of the second monomer. While PMA is soluble in DMSO, PS, P*t*BA, and PCL are not. Consequently, the synthesis of PHD in DMSO from PS, P*t*BA, or PCL macroinitiators is not feasible. An alternate synthetic route involves first synthesizing PHD in DMSO and subsequently using it initiate the polymerization of the other block in a mutual solvent for both polymers. Unfortunately, the halide end-groups of poly(DMAEMA) or other nitrogen-containing polymers can be removed during polymer clean-up, resulting in an inability for PHD copolymers to initiate subsequent polymerizations.[48,49,50,51] We found that polymers with

hydroxyl side groups (e.g., hydroxyethyl acrylate or HEMA) are also not effective as macroinitiators, presumably for the same reason.

PHD-CONTAINING BLOCK COPOLYMERS BY RAFT.

One can overcome the technical challenges associated with ATRP synthesis of PHD-containing block copolymers by employing alternate polymerization techniques that do not rely on alkyl halides, such as RAFT. The chain transfer agents (CTAs) used in RAFT are less susceptible to attack (and loss) than alkyl halides, due to the fact that the leaving group of the CTA is more sterically hindered and is less polar than the terminal halide of the ATRP chain end. Notably, the synthesis of DMAEMA-containing block copolymers using RAFT has been demonstrated.[9,52,53]

We first carried out the polymerization of DMAEMA in isopropanol using a monofunctional CTA, CDB (see Chapter 2), which was provided by Dr. Brent Sumerlin at Southern Methodist University. The poly(DMAEMA) macro-CTA (PD 8.2, M_n = 8.2 kg/mol, M_w/M_n = 1.12) was subsequently used for the polymerization of HEMA, with AIBN as the initiator. The final number-average molecular weight of poly(HEMA) was determined by ^{1}H NMR to be 17 kg/mol, given the absolute M_n of PD 8.2. The final block copolymer is labeled PD/PH 8.2/17, where PD denotes poly(DMAEMA), PH denotes poly(HEMA), and 8.2 and 17 denote the number average molecular weights of the PD and PH blocks, in kg/mol, respectively. GPC traces of PD 8.2 and of PD/PH 8.2/17 (M_w/M_n = 1.09) are shown in Figure 4.18. Both peaks are narrow and monomodal, and there is a pronounced shift in elution volume between PD 8.2 and PD/PH 8.2/17, confirming the addition of HEMA to PD 8.2. We successfully synthesized a series of PD/PH block copolymers by RAFT. The characteristics of each of these block copolymers is presented in Table 4.2.

Previously, we were only able to synthesize PS/PHD$_{28}$ diblock copolymers by ATRP in DMF, due to the fact that PS macroinitiators are insoluble in DMSO. Using RAFT, we were able to synthesize PS/PHD diblock copolymers containing statistical PHD blocks with various DMAEMA contents. For example, PHD$_{75}$ 14 ($\overline{F_D}$ = 0.75; M_n = 14 kg/mol, M_w/M_n = 1.20) was synthesized in DMSO with CDB as the CTA and AIBN as the initiator. Subsequently, the polymer was purified (see Chapter 2 for details) and was used as the macro-CTA for the polymerization of styrene in DMF, resulting in PS/PHD$_{75}$ 6.7/14 (M_w/M_n = 1.13). GPC traces of the PHD$_{75}$ 14 (solid) and of PS/PHD$_{75}$ 6.7/14 (dashed) are shown in Figure 4.19. Both traces are narrow and monomodal. The GPC trace of the block copolymer is shifted to a lower elution volume than that of PHD$_{75}$ 14, but not to the same extent compared to other block copolymers of comparable molecular weights. The fact that the addition of PS to PHD$_{75}$ does not cause a pronounced shift in the GPC trace is consistent with the "salting out" of PS homopolymers that has been previously observed during GPC analysis performed in DMF with LiBr.[54] The microstructure of PS/PHD$_{75}$ 6.7/14 was investigated by SAXS after casting from THF. The SAXS profile (Figure 4.20) exhibits a narrow primary peak at q* = 0.211 nm^{-1}, with higher-order reflections (▼) at q/q* = 2 and 3. Given the SAXS trace and v_{PHD} = 0.633, we can establish that PS/PHD$_{75}$ 6.7/14 is organized as L,[32] with an interdomain spacing of 29.8 nm.

RAFT is also a useful technique for the synthesis of triblock copolymers with PHD midblocks, which we were previously unable to synthesize by ATRP due to the loss of halide functionalities from the PHD chain ends. To demonstrate the use of RAFT to synthesize these triblock copolymers, PHD$_{28}$ 16 ($\overline{F_D}$ = 0.28; M_n = 16 kg/mol, M_w/M_n = 1.15) was first synthesized using the bifunctional CTA, TBTPB, and was subsequently used as the macro-CTA for the polymerization of styrene, resulting in PS/PHD$_{28}$/PS

4.5/16/4.5 (M_w/M_n = 1.12). PS/PHD_{28}/PS 4.5/16/4.5 was solvent-cast from THF to induce microphase separation. The SAXS profile of PS/PHD_{28}/PS 4.5/16/4.5 is shown in Figure 4.21. The SAXS profile of PHD_{28}/PS/PHD_{28} 4.5/15.6/4.5 (Figure 4.16b) exhibits a primary peak at q* = 0.322 nm^{-1} and higher-order reflections (▼) at q/q* = 2, 3, and 4, which indicate that the sample adopts the alternating lamellar morphology,[32] with a 19.5 nm interdomain spacing. We also synthesized and characterized the lamella-forming triblock copolymer of PS/PHD_{75}/PS 5.9/20/5.9 in a similar fashion.

CONCLUSIONS

In this chapter, we demonstrated that a diverse collection of diblock and triblock copolymers containing compositionally uniform PHD statistical copolymers can be synthesized using controlled free-radical polymerization techniques. Specifically, we demonstrated that PS, P*t*BA, and PMA can be synthesized by ATRP and subsequently used as macroinitiators to initiate the copolymerization of HEMA and DMAEMA at their compositional azeotrope in DMF, or in the case of PMA, across the entire composition range in DMSO. ATRP macroinitiators need not be limited to polymers that are synthesized by ATRP, as we demonstrated with the synthesis of PCL/PHD_{28} 9.0/17.8, where PCL was first synthesized by ROP and subsequently converted into an ATRP macroinitiator for polymerization of HEMA and DMAEMA. Further, we demonstrated that bifunctional macroinitiators can be utilized to produce triblock copolymers. In cases in which the PHD block must be synthesized first, such as when the hydrophobic macroinitiator is not soluble in the required solvent (DMSO), we were unable to synthesize block copolymers by ATRP. This limitation is principally attributed to a loss of the active chain end from PHD copolymers during polymer clean-up. This limitation, however, can be overcome by selecting a different controlled free-radical polymerization scheme, as we have demonstrated with the RAFT polymerization a variety of PD/PH,

PS/PHD, and PS/PHD/PS block copolymers. Whether synthesis is carried out by ATRP or by RAFT, diblock and triblock copolymers containing compositionally uniform PHD microphase separate to form periodic nanoscale structures (lamellae, cylinders, or spheres), depending on the relative size of each block, the solvent quality, and χN.

The diblock and triblock copolymers that we have described in this chapter can are functional materials due to the inclusion of DMAEMA within the PHD block. The functionality of these materials can be tuned by synthetically altering the composition of the PHD block. The characteristics of these functional block copolymer structures can be further tuned by the judicious selection of the other block (e.g., PS or PMA), by the block copolymer architecture (e.g., diblock or triblock), as well as by the solid-state structure (e.g., L or H), which is controlled by the relative length of each block. When swollen with water, well-characterized PHD-containing amphiphilic block copolymers are thus model hydrogels with highly tunable environmental response.

TABLES

Table 4.1. The Physical Characteristics of PHD-containing Block Copolymers.

Name	M_n[a]	$M_{n,PHD}$	M_w/M_n	v_{PHD}[c]	F_D[d]	Solid-State Structure[e]	d (nm)[f]
PS/PHD_{28} 6.5/27	6.5[b]	27	1.16	0.784	0.283	H^{ii}	25.5
						S^{ii}	18.6
PS/PHD_{28} 6.5/16	6.5[b]	16	1.14	0.688	0.287	L^{i}	27.8
						H^{ii}	20.4
PS/PHD_{28} 6.8/5.8	6.8[b]	5.8	1.16	0.427	0.281	L^{i}	18.1
PS/PHD_{28} 6.8/27	6.8[b]	27	1.14	0.775	0.280	H^{i}	25.3
PS/PHD_{50} 5.4/9.8	5.4	9.8[b]	1.10	0.608	0.504	L^{i}	26.6
PS/PHD_{75} 6.7/14	6.7	14[b]	1.13	0.633	0.748	L^{i}	29.8
PS/PHD_{28}/PS 4.5/16/4.5	4.5	15[b]	1.12	0.605	0.281	L^{i}	19.5
PS/PHD_{75}/PS 5.9/20/5.9	5.9	20[b]	1.19	0.584	0.751	L^{i}	25.7
P*t*BA/PHD_{28} 15/18	15[b]	18	1.12	0.476	0.279	L^{i}	30.2
PHD_{28}/P*t*BA/PHD_{28} 8.5/16/8.5	16[b]	8.5	1.07	0.451	0.276	L^{i}	23.7
PCL/PHD_{28} 9.0/18	9.0[b]	18	1.11	0.653	0.278	H^{i}	24.8
PMA/PHD_{75} 13/11	13[b]	11	1.10	0.440	0.753	L^{iii}	21.7
PMA/PHD_{63} 10/9.7	10[b]	9.7	1.07	0.491	0.633	L^{iii}	16.0
PMA/PHD_{50} 12/15	12[b]	15	1.11	0.556	0.500	L^{iv}	21.5
PMA/PHD_{28} 8.0/13	8.0[b]	13	1.15	0.610	0.279	L^{iv}	17.8

[a]Denotes the molecular weight of the block that is not PHD.
[b]Indicates the first block. Block copolymers with PHD as the first block were synthesized by RAFT. All other block copolymers were synthesized by ATRP.
[c]Volume fraction of PHD; calculated using molar compositions from ^{1}H NMR and polymer densities of ρ_{PHD75}[38] = 1.27 g/cm^3, ρ_{PHD63}[38] = 1.25 g/cm^3, ρ_{PHD50}[38] = 1.21 g/cm^3, ρ_{PHD28}[26] = 1.20 g/cm^3, ρ_{PMA}[38] = 1.24 g/cm^3, ρ_{PtBA} = 0.93 g/cm^3, ρ_{PCL}[30] = 1.09 g/cm^3 (amorphous), and ρ_{PS}[30] = 1.05 g/cm^3. Polymer densities were determined using a pycnometer according to ASTM D153-84[31] with cyclohexanes as nonsolvent.
[d]Mole fraction of DMAEMA within PHD.
[e]Determined by SAXS, after [i]casting from THF, [ii]casting from DMF, or thermally annealed at [iii]90°C or [iv]110°C.
[f]$d = 2\pi/q^*$.

Table 4.2. The Physical Characteristics of PD/PH Block Copolymers.

Name	$M_{n,PD}$	$M_{n,PH}$	M_w/M_n	F_D [b]
PD/PH 25/5.2	25 [a]	5.2	1.27	0.800
PD/PH 25/13	25 [a]	13	1.29	0.617
PD/PH 8.2/17	8.2 [a]	17	1.09	0.288
PD/PH 29/36	29	36 [a]	1.21	0.508

[a]Indicates the first block.
[b]Mole fraction of DMAEMA within PD/PH.

FIGURES

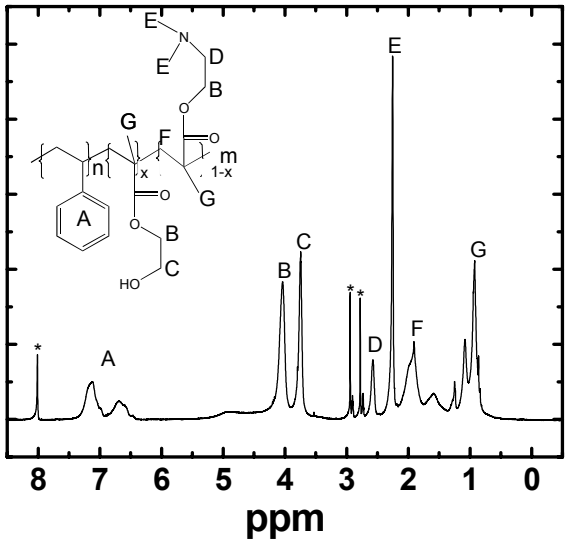

Figure 4.1. ^{1}H NMR spectrum of PS/PHD$_{28}$ 6.5/27 in deuterated DMF. The proton contributions are labeled for clarity. * indicates solvent (d-DMF) peaks.

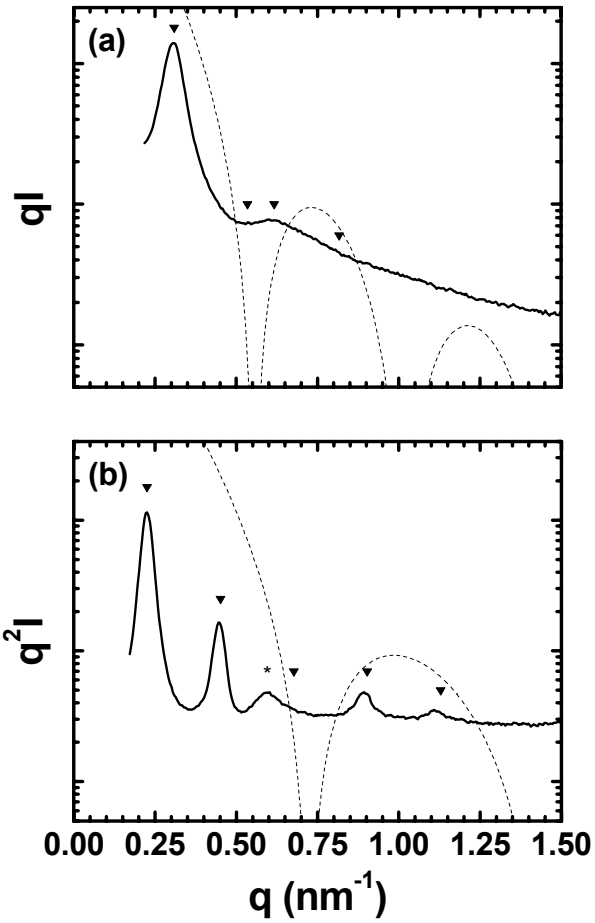

Figure 4.2. Small-angle x-ray scattering profiles of PS/PHD$_{28}$ 6.5/16 cast from (a) DMF and (b) THF. In (a), the primary peak position, q*, is 0.309 nm^{-1}, and markers (▼) are placed at q/q* ratios of 1, √3, √4, and √7. The form factor curve[33] for isolated cylinders of radius 6.9 nm is also shown (dashed curve). In (b), the primary peak position, q*, is 0.226 nm^{-1}, markers (▼) are placed at q/q* ratios of 1, 2, 3, 4, 5, and an additional marker (*) is placed at q/q* = √7. The form factor curve[33] for isolated lamellae of thickness 8.6 nm is also shown (dashed curve).

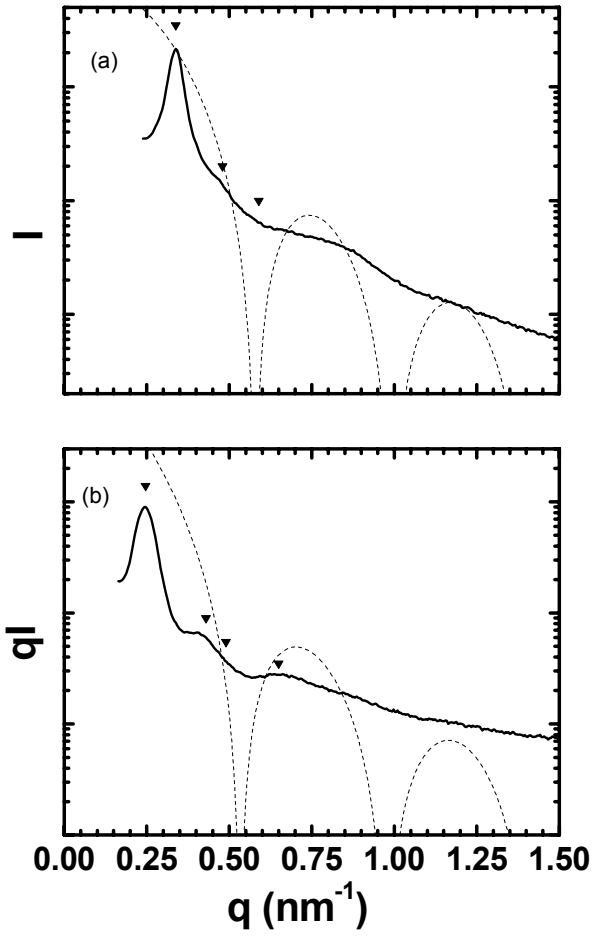

Figure 4.3. Small-angle x-ray scattering profiles of PS/PHD$_{28}$ 6.5/27 cast from (a) DMF and (b) THF. In (a), the primary peak position, q*, is 0.338 nm^{-1}, and markers (▼) are placed at q/q* ratios of 1, √2, √3. The form factor curve[33] for isolated spheres of radius 7.8 nm is also shown (dashed curve). In (b), the primary peak position, q*, is 0.247 nm^{-1}, and markers (▼) are placed at q/q* ratios of 1, √3, √4, √7. The form factor curve[33] for isolated lamellae of thickness 7.2 nm is also shown (dashed curve).

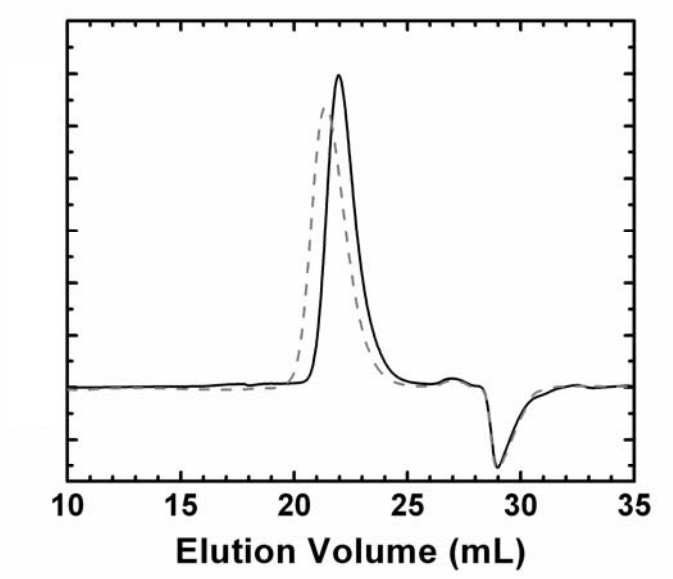

Figure 4.4. Gel permeation chromatography traces with DMF (+ 0.01M LiBr) as the eluent at 1 mL/min of PMA 13 (solid line, $M_w/M_n = 1.02$) and PMA/PHD_{75} 13/11 (dashed line, $M_w/M_n = 1.10$).

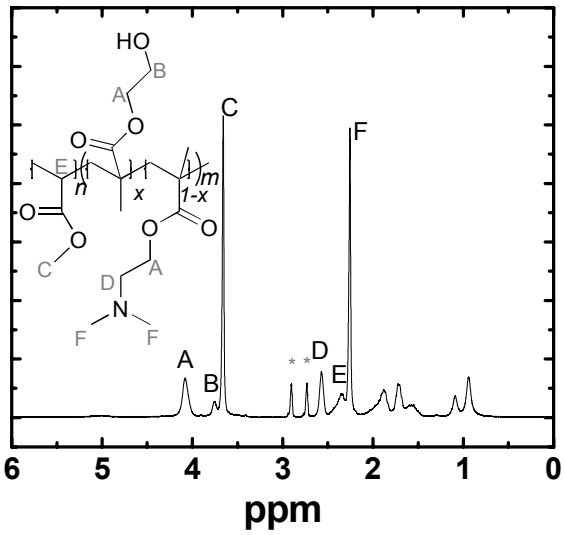

Figure 4.5. ^{1}H NMR spectrum of PMA/PHD$_{75}$ 13/11 in deuterated DMF. The proton contributions are labeled for clarity. * indicates solvent (d-DMF) peaks.

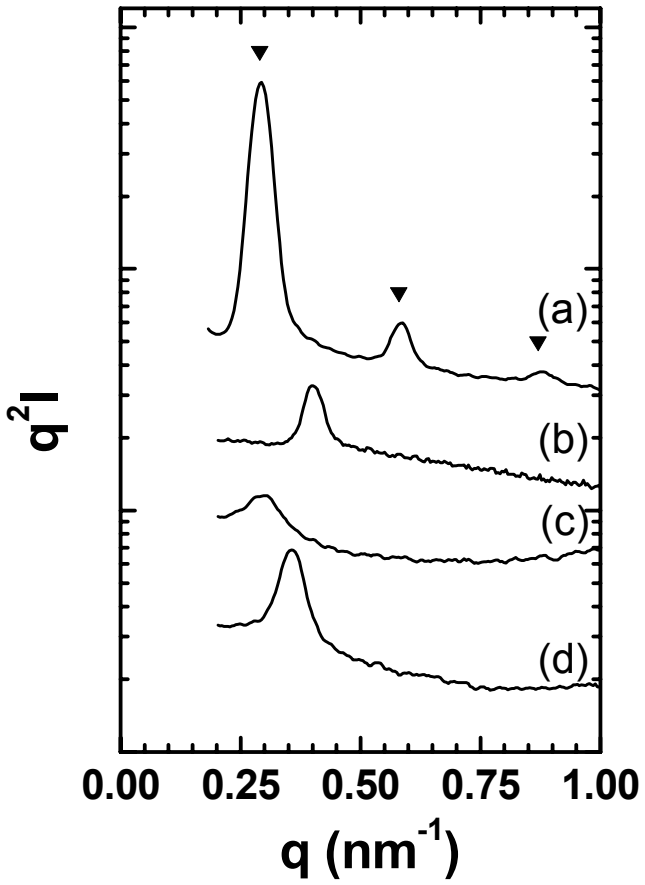

Figure 4.6. Small-angle x-ray scattering profiles of (a) PMA/PHD_{75} 13/11, (b) PMA/PHD_{63} 10/9.7, (c) PMA/PHD_{50} 12/15, (d) PMA/PHD_{28} 8.0/13. In (a), the primary peak position, q*, is 0.290 nm^{-1}, and markers (▼) are placed at q/q* ratios of 1, 2, and 3.

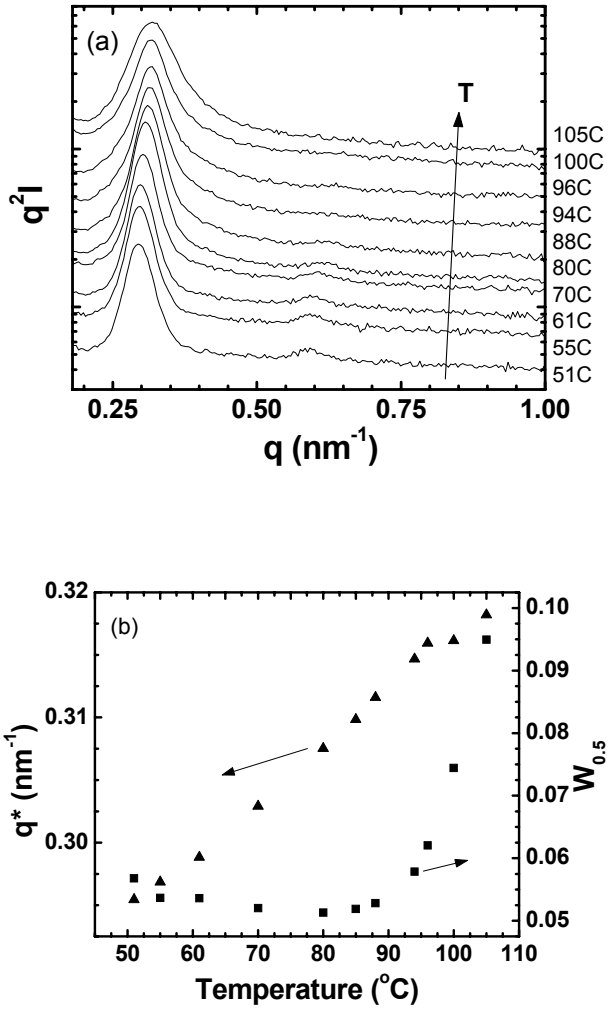

Figure 4.7. (a) Small-angle x-ray scattering profiles for PMA/PHD_{75} 13/11 during a temperature ramp experiment; (b) the primary peak position (q*, ▲) and the primary peak width at half its maximum intensity (■) plotted as a function of temperature.

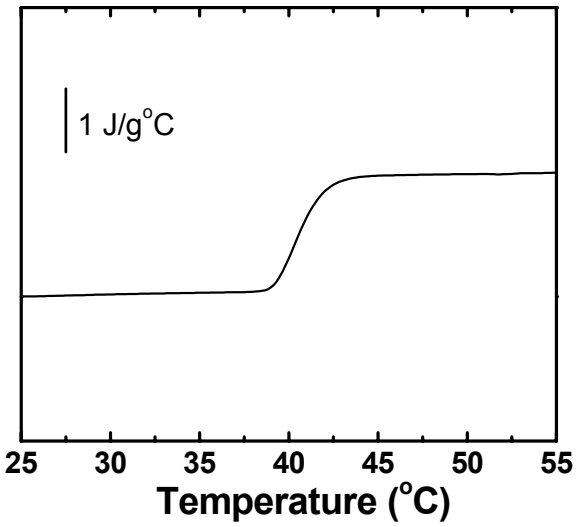

Figure 4.8. DSC thermogram of P*t*BA 15 (M_n = 15 kg/mol, M_w/M_n = 1.02), collected on second heat. The glass transition temperature, extracted at the midpoint of the step change in heat capacity, is 41°C.

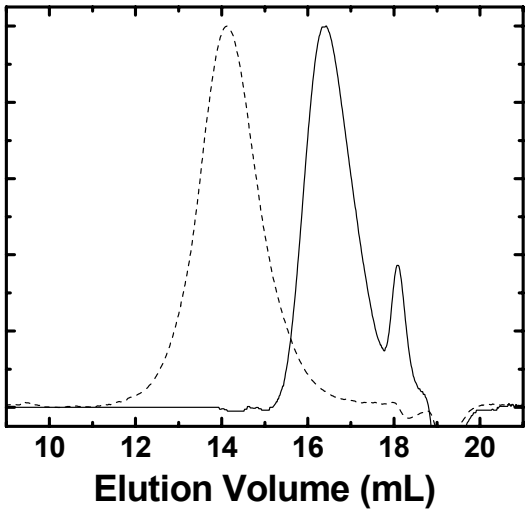

Figure 4.9. Gel permeation chromatography traces with DMF (+ 0.05M LiBr) as the eluent at 1 mL/min of P*t*BA 15 (solid line, $M_w/M_n = 1.02$) and P*t*BA/PHD_{28} 15/18 (dashed line, $M_w/M_n = 1.12$). The small peak at 18.3 mL, which overlaps with the peak associated with P*t*BA 15, is associated with the elution of solvent.

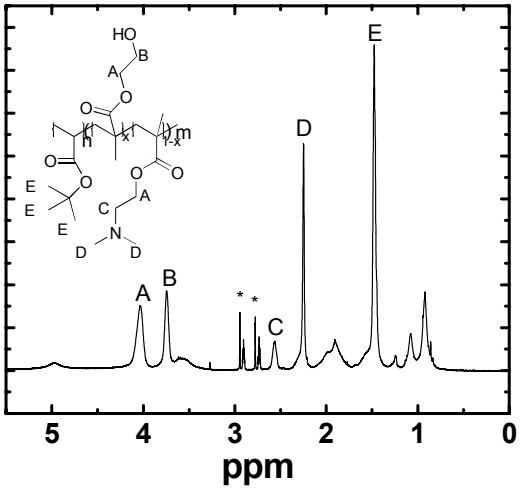

Figure 4.10. ^{1}H NMR spectrum of P*t*BA/PHD$_{28}$ 15/18 in deuterated DMF. The proton contributions are labeled for clarity. * indicates solvent (d-DMF) peaks.

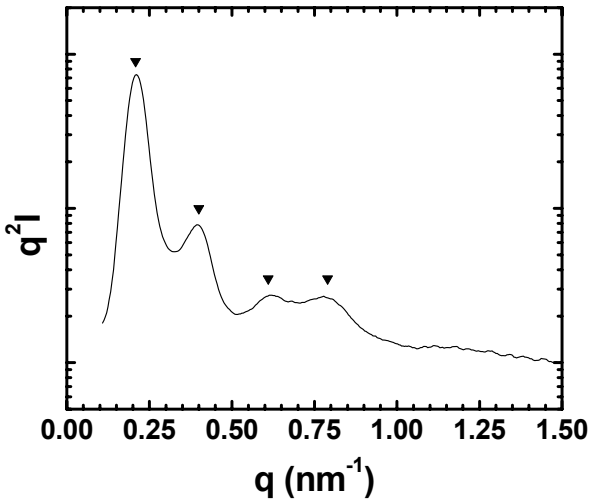

Figure 4.11. Small-angle x-ray scattering profile of P*t*BA/PHD$_{28}$ 15/18. The primary peak position, q*, is 0.208 nm^{-1}, and markers (▼) are placed at q/q* ratios of 1, 2, 3, 4.

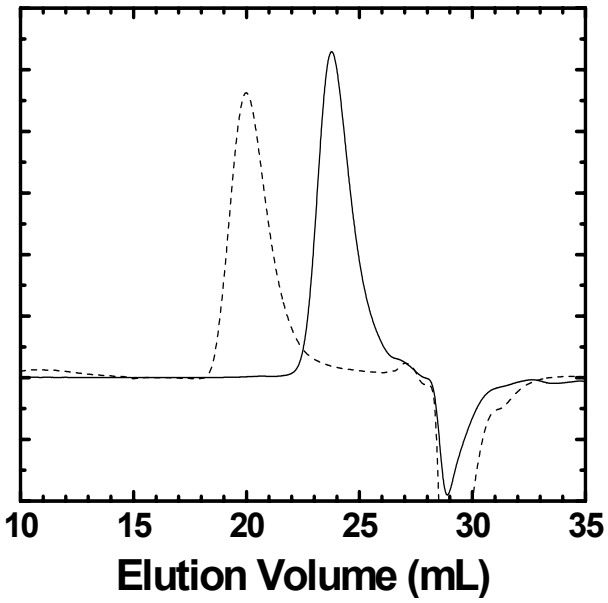

Figure 4.12. Gel permeation chromatography traces with DMF (+ 0.01M LiBr) as the eluent at 1 mL/min of bifunctional P*t*BA 16 (solid line, $M_w/M_n = 1.05$) and PHD_{28}/P*t*BA/PHD_{28} 8.5/16/8.5 (dashed line, $M_w/M_n = 1.07$).

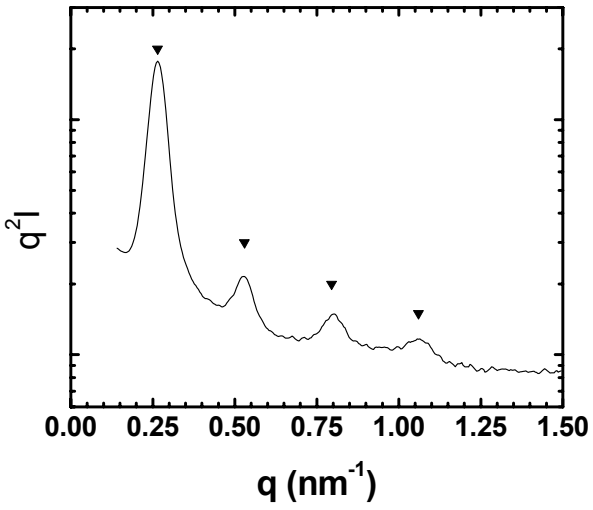

Figure 4.13. Small-angle x-ray scattering profile of PHD_{28}/PtBA/PHD_{28} 8.5/16/8.5. The primary peak position, q*, is 0.265 nm^{-1}, and markers (▼) are placed at q/q* ratios of 1, 2, 3, 4.

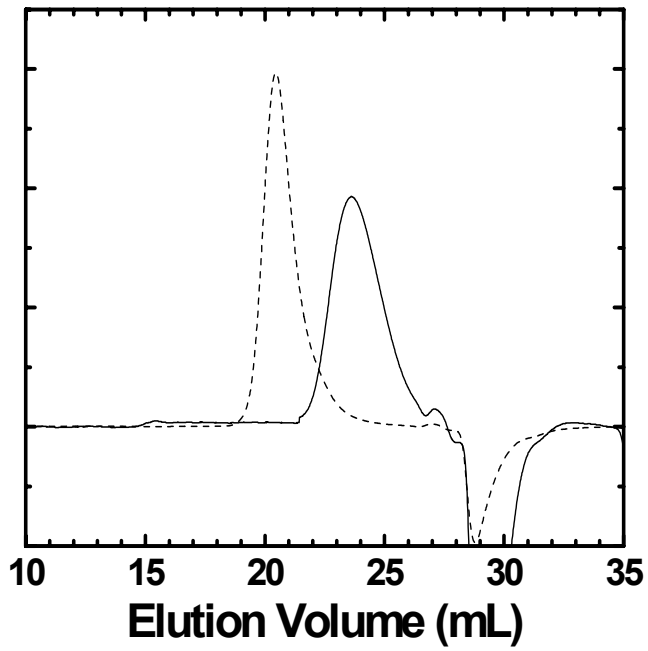

Figure 4.14. Gel permeation chromatography traces with DMF (+ 0.01M LiBr) as the eluent at 1 mL/min of PCL 9.0 (solid line, $M_w/M_n = 1.06$) and PCL/PHD_{28} 9.0/18 (dashed line, $M_w/M_n = 1.11$).

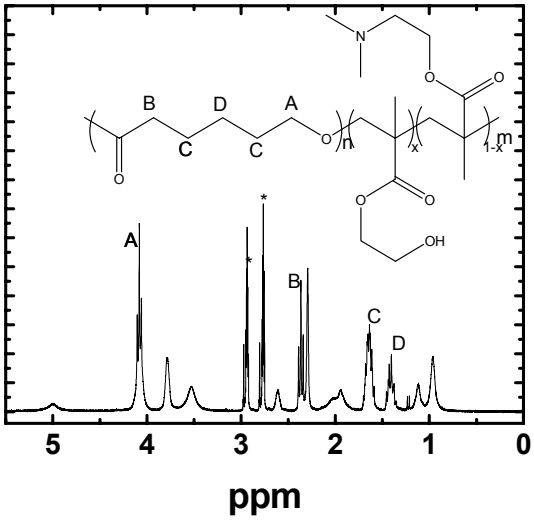

Figure 4.15. ^{1}H NMR spectrum of PCL/PHD$_{28}$ 9.0/18 in deuterated DMF. The proton contributions are labeled for clarity. * indicates solvent (d-DMF) peaks.

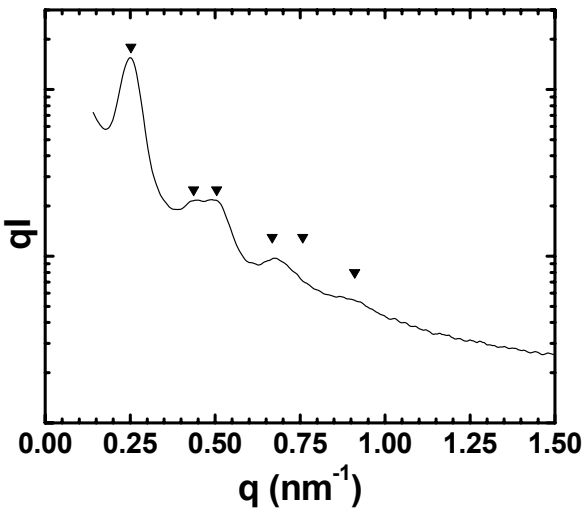

Figure 4.16. Small-angle x-ray scattering profile of PCL/PHD_{28} 9.0/18. The primary peak position, q*, is 0.253 nm^{-1}, and markers (▼) are placed at q/q* ratios of 1, √3, √4, √7, √9, √13.

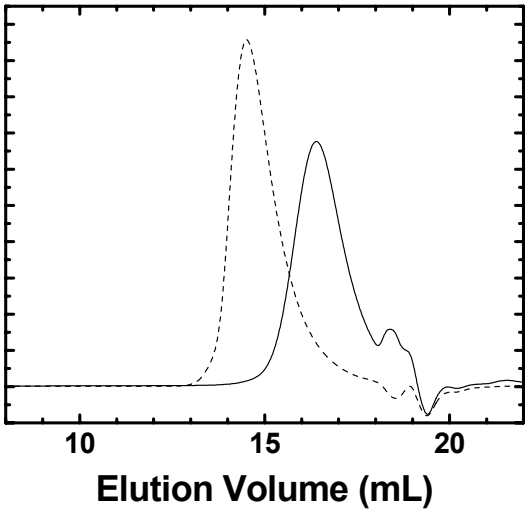

Figure 4.17. Gel permeation chromatography traces with DMF (+ 0.05M LiBr) as the eluent at 1 mL/min of PD 8.2 (solid line, $M_w/M_n = 1.12$) and PD/PH 8.2/17 (dashed line, $M_w/M_n = 1.09$).

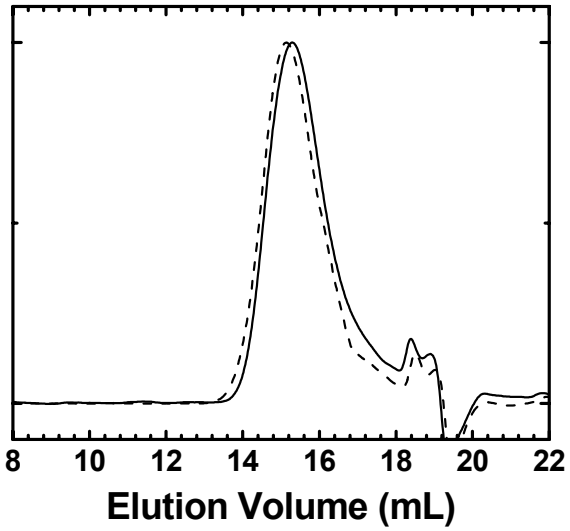

Figure 4.18. Gel permeation chromatography traces with DMF (+ 0.05M LiBr) as the eluent at 1 mL/min of PHD_{75} 14 (solid line, $M_w/M_n = 1.20$) and PS/PHD_{75} 6.7/14 (dashed line, $M_w/M_n = 1.13$).

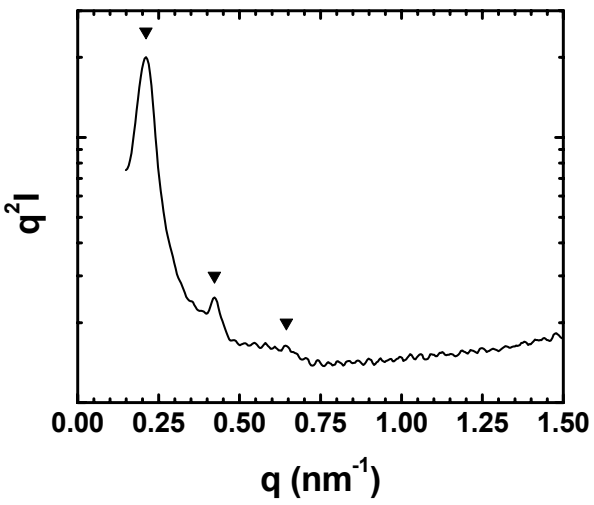

Figure 4.19. Small-angle x-ray scattering profile of PS/PHD$_{75}$ 6.7/14. The primary peak position, q*, is 0.211 nm^{-1}, and markers (▼) are placed at q/q* ratios of 1, 2, 3.

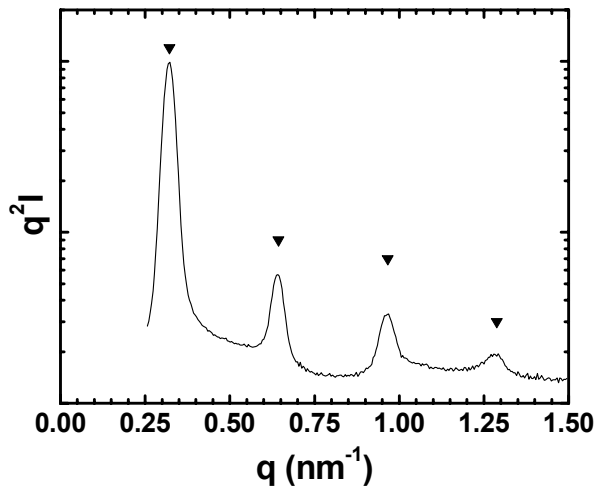

Figure 4.20. Small-angle x-ray scattering profile of PS/PHD_{28}/PS 4.5/16/4.5. The primary peak position, q*, is 0.322 nm^{-1}, and markers (▼) are placed at q/q* ratios of 1, 2, 3, 4.

REFERENCES

1. Dong, L.; Agarwal, A. K.; Beebe, D. J.; Jiang, H. *Nature* **2006,** 442, 551-554.

2. Du, R.; Zhao, J. *Journal of Applied Polymer Science* **2004,** 91, 2721-2728.

3. Yilmaz, Z.; Akkas, P. K.; Sen, M.; Guven, O. *Journal of Applied Polymer Science* **2006,** 102, 6023-6027.

4. Kroupova, J.; Horak, D.; Pachernik, J.; Dvorak, P.; Slouf, M. *Journal of Biomedical Materials Research, Part B: Applied Biomaterials* **2006,** 76B, 315-325.

5. Satish, C. S.; Shivakumar, H. G. *Journal of Macromolecular Science, Part A: Pure and Applied Chemistry* **2007,** 44, 379-387.

6. Traitel, T.; Cohen, Y.; Kost, J. *Biomaterials* **2000,** 21, 1679-1687.

7. Brahim, S.; Narinesingh, D.; Guiseppi-Elie, A. *Biomacromolecules* **2003,** 4, 1224-1231.

8. Brahim, S.; Narinesingh, D.; Guiseppi-Elie, A. *Biomacromolecules* **2003,** 4, 497-503.

9. Triftaridou, A. I.; Hadjiyannakou, S. C.; Vamvakaki, M.; Patrickios, C. S. *Macromolecules* **2002,** 35, 2506-2513.

10. Haraguchi, K.; Takehisa, T. *Advanced Materials* **2002,** 14, 1120-1124.

11. Huglin, M. B.; Zakaria, M. B. *Polymer* **1984,** 25, 797-802.

12. Liu, R.; Oppermann, W. *Macromolecules* **2006,** 39, 4159-4167.

13. Kopecek, J.; Yang, J. *Polymer International* **2007,** 56, 1078-1098.

14. Malkoch, M.; Vestberg, R.; Gupta, N.; Mespouille, L.; Dubois, P.; Mason, A. F.; Hedrick, J. L.; Liao, Q.; Frank, C. W.; Kingsbury, K.; Hawker , C. J. *Chemical Communications* **2006,** 26, 2774-2776.

15. Burke, S. A.; Ritter-Jones, M.; Lee, B. P.; Messersmith, P. B. *Biomedical Materials* **2007,** 2, 203-210.

16. Koshiro, Y.; Morone, N.; Fukutomi, T. *Polymer Gels and Networks* **1995,** 3, 59-70.

17. Achilleos, M.; Krasia-Christoforou, T.; Patrickios, C. S. *Macromolecules* **2007,** 40, 5575-5581.

18. Krasia, T. C.; Patrickios, C. S. *Macromolecules* **2006,** 39, 2467-2473.

19. Suevegh, K.; Domjan, A.; Vanko, G.; Ivan, B.; Vertes, A. *Macromolecules* **1998,** 31, 7770-7775.

20. Themistou, E.; Patrickios, C. S. *Macromolecules* **2007,** 40, 5231-5234.

21. Leibler, L. *Macromolecules* **1980,** 13, 1602-17.

22. Matsen, M. W.; Bates, F. S. *Macromolecules* **1996,** 29, 1091-1098.

23. Topham, P. D.; Howse, J. R.; Crook, C. J.; Gleeson, A. J.; Bras, W.; Armes, S. P.; Jones, R. A. L.; Ryan, A. J. *Macromolecular Symposia* **2007,** 256, 95-104.

24. Nykaenen, A.; Nuopponen, M.; Laukkanen, A.; Hirvonen, S.-P.; Rytelae, M.; Turunen, O.; Tenhu, H.; Mezzenga, R.; Ikkala, O.; Ruokolainen, J. *Macromolecules* **2007,** 40, 5827-5834.

25. Victorov, A. I. *Fluid Phase Equilibria* **2006,** 241, 334-343.

26. Guice, K. B.; Loo, Y.-L. *Macromolecules* **2006,** 39, 2474-2480.

27. Teoh, R. L.; Guice, K. B.; Loo, Y.-L. *Macromolecules* **2006,** 39, 8609-8615.

28. Young, R. J.; Lovell, P. A., *Introduction to Polymers*. 2nd ed.; Chapman & Hall: London, 1991.

29. Caykara, T.; Ozyurek, C.; Kantoglu, O.; Guven, O. *Journal of Polymer Science, Part B: Polymer Physics* **2002,** 40, 1995-2003.

30. Polymer Handbook, 4th Ed. In Brandrup, J.; Immergut, E. H.; Grulke, E. A., Eds. Wiley-Interscience: New York, 1999, VI-203.

31. *ASTM D153-84, Standard Test Methods for Specific Gravity of Pigments* **2003**.

32. Shibayama, M.; Hashimoto, T.; Kawai, H. *Macromolecules* **1983,** 16, 16-28.

33. Porod, G., The Principles of Diffraction, Section 1, General Theory. In *Small-Angle X-ray Scattering*, Glatter, O., Kratky, O., Ed. Academic Press: London, 1982, pp. 17-51.

34. Sakurai, S.; Momii, T.; Taie, K.; Shibayama, M.; Nomura, S.; Hashimoto, T. *Macromolecules* **1993,** 26, 485-491.

35. Senshu, K.; Yamashita, S.; Ito, M.; Hirao, A.; Nakahama, S. *Langmuir* **1995,** 11, 2293-2300.

36. Lee, J.; Aoai, T.; Kondo, S. I.; Miyagawa, N.; Takahara, S.; Yamaoka, T. *Journal of Polymer Science, Part A: Polymer Chemistry* **2002,** 40, 1858-1867.

37. Bories-Azeau, X.; Armes, S. P. *Macromolecules* **2002,** 35, 10241-10243.

38. Guice, K. B.; Loo, Y.-L. *Macromolecules* **2007,** 40, 9053 -9058.

39. Bucholz, T. L.; Loo, Y.-L. *Macromolecules* **2006,** 39, 6075-6080.

40. Gomez, E. D.; Das, J.; Chakraborty, A. K.; Pople, J. A.; Balsara, N. P. *Macromolecules* **2006,** 39, 4848-4859.

41. Handlin, D. L., Jr.; Thomas, E. L. *Macromolecules* **1983,** 16, 1514-25.

42. Bucholz, T. L.; Li, S. P.; Loo, Y.-L. *Journal of Materials Chemistry* **2008,** 18, 530-536.

43. Meng, F.; Xu, Z.; Zheng, S. *Macromolecules* **2008,** 41, 1411-1420.

44. Bougard, F.; Jeusette, M.; Mespouille, L.; Dubois, P.; Lazzaroni, R. *Langmuir* **2007,** 23, 2339-2345.

45. Tsuji, H.; Horikawa, G.; Itsuno, S. *Journal of Applied Polymer Science* **2007,** 104, 831-841.

46. Loo, Y.-L.; Register, R. A.; Ryan, A. J. *Macromolecules* **2002,** 35, 2365-2374.

47. Loo, Y.-L. Controlled polymer crystallization through block copolymer self-assembly, Ph.D. Dissertation, Princeton University, Princeton, N.J. **2001**, p. 42.

48. Tsarevsky, N. V.; Matyjaszewski, K. *Chemical Reviews* **2007,** 107, 2270-2299.

49. Tsarevsky, N. V.; Pintauer, T.; Matyjaszewski, K. *Macromolecules* **2004,** 37, 9768-9778.

50. Lee, S. B.; Russell, A. J.; Matyjaszewski, K. *Biomacromolecules* **2003,** 4, 1386-1393.

51. Jin, X.; Shen, Y.; Zhu, S. *Macromolecular Materials and Engineering* **2003,** 288, 925-935.

52. dos Santos, A. M.; Pohn, J.; Lansalot, M.; D'Agosto, F. *Macromolecular Rapid Communications* **2007,** 28, 1325-1332.

53. Sahnoun, M.; Charreyre, M.-T.; Veron, L.; Delair, T.; D'Agosto, F. *Joural of Polymer Science, Part A: Polymer Chemistry* **2005,** 43, 3551-3565.

54. Dubin, P. L.; Koontz, S.; Wright, K. L., III. *Journal of Polymer Science, Polymer Chemistry Edition* **1977,** 15, 2047-2057.

Chapter 5. pH-Responsive Model Hydrogels Containing PS and PHD

INTRODUCTION

Poly(DMAEMA) is stimuli-responsive, with its solubility in aqueous environments significantly influenced by both pH[1] and temperature.[2] The pH response of poly(DMAEMA), which is the subject of this chapter, is associated with protonation of the pendant tertiary amine functional group of DMAEMA below its pKa.[1] The pKa for poly(DMAEMA) has been reported to be 7.5,[1] which is in a suitable range for physiological use.[3] Hydrogels containing DMAEMA imbibe more water upon protonation of tertiary amine groups in order to counteract ionic repulsions.[1] Because of this pH-responsiveness, DMAEMA-containing hydrogels are attractive materials for a range of applications, including nanofiltration,[4,5] gene[1] and drug delivery,[6-10] and tissue scaffolds.[11]

DMAEMA-containing hydrogels can also be synthetically modified by copolymerizaton with other monomers.[6-8,11,12] In particular, HEMA, a monomer that is biocompatible and is moderately water-swellable in its polymeric form, has been widely studied as a comonomer to tune the properties of DMAEMA-based hydrogels. [2,6,8,11,13,14] For example, a 10% increase in the HEMA content in PHD hydrogels (e.g., from PHD_{20} to PHD_{10}) can decrease the water uptake in PHD hydrogels, under acidic conditions, by over 35%.[6]

While the PHD hydrogels that have been previously investigated are undoubtedly useful, fundamental study of these systems is limited by characteristically large composition distributions within the hydrogels.[15] In order to overcome the non-uniform crosslink distributions associated with traditional hydrogels, model network architectures have been investigated by several research groups.[16-20] Typically, these model hydrogels

are derived from amphiphilic block copolymers, with the glassy hydrophobic blocks serving as physical crosslinks that are regularly spaced in a swellable hydrophilic matrix.[18,16] As an added advantage, the dimensional changes within well-ordered amphiphilic block copolymer hydrogels can be probed directly by SAXS.[16]

In Chapter 4, we demonstrated that block copolymers containing compositionally-uniform PHD can be synthesized with controlled molecular weights and narrow molecular weight distributions,[21,22] and that the resulting block copolymers microphase separate to form well-ordered microstructures in the solid state.[21,22] The distinguishing feature of these PHD-containing block copolymers, relative to other block copolymers that have been investigated as model hydrogels,[16-20] is that our hydrophilic block is comprised of a statistical PHD copolymer. When swollen in water, PHD-containing block copolymers are uniquely suited to serve as a model hydrogel system for investigating the temperature and pH-dependent swelling of hydrogels comprised of two comonomers (e.g., HEMA and DMAEMA).

In this chapter, we investigated the pH response of model hydrogels derived from lamella-formers of PS/PHD. The hydrophobic PS microdomains are glassy during the course of the swelling experiments. The glassy microdomains are crucial as they serve to anchor the swellable component.[18,19,23-28] Of specific relevance to this study is whether or not the glassy PS microdomains can effectively preserve the phase-separated microstructure during swelling of PS/PHD diblock copolymers. It has been widely assumed that only amphiphilic block copolymers containing two or more glassy, hydrophobic blocks (i.e., at least a triblock copolymer architecture) can retain their microstructures during swelling. The swelling behavior of hydrogels in which the swellable component is not anchored at both ends, however, has not been looked into carefully. In this chapter, we compare the swelling characteristics of PS/PHD/PS and

PS/PHD at varying PHD compositions in order to probe the limits of the swelling of diblock copolymer hydrogels. Further, we demonstrate the tunability of the swelling characteristics of these block copolymer hydrogels by controlling the DMAEMA content that is present.

SWELLING OF PS/PHD/PS LAMELLAR TRIBLOCK COPOLYMERS

PS/PHD diblock and PS/PHD/PS triblock copolymers were cast from THF, annealed at 40°C, and then characterized by SAXS. With one exception (discussed later in the chapter), the SAXS profiles of all block copolymers revealed alternating lamellar morphologies.[29] The difference between the triblock copolymer lamellar morphology and that of the diblock copolymer is illustrated at the level of individual polymer chains in Figure 5.1. In the case of the triblock copolymer (Figure 5.1a), the PS endblocks (shown in white) can occupy different lamellae, effectively serving as anchors for the PHD midblock (shown in black). When swollen in aqueous environments, the neighboring PS microdomains can serve as physical crosslinks, effectively maintaining the structural integrity of the lamellar microdomains. In contrast, the diblock copolymer (Figure 5.1b) is not able to arrange in this fashion due to the lack of a second PS endblock.

To explore the swelling properties associated with PS/PHD/PS and PS/PHD, the microphase-separated block copolymers were weighed before they were immersed in a 0.1 M pH 8.8 phosphate buffer for 24 h. Buffers with pHs ranging from 4.7 to 8.8 were prepared using potassium phosphate monobasic and potassium phosphate dibasic and appropriately diluted with deionized water. Subsequently, the resulting hydrogels were reweighed and characterized by SAXS. In this manner, we were able to collect both gravimetric swelling and microdomain characteristic dimension data[16] for each hydrogel as a function of pH. To examine the swelling characteristics of the same hydrogel at

subsequent pHs, the sample was then immersed in deionized water for 6 h and re-immersed in the next phosphate buffer for 24 h. The swelling behavior of each hydrogel was systematically investigated from the most basic (pH = 8.8) to the most acidic (pH = 4.7) buffer solution.

The SAXS profiles of PS/PHD_{28}/PS 4.5/16/4.5 in the solid state and upon immersion in a series of phosphate buffers are shown in Figure 5.2a. The SAXS profile of the block copolymer in the solid state (Figure 5.2a-i) exhibits a narrow and intense primary peak at $q^* = 0.322\ nm^{-1}$ and higher-order reflections at q/q* ratios of 2, 3, and 4, consistent with that of an alternating lamellar morphology.[29] The SAXS profile collected in the pH 8.8 phosphate buffer (Figure 5.2a-ii) exhibits a primary peak at $q^* = 0.290 nm^{-1}$, and higher-order reflections at q/q* ratios of 2 and 3. The position of the higher-order reflections indicates that its lamellar morphology is retained after swelling.[29] The primary peak position has shifted to a lower q compared to that of the block copolymer in the solid state, which indicates that the microdomain spacing, $d = 2\pi/q^*$, is swollen relative to that in the solid state. To facilitate discussion, we define a microdomain spacing ratio, d/d_o, where d is the characteristic lamellar interdomain spacing of the swollen hydrogel and d_o is the interdomain spacing of the lamellae in the solid state. After immersion in the pH 8.8 phosphate buffer, d/d_o for PS/PHD_{28}/PS 4.5/16/4.5 is 1.11. The gravimetric swelling ratio, M/M_o, was determined to be 1.16 from the gravimetric weights of the block copolymer before, M_o, and after, M, immersion in the phosphate buffer.

PS/PHD_{28}/PS 4.5/16/4.5 was sequentially immersed in phosphate buffers that were progressively more acidic. SAXS profiles collected at each successive pH are also shown in Figure 5.2a. In general, the primary peak positions in the SAXS profiles shift to smaller q's with decreasing pH. This increased swelling with decreasing solution pH

is consistent with the swelling behavior that had been previously observed for cationic hydrogels.[7] Moreover, the second- and third-order reflections remain visible in all of the SAXS profiles, which confirms that the lamellar morphology is maintained throughout the swelling study.[29]

The SAXS profile collected on PS/PHD_{28}/PS 4.5/16/4.5 that is immersed in the most acidic phosphate buffer (pH 4.7, Figure 5.2a-viii) exhibits a primary peak at q* = 0.265 nm^{-1}, and higher-order reflections at q/q* ratios of 2 and 3. As in the sample that is swollen in the pH 8.8 phosphate buffer, the sample in the pH 4.7 buffer exhibits higher-order reflections consistent with that of the lamellar morphology.[29] The primary peak position is shifted to an even lower q, which indicates further swelling of the lamellar microdomains (d/d_o = 1.22). Increased interdomain swelling in at pH 4.7 is consistent with increases in water uptake (M/M_o = 1.42). The compiled microdomain spacing ratio and gravimetric swelling ratio for PS/PHD_{28}/PS 4.5/16/4.5 at each pH are shown in Figure 5.2b. The block copolymer hydrogel behaves like a cationic hydrogel, with a large extent of swelling in acidic media and a pronounced change in swelling upon crossing the pKa of poly(DMAEMA) at pH 7.5.[1,7,30]

It is not surprising that the SAXS profile of the swollen PS/PHD_{28}/PS 4.5/16/4.5 sample exhibits higher-order reflections consistent with that of an alternating lamellar morphology. PS is hydrophobic and glassy at ambient temperatures.[31] As a result, the PS microdomains do not sorb water, and they maintain their rigidity during swelling of PHD_{28}. In PS/PHD_{28}/PS 4.5/16/4.5 triblock copolymers, PS endblocks that are embedded in two neighboring microdomains can anchor PHD. These PS microdomains effectively serve as physical crosslinks, retaining the lamellar morphology of the solid state during swelling.[19]

In order to examine the effects of the composition of PHD on the swelling behavior of PS/PHD/PS hydrogels, we also examined the swelling behavior of PS/PHD_{75}/PS 5.9/20/5.9. The SAXS profiles of PS/PHD_{75}/PS 5.9/20/5.9 in the solid state and upon immersion in buffer solutions at pH 8.8 and pH 4.7 are shown in Figure 5.3a. Similar to that of PS/PHD_{28}/PS 4.5/16/4.5 in the solid state, the SAXS profile of PS/PHD_{75}/PS 5.9/20/5.9 in the solid state (Figure 5.3a-i) exhibits a lamellar morphology, with a primary peak at $q^* = 0.244$ nm^{-1}, and a higher-order reflection at $q/q^* = 2$. Upon immersion in a basic phosphate buffer at pH 8.8 (Figure 5.3a-ii), the sample imbibes water ($M/M_o = 1.47$), and the primary peak position in the SAXS profile of the swollen sample shifts to a lower q ($q^* = 0.207$ nm^{-1}; $d/d_o = 1.18$). The SAXS profile maintains a higher-order reflection at $q/q^* = 2$, indicating that the lamellar morphology is retained. At pH 4.7 (Figure 5.3a-iii), the sample takes in even more water ($M/M_o = 2.77$). The primary peak position in the SAXS profile of the swollen sample has shifted to a significantly lower q compared to that of the PS/PHD_{75}/PS 5.9/20/5.9 sample in the solid state ($q^* = 0.149$ nm^{-1}; $d/d_o = 1.64$), and two higher-order reflections associated with the lamellar morphology ($q/q^* = 2$ and 3) are observed.[29] Gravimetric swelling data and microdomain spacing ratios for PS/PHD_{75}/PS 5.9/20/5.9 hydrogel as a function of pH are presented in Figure 5.3b.

As with PS/PHD_{28}/PS 4.5/16/4.5, PS/PHD_{75}/PS 5.9/20/5.9 displays swelling behavior that is typical of that of cationic hydrogels.[7] PS/PHD_{75}/PS 5.9/20/5.9 retains both its macroscopic integrity and its microscopic lamellar morphology during swelling due to its triblock copolymer architecture in which the PS microdomains effectively serve as physical crosslinks for the swellable PHD_{75} phase. The extent of swelling observed in PS/PHD_{75}/PS 5.9/20/5.9, however, is significantly greater than that observed in PS/PHD_{28}/PS 4.5/16/4.5. We attribute this difference to the compositional difference of

the swellable PHD midblock. There is significantly more DMAEMA in the midblock of PS/PHD_{75}/PS 5.9/20/5.9 compared to that of PS/PHD_{28}/PS 4.5/16/4.5. At ambient temperatures, DMAEMA is more hydrophilic than HEMA.[22] As such, the incorporation of more DMAEMA into the PHD block should result in greater swelling. Further, DMAEMA can be protonated below its pKa.[1] The additional DMAEMA present in PHD_{75} results in a greater swelling change in PS/PHD_{75}/PS 5.9/20/5.9 upon crossing the pKa of poly(DMAEMA). While not surprising, we note a monotonic increase in the extent of swelling of PS/PHD/PS model hydrogels with increasing DMAEMA content from PHD_{28} to PHD_{75}. This result is contrary to a recent report, wherein the swelling characteristics of PHD hydrogels plateau at 15 mol% DMAEMA.[7] The discrepancy between the two observations is likely related to differences in hydrogel synthesis. Specifically, the PHD hydrogels described in the previous report were synthesized by copolymerization of HEMA and DMAEMA in the bulk, in the presence of a crosslinker.[7] Given the reactivity ratios that have been reported for HEMA and DMAEMA in the bulk (r_H = 1.6, r_D = 0.45),[32] the distribution of HEMA and DMAEMA throughout these hydrogels is not likely to be uniform. As a consequence, differences result in the uniformity of comonomer and/or crosslink distributions within the hydrogels.

SWELLING OF PS/PHD LAMELLAR DIBLOCK COPOLYMERS

To assess the importance of block copolymer architecture on the swelling behavior of PS/PHD/PS, we examined the swelling behavior of PS/PHD diblock copolymers having similar compositions. Specifically, we investigated the swelling behavior of PS/PHD_{75} 6.7/14, a lamella-forming diblock copolymer with comparable PHD composition to that of PS/PHD_{75}/PS 5.9/20/5.9. The SAXS profiles of PS/PHD_{75} 6.7/14 in the solid state and upon immersion in buffer solutions at pH 8.8 and pH 4.7 are shown in Figure 5.4a. In the solid state, PS/PHD_{75} 6.7/14 exhibits a SAXS profile (Figure

5.4a-i) that is consistent with an alternating lamellar morphology,[29] with a primary peak at $q^* = 0.211$ nm^{-1}, and a higher-order reflection at $q/q^* = 2$. When immersed in the pH 8.8 phosphate buffer, PS/PHD$_{75}$ 6.7/14 swells significantly ($M/M_o = 1.60$). Correspondingly, the primary peak in the SAXS profile of the swollen PS/PHD$_{75}$ 6.7/14 sample (Figure 5.4a-ii) shifts to a smaller q ($q^* = 0.184$ nm^{-1}; $d/d_o = 1.15$), relative to that of the solid state. A higher-order peak at $q/q^* = 2$ remains in the SAXS profile, suggesting that the lamellar morphology is maintained. The SAXS profile of PS/PHD$_{75}$ 6.7/14 at pH 4.7 is shown in Figure 5.4a-iii. Under these conditions, we observe a significant shift in the primary peak position ($q^* = 0.120$ nm^{-1}; $d/d_o = 1.76$). Higher-order reflections are also still visible at peak ratios of $q/q^* = 2$ and 3, indicating that the hydrogel maintains its lamellar morphology even at pHs below the pKa of poly(DMAEMA).

Microdomain spacing and gravimetric swelling data for PS/PHD$_{75}$ 6.7/14 are presented as a function of pH in Figure 5.4b. Over the course of our pH experiments, the PS/PHD$_{75}$ 6.7/14 hydrogel broke into many smaller pieces, most of which we were unable to recover for gravimetric analysis. This phenomenon was first observed when we immersed PS/PHD$_{75}$ 6.7/14 in the pH 7 buffer solution, which is just below the pKa of poly(DMAEMA).[1] This phenomenon is expected because neighboring lamellar microdomains cannot anchor the sample microscopically during swelling. PS/PHD$_{75}$ 6.7/14 continued to break into smaller pieces with each subsequent reduction in pH. As such, the swelling data presented in Figure 5.4b does not include gravimetric swelling information below pH 7. We were, however, able to collect several of the smaller pieces that were still large enough for SAXS. SAXS on these smaller pieces indicate that, while the PS/PHD$_{75}$ 6.7/14 hydrogel no longer maintains its original macroscopic integrity, the alternating lamellar morphology is retained on swelling below pH 7. As evinced by the

microdomain spacing data in Figure 5.4b, the lamellar microdomains continue to respond to decreasing pH.

Unlike PS/PHD$_{75}$/PS 5.9/20/5.9, PS/PHD$_{75}$ 6.7/14 disintegrated macroscopically because the PHD segments are not anchored by PS glassy microdomains on both ends. Within the smaller pieces of samples, however, the periodic lamellar structure is retained, presumably because the long-range electrostatic repulsion generated by protonated DMAEMA units within an individual lamella is not significant enough to force a complete separation.[34] As such, the loss of macroscopic integrity in PS/PHD$_{75}$ 6.7/14 is likely to originate at structural defects, such as grain boundaries that were predefined during solvent casting of the solid-state sample.[35]

We also examined the swelling behavior of PS/PHD$_{50}$ 5.4/9.8. PS/PHD$_{50}$ 5.4/9.8 imbibes water (M/M_o = 1.22, d/d_o = 1.16) when swollen in the pH 8.8 phosphate buffer. Similar to PS/PHD$_{75}$ 6.7/14, PS/PHD$_{50}$ 5.4/9.8 loses macroscopic integrity, as determined by gravimetric analysis, upon crossing the pKa of poly(DMAEMA). SAXS analysis performed on collected pieces of the PS/PHD$_{50}$ sample confirm that its alternating lamellar morphology is retained even after the loss of macroscopic integrity. Further, the PS/PHD$_{50}$ 5.4/9.8 sample continues to undergo microdomain swelling that is characteristic of a cationic hydrogel (d/d_o = 1.36 at pH 4.7). We note that the swelling in PS/PHD$_{50}$ 5.4/9.8 is less than that of PS/PHD$_{75}$ 6.7/14 due to the fact that less DMAEMA is present in PS/PHD$_{50}$ 5.4/9.8. In both cases, the swelling that occurs upon protonation of DMAEMA is sufficient to macroscopically destabilize the samples.

The SAXS profiles of PS/PHD$_{28}$ 6.8/5.8 in the solid state and upon immersion in phosphate buffers of different pH's (pH 8.8 and pH 4.7) are shown in Figure 5.5a. Similar to that of PS/PHD$_{28}$/PS 4.5/16/4.5, the SAXS profile of PS/PHD$_{28}$ 6.8/5.8 in the solid state (Figure 5.5a-i) indicates that the sample adopts a lamellar morphology, with a

primary peak position of $q^* = 0.348\ nm^{-1}$, and higher-order reflections at q/q^* ratios of 2, 3, and 4. Upon immersion in the basic phosphate buffer at pH 8.8 (Figure 5.5a-ii), the primary peak position shifts to a lower q ($q^* = 0.323\ nm^{-1}$; $d/d_o = 1.08$), but the higher-order reflections at q/q^* ratios of 2 and 3 remain.[29] Upon immersion in the acidic phosphate buffer solution at pH 4.7 (Figure 5.5a-iii), the primary peak position shifts to even smaller q ($q^* = 0.298\ nm^{-1}$; $d/d_o = 1.17$). The microdomain spacing ratio of PS/PHD_{28} 6.8/5.8 is shown, as a function of the pH of the phosphate buffer, in Figure 5.5b. Gravimetric data, which was also collected over the full pH range, is also shown in Figure 5.5b. In contrast to PS/PHD_{75} 6.7/14 and PS/PHD_{50} 5.4/9.8, PS/PHD_{28} 6.8/5.8 does not lose its macroscopic integrity during the entire swelling process despite being a diblock copolymer.

It has been widely assumed that a triblock copolymers with two hydrophobic end-blocks are necessary to provide structural integrity to model hydrogels.[18,19,23-28] Diblock copolymers, on the other hand, are incapable of anchoring the swellable block so macroscopic disintegration is generally expected. The swelling experiments of PS/PHD_{75} 6.7/14 and PS/PHD_{50} 5.4/9.8 confirm that diblock copolymer hydrogels are indeed destabilized upon protonation of the ionic component. In the case of PS/PHD_{28} 6.8/5.8, however, the diblock copolymer architecture is sufficient to preserve the macroscopic integrity of the hydrogel when swollen across four decades of pH. When protonated, PHD_{28} has a lower charge density than PHD_{75}. The water driven into the PHD phase thus generates a lower osmotic pressure in PHD_{28} compared to PHD_{75}. From the swelling behavior of the diblock copolymers with varying DMAEMA content, there appears to be a threshold concentration of DMAEMA within the swellable block that governs whether the diblock copolymer architecture can suitably withstand the osmotic pressure generated within the hydrogel upon the protonation of DMAEMA units below the pKa of

poly(DMAEMA). In our system, we estimate this threshold concentration to be between 28 and 50 mol%. Given that the DMAEMA content within PHD_{28} is relatively low, PS/PHD_{28} 6.8/5.8 is able to maintain its macroscopic integrity during swelling. Its swelling behavior thus mirrors that of the physically crosslinked PS/PHD_{28}/PS 4.5/16/4.5 triblock copolymer hydrogel.

EQUILIBRIUM SWELLING OF MODEL LAMELLAR HYDROGELS

The swelling properties of PS/PHD and PS/PHD/PS lamellar hydrogels are related to four factors: the relative volume fraction of the PHD block (v_{PHD}), the fraction of DMAEMA in the PHD block (x_D), the overall molecular weight of the PHD block, and the block copolymer architecture. By normalizing microdomain swelling against the characteristic microdomain size of the block copolymer in the solid state (d/d_o), we have accounted for differences in the molecular weight of the block copolymers. The overall composition of DMAEMA in the hydrogel can be described by the volume fraction of the PHD block and the composition DMAEMA within the PHD block ($c = v_{PHD} \cdot x_D$). In Figure 5.6, we have plotted the microdomain spacing ratio (d/d_o) at pH 4.7 (■) as a function of the overall DMAEMA composition for all lamella-forming block copolymers investigated in this chapter. The microdomain swelling properties in PS/PHD and PS/PHD/PS hydrogels are strongly correlated with the DMAEMA concentration. As observed in Figure 5.6, a 35% increase in the overall DMAEMA concentration in the hydrogel results in a 4.5-fold increase in the swelling response at pH 4.7. The microdomain spacing ratio at pH 8.8 (▼) is also plotted as a function of DMAEMA concentration in Figure 5.6. As with the data at pH 4.7, the microdomain spacing ratio at pH 8.8 also increases with increasing DMAEMA content. Above the pKa of poly(DMAEMA), however, DMAEMA units are not protonated[11] and therefore only

contribute towards the hydrophilicity of the hydrogel.[22] The dependence of swelling on the overall DMAEMA composition is therefore less apparent at basic conditions.

We assessed the dependence of microdomain swelling on the overall DMAEMA composition in our block copolymer hydrogels with models derived for traditional, chemically-crosslinked hydrogels. Most useful in this regard is a swelling model, proposed by Brannon-Peppas et al., that describes the swelling equilibrium of ionic hydrogels as a balance between the ionic chemical potential and the combined mixing and elastic potentials of the hydrogel.[30] The Brannon-Peppas model assumes that the crosslinks are point crosslinks connected to four extended polymer arms, and that the crosslinks are introduced in the swollen state.[30] Since our crosslinks are introduced in the dry state, we use the more appropriate Flory-Rehner model to describe the mixing and elastic potentials,[36] while retaining the Brannon-Peppas derivation of ionic potential.[30] The complete swelling equilibrium condition of our hydrogels, expressed in terms of the concentration of the ionizable component, c, was previously presented as Equation 2.10.

For the purpose of evaluating our PS/PHD and PS/PHD/PS hydrogels, we assumed that any differences in molecular weight are accounted for by normalizing the microdomain swelling of each lamellar-forming hydrogel against the characteristic microdomain spacing in the solid state. In a particular buffer of known pH, Equation 2.10**,** simplifies into an equation of two variables, c and $v_{2,s}$, the volume fraction of polymer in the hydrogel. Assuming isotropic swelling in PS/PHD and PS/PHD/PS hydrogels, the microdomain spacing ratio is related to $v_{2,s}$ as shown in Equation 5.1:

$$\left(\frac{d}{d_o}\right)^3 \approx \frac{1}{v_{2,s}} \qquad \text{(Equation 5.1)}$$

As a further approximation, we simplified our model in the limit of large swelling (small $v_{2,s}$),[36] as shown in Equation 5.2.

$$\left(\frac{d}{d_o}\right)^{-1} \approx A - Bc^2 \quad \text{(Equation 5.2)}$$

In Equation 5.2, A is a unitless constant and B is defined by Equation 5.3:

$$\lim_{v_{2,s}\to 0} B = \left(\frac{2M_c}{M_n} - 1\right)^{-1}\left(\frac{K_b}{10^{pH-14} + K_b}\right)^2\left(\frac{v \cdot M_c}{4I}\right)\cdot\left(V_{PHD}\right)^2 \quad \text{(Equation 5.3)}$$

In Equation 5.3, I is the ionic strength, K_b is the dissociation constant, v is the specific volume of the polymer, and V_{PHD} is the molar volume of dry PHD.

Subjecting our pH 4.7 data to a best fit of Equation 5.2 yields A = 0.866 and B = 1.33 (correlation coefficient = 0.996). In Figure 5.6, the dashed curve represents a fit according to Equation 5.2 to the microdomain spacing ratio data at pH 4.7. The pH 8.8 data can also be fitted to Equation 5.2 with reasonable agreement (A = 0.916, B = 0.406; correlation coefficient = 0.947). The solid curve in Figure 5.6 represents the fit to the pH 8.8 data. The simplified model adequately describes our data for amphiphilic PS/PHD and PS/PHD/PS hydrogels. Further, that the microdomain swelling behavior of diblock and triblock copolymers can be modeled together with good agreement suggests that architectural differences do not significantly affect the microdomain swelling behavior of the lamellar structures within our hydrogels.

Our results thus far have focused on the swelling behavior of block copolymer hydrogels from the most basic (pH = 8.8) to the most acidic (pH = 4.7) buffer solution. In order to examine the reversibility of swelling in PS/PHD lamellar hydrogels, we also examined the swelling response of PS/PHD_{28} 6.8/5.8 on return, i.e. from the most acidic to the most basic condition. Microdomain spacing ratios collected with increasing pH are shown in Figure 5.7 (▲; dashed line). For comparison, we have also presented the original microdomain spacing ratio data collected from basic to acidic pH for PS/PHD_{28} 6.8/5.8 in Figure 5.7 (■; solid line). While we observe a decrease in microdomain

spacing with increasing pH, the hydrogel does not return to the same extent of swelling as compared to the hydrogel swelling experiment on decreasing pH. Upon returning to pH 8.8, PS/PHD$_{28}$ 6.8/5.8 was immersed in deionized water to remove any uncomplexed ions. The sample was then dried, dissolved in THF, and cast onto a Si test wafer for FTIR analysis. The IR spectra of the PS/PHD$_{28}$ 6.8/5.8 before any swelling experiments and after the completion of the deswelling experiment are shown in Figures 5.8a and 5.8b, respectively. In the FTIR spectrum collected on PS/PHD$_{28}$ 6.8/5.8 before swelling (Figure 5.8a), we observe narrow absorption bands at 1728 cm^{-1} and 1159 cm^{-1}, associated with the ester C=O and the aldehyde C-O stretches, respectively.[37] We also observe a C-H stretch[38] at 2900 cm^{-1}. In the FTIR spectrum of the previously swollen sample (Figure 5.8b), we observe an additional region of reduced transmission between 2700 and 2300 cm^{-1}. This region is commonly associated with an NR_3^+ stretch.[5] The persistence of the NR_3^+ stretch after return of PS/PHD$_{28}$ 6.8/5.8 to the pH 8.8 phosphate buffer (i.e., above the pKa of DMAEMA) and dialysis in deionized water suggests the presence of residual ions coordinating with DMAEMA. In particular, amine cations have been demonstrated to form stable complexes with phosphate anions.[39] We speculate that it is this trapping of ions within the hydrogel that is responsible for irreversibility observed in the swelling and deswelling characteristics of PS/PHD hydrogels.[5] Upon reimmersion in the pH 4.7 buffer, we note that we are always able to reproduce the most swollen swelling state.

SWELLING OF A PS/PHD CYLINDRICAL DIBLOCK COPOLYMER

In order to examine the role of morphology on the swelling in PS/PHD hydrogels, we investigated the swelling of a cylinder-forming PS/PHD$_{28}$ 6.8/27. The SAXS profiles collected on PS/PHD$_{28}$ 6.8/27 in the solid state and upon immersion in pH 8.8, 8.1, 7.5, and 7.1 phosphate buffer solutions are shown in Figure 5.9a. The SAXS profile of

PS/PHD_{28} 6.8/27 in the solid state (Figure 5.9a-i) exhibits a primary peak at q* = 0.248 nm^{-1}, with higher-order reflections at q/q* = √3, √7, and √13. The spacing of the higher-order reflections is consistent with the hexagonally-packed cylindrical morphology.[29] Given the volume fraction (v_{PHD} = 0.775; Table 4.1), PS is expected to form discrete cylinders of radius 7.3 nm within the PHD_{28} matrix. We have plotted the form factor[40] (Equation 2.18) for cylinders of radius 7.3 nm as a dashed curve in Figure 5.9. The first minimum in the form factor curve occurs in the location of q/q* = √4, which is commonly observed for the H morphology but is absent in the SAXS profile.[29]

Upon immersion in the pH 8.8 phosphate buffer (Figure 5.9a-ii), the primary peak position in the SAXS profile shifts to a lower q of q* = 0.199 nm^{-1} (d/d_o = 1.25), and the higher-order reflection at q/q* = √3 is retained. The existence of the higher-order reflection at q/q* = √3 suggests that the H morphology is retained during swelling in the pH 8.8 buffer.[29] There is no further change in the SAXS profile upon immersion of PS/PHD_{28} 6.8/27 in a pH 8.1 phosphate buffer (Figure 5.9a-iii). Upon immersion in the pH 7.5 phosphate buffer (Figure 5.9a-iv), which is around the pKa of poly(DMAEMA), the primary peak in the SAXS profile of PS/PHD_{28} 6.8/27 shifts to even lower q, q* = 0.170 (d/d_o = 1.46), and extra intensity is visible in the SAXS profile near q/q* = √4. After immersion in the pH 7.1 phosphate buffer, the primary peak is no longer visible in the SAXS profile of PS/PHD_{28} 6.8/27 (Figure 5.9a-v), although a large bump is visible in the range q ≈ 0.25-0.50 nm^{-1}. Without a primary peak, however, we are unable to identify the morphology or to assess the microdomain swelling in PS/PHD_{28} 6.8/27 at pH 7.1.

Notably, the PS/PHD_{28} 6.8/27 hydrogel does not disintegrate at pH 7.1, despite our inability to assign a structure from the SAXS profile. We were able to continue to monitor the gravimetric water uptake of PS/PHD_{28} 6.8/27 over the full pH range. The

gravimetric swelling ratio is shown as a function of pH in Figure 5.9b. At pH 4.7, the gravimetric swelling ratio for PS/PHD$_{28}$ 6.8/27 is 2.34, which is significantly larger than that of PS/PHD$_{28}$ 6.8/5.8, the lamellar equivalent (M/M_o = 1.23). More swelling is expected in PS/PHD$_{28}$ 6.8/27 than in PS/PHD$_{28}$ 6.8/5.8, because the PHD$_{28}$ content is higher in PS/PHD$_{28}$ 6.8/27 (v_{PHD} = 0.775) than in PS/PHD$_{28}$ 6.8/5.8 (v_{PHD} = 0.427).

As a final point, the swelling data collected by gravimetric techniques only qualitatively describe the volumetric expansion of PS/PHD and PS/PHD/PS lamellar hydrogels predicted by the microdomain swelling ratios. In all cases, the volumetric expansion in PS/PHD and PS/PHD/PS is greater than the volume of water imbibed by the hydrogel, as measured by gravimetric techniques. In accordance with the lattice models of polymer-solvent mixing,[41] this discrepancy suggests an increase in free volume within the samples when they are swollen. Similar free volume effects have been observed during the swelling of DMAEMA-containing hydrogels with hydrophobic groups.[42] Further, we observe that the free volume in swollen PS/PHD or PS/PHD/PS samples decreases with increasing DMAEMA content within PHD and is generally not affected by pH. More specifically, the volume expansion of PS/PHD$_{28}$ 6.8/5.8 and PS/PHD$_{28}$/PS 4.5/16/4.5 as measured by SAXS is 1.9 times greater (standard deviation = ± 0.2) than that predicted by the gravimetric data. In contrast, the volumetric expansion of PS/PHD$_{50}$ 5.4/9.8 is 1.7 times greater (standard deviation = ± 0.3) than the gravimetric volume expansion, and the volumetric expansion of PS/PHD$_{75}$ 6.7/14 and PS/PHD$_{75}$/PS 5.9/20/5.9 is 1.4 times greater (standard deviation = ± 0.3) than the gravimetric volume expansion. Given that the free volume present in PS/PHD or PS/PHD/PS hydrogels is not significantly affected by pH and therefore not directly related to the amount of water present in the sample, we are left to speculate that the change in free volume is largely related to the Flory interaction parameter, χ, between the polymer and water. For

DMAEMA-containing polymers in water, it has been demonstrated that χ is highly dependent on the DMAEMA content of the polymer.[43] The incorporation of HEMA into PHD microdomains results in an increase in χ between PHD and water, thus increasing the free volume within the swellable component of the hydrogel.

CONCLUSIONS

PS/PHD diblock copolymers and PS/PHD/PS triblock copolymers with varying DMAEMA content microphase separate to form well-ordered structures in the solid state, with glassy PS microdomains serving to anchor the swelling of PHD upon immersion in buffers of varying pH. PS/PHD/PS and PS/PHD hydrogels are shown to be pH-responsive, and the magnitude of their pH responsive can be controlled synthetically by adjusting the DMAEMA content. When PS/PHD/PS triblock copolymers are swollen in water, PS microdomains serve as physical crosslinks to hold the hydrogel together. In contrast, PS microdomains within PS/PHD diblock copolymers are not capable of serving as physical crosslinks. As such, PS/PHD diblock copolymers with high DMAEMA content (PS/PHD_{75} 6.7/14.0 or PS/PHD_{50} 5.4/9.8) fall apart after protonation of DMAEMA units. While we observe a loss of macroscopic integrity for these diblock copolymers, the lamellar microdomains within the samples continue to exhibit pH response characteristic of cationic hydrogels. Moreover, we demonstrated that lamella- and cylinder-forming diblock copolymer hydrogels containing PHD_{28} are capable of withstanding the osmotic pressure induced by protonation of the DMAEMA units. As a result, the diblock copolymer hydrogels exhibit microdomain and gravimetric swelling behavior equivalent to what has been observed for physically-crosslinked triblock copolymer hydrogels.

FIGURES

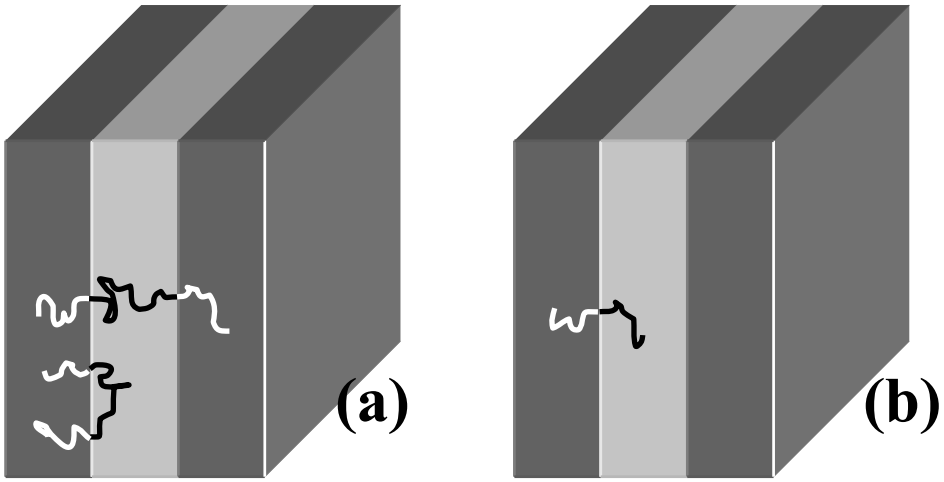

Figure 5.1. Illustration of lamella-forming (a) PS/PHD/PS triblock copolymer and (b) PS/PHD diblock copolymer. PS endblocks (white) in the triblock copolymer can anchor the PHD midblock (black) during swelling, provided that the two endblocks are localized in neighboring PS microdomains.

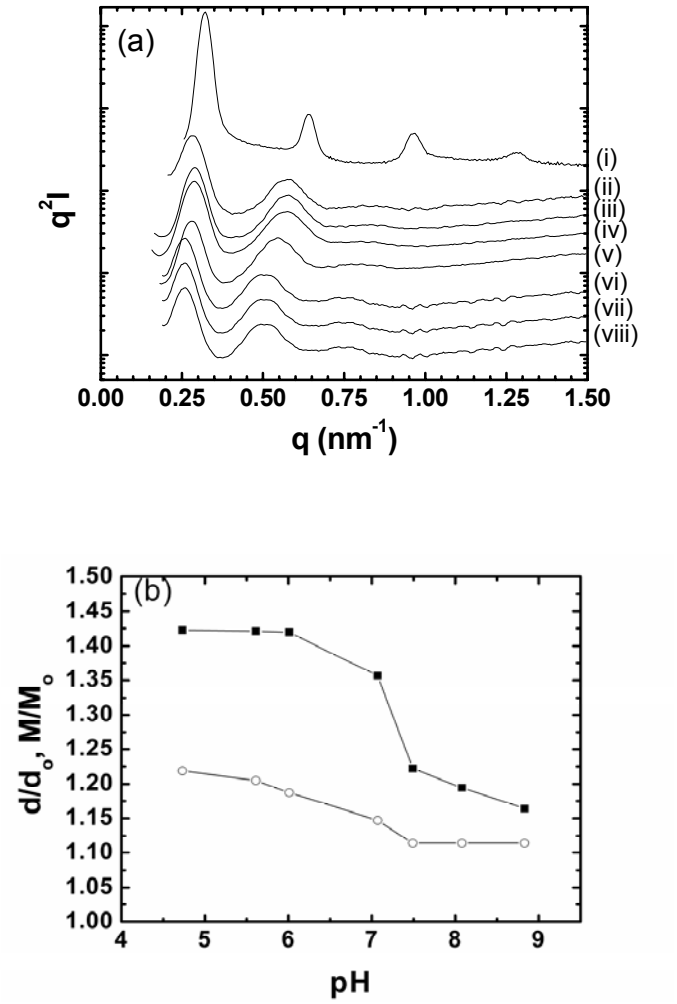

Figure 5.2. **(a)** Small-angle x-ray scattering profiles of PS/PHD_{28}/PS 4.5/16/4.5 in the solid state **(i)** and swollen in buffer solutions at pH 8.8 **(ii)**, pH 8.1 **(iii)**, pH 7.5 **(iv)**, pH 7.1 **(v)**, pH 6.0 **(vi)**, pH 5.6 **(vii)**, and pH 4.7 **(viii)**. **(b)** Gravimetric (M/M_o, ■) and microdomain (d/d_o, ○) swelling of PS/PHD_{28}/PS 4.5/16/4.5 as a function of decreasing pH.

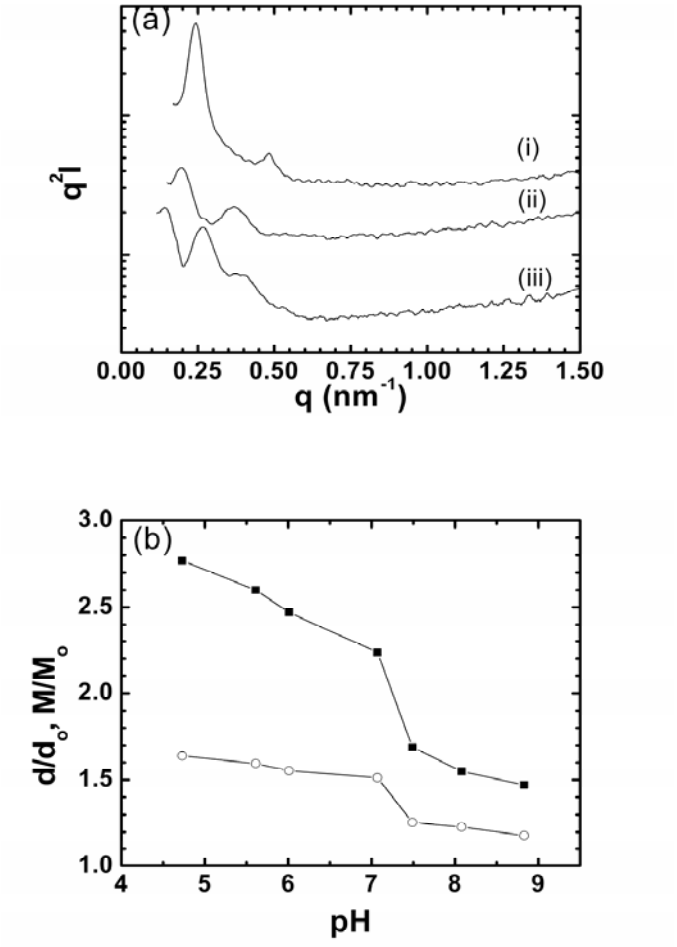

Figure 5.3. **(a)** Small-angle x-ray scattering profiles of PS/PHD_{75}/PS 5.9/20/5.9 in the solid state **(i)** and swollen in a phosphate buffer solution at pH 8.8 **(ii)** and pH 4.7 **(iii)**. **(b)** Gravimetric (M/M_o, ■) and microdomain (d/d_o, ○) swelling of PS/PHD_{75}/PS 5.9/20/5.9 as a function of decreasing pH.

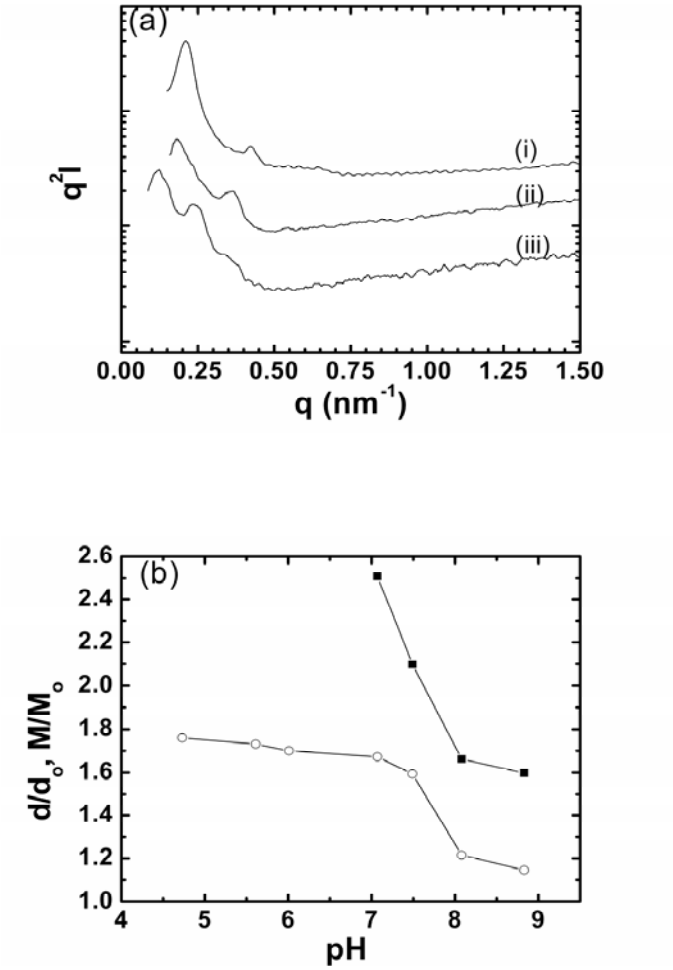

Figure 5.4. **(a)** Small-angle x-ray scattering profiles of PS/PHD$_{75}$ 6.7/14 in the solid state **(i)** and swollen in a phosphate buffer solution at pH 8.8 **(ii)** and pH 4.7 **(iii)**. **(b)** Gravimetric (M/M_o, ■) and microdomain (d/d_o, ○) swelling of PS/PHD$_{75}$ 6.7/14 as a function of decreasing pH. Below pH 7, PS/PHD$_{75}$ 6.7/14 loses macroscopic integrity so its macroscopic swelling cannot be assessed. The PS/PHD$_{75}$ 6.7/14 hydrogel maintains a lamellar microstructure throughout the experiment.

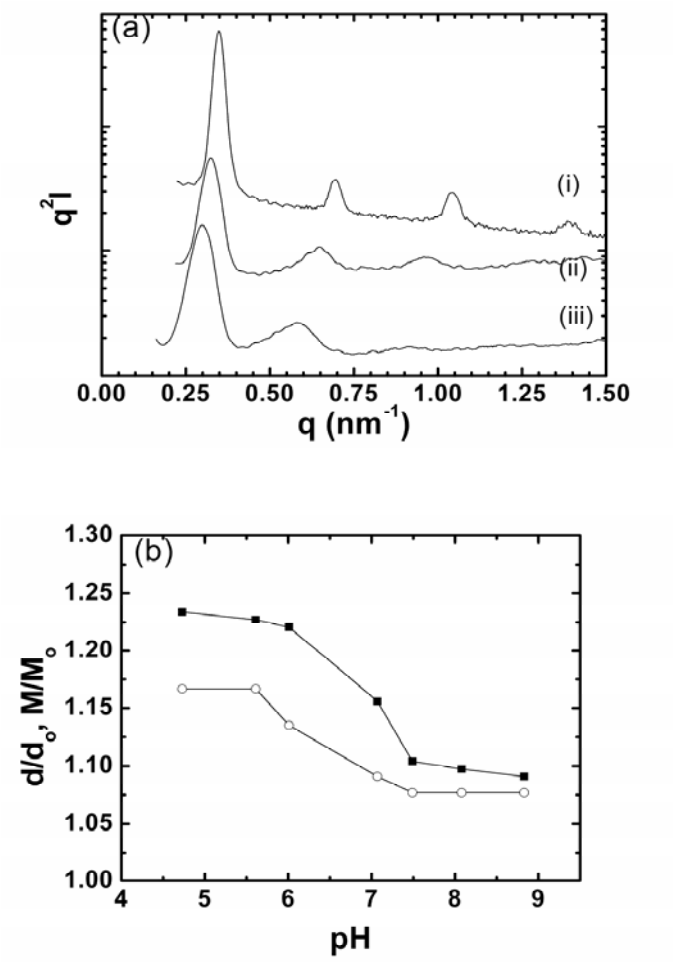

Figure 5.5. **(a)** Small-angle x-ray scattering profiles of PS/PHD$_{28}$ 6.8/5.8 in the solid state **(i)** and swollen in a phosphate buffer solution at pH 8.8 **(ii)** and pH 4.7 **(iii)**. **(b)** Gravimetric (M/M_o, ■) and microdomain (d/d_o, ○) swelling of PS/PHD$_{28}$ 6.8/5.8 as a function of decreasing pH.

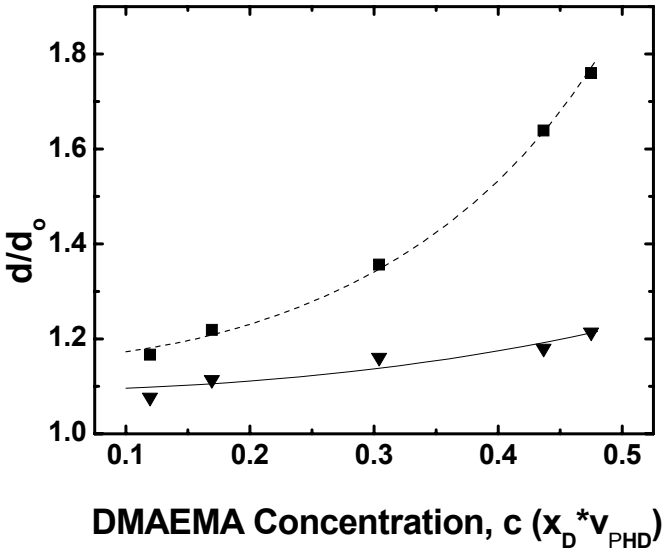

Figure 5.6. Normalized microdomain expansion in hydrogels of PS/PHD and PS/PHD/PS at pH 4.7 (■) and at pH 8.8 (▼), expressed in terms of the DMEAMA unit density. The dashed curve represents a fit to the pH 4.7 data derived from a modified Brannon-Peppas model for ionic hydrogels (Equation 5.2),[30] and the solid curve represents a fit to the pH 8.8 data.

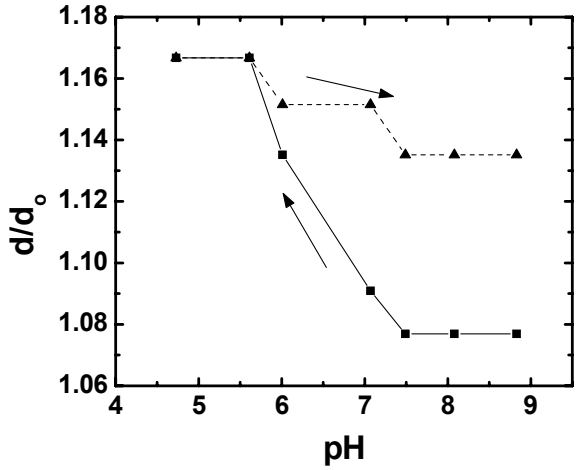

Figure 5.7. Microdomain swelling of PS/PHD$_{28}$ 6.8/5.8 with decreasing pH (■) and then with increasing pH (▲).

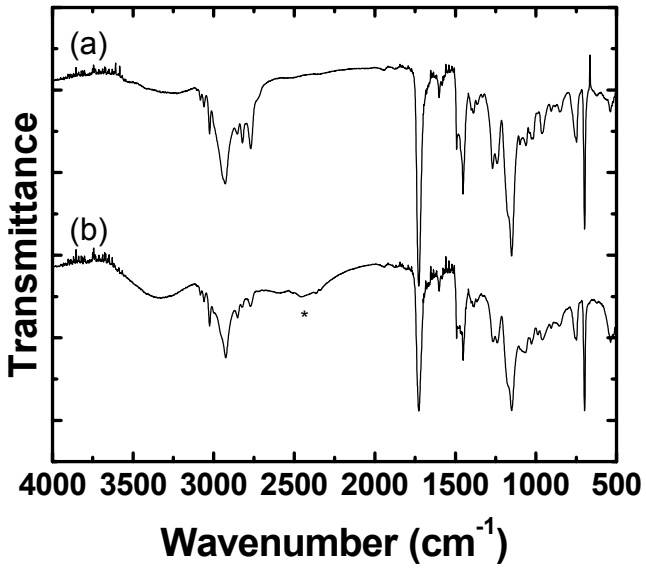

Figure 5.8. FTIR Transmittance of (a) PS/PHD$_{28}$ 6.8/5.8 and (b) PS/PHD$_{28}$ 6.8/5.8 after swelling to pH 4.7, return to pH 8.8, and dialysis to remove residual ions. In (b), * represents an NR_3^+ stretch.

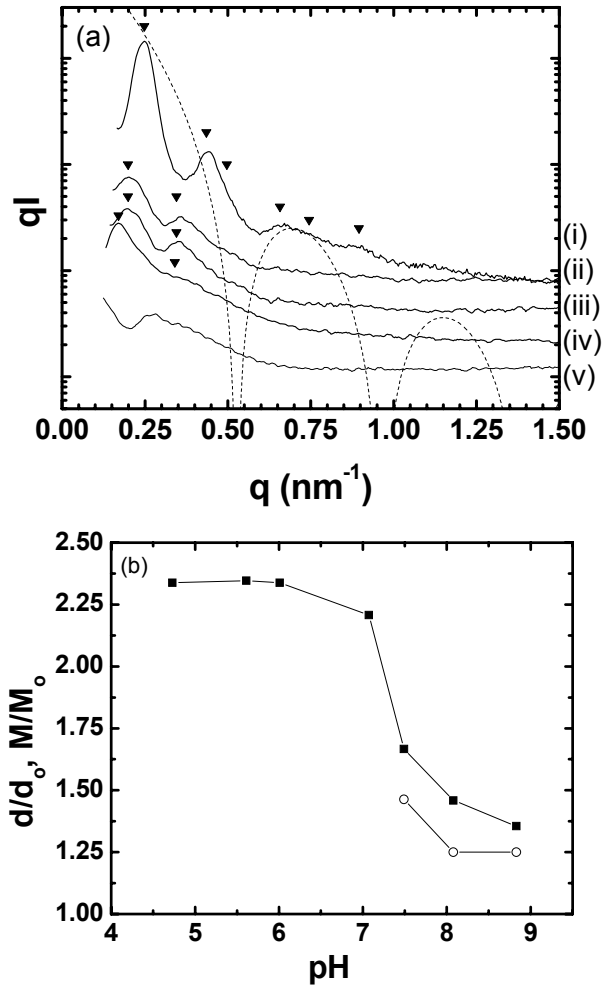

Figure 5.9. **(a)** Small-angle x-ray scattering profiles of PS/PHD$_{28}$ 6.8/27 in the solid state **(i)** and swollen in a phosphate buffer solution at pH 8.8 **(ii)**, pH 8.1 **(iii)**, pH 7.5 **(iv)**, and pH 7.1 **(v)**. The form factor curve[40] for individual cylinders of radius 7.3 nm is also shown (dashed curve). Markers (▼) are added at q/q* ratios of 1, √3, √4, √7, √9, √13 in **(i)**, at q/q* ratios of 1, √3 in **(ii)** and **(iii)**, and at q/q* ratios of 1, √4 in **(iv)**. **(b)** Gravimetric (M/M_o, ■) and microdomain (d/d_o, ○) swelling of PS/PHD$_{28}$ 6.8/27 as a function of decreasing pH. At pH's below pH 7.5, the primary peaks can no longer be resolved in the SAXS profiles, so microdomain swelling cannot be assessed. The PS/PHD$_{28}$ 6.8/27 hydrogel maintained its macroscopic integrity throughout the swelling experiments.

REFERENCES

1. Van de Wetering, P.; Moret, E. E.; Schuurmans-Nieuwenbroek, N. M. E.; Van Steenbergen, M. J.; Hennink, W. E. *Bioconjugate Chemistry* **1999,** 10, 589-597.

2. Fournier, D.; Hoogenboom, R.; Thijs, H. M. L.; Paulus, R. M.; Schubert, U. S. *Macromolecules* **2007,** 40, 915-920.

3. Van Tomme, S. R.; van Steenbergen, M. J.; De Smedt, S. C.; van Nostrum, C. F.; Hennink, W. E. *Biomaterials* **2005,** 26, 2129-2135.

4. Du, R.; Zhao, J. *Journal of Applied Polymer Science* **2004,** 91, 2721-2728.

5. Yilmaz, Z.; Akkas, P. K.; Sen, M.; Guven, O. *Journal of Applied Polymer Science* **2006,** 102, 6023-6027.

6. Brahim, S.; Narinesingh, D.; Guiseppi-Elie, A. *Biomacromolecules* **2003,** 4, 1224-1231.

7. Brahim, S.; Narinesingh, D.; Guiseppi-Elie, A. *Biomacromolecules* **2003,** 4, 497-503.

8. Traitel, T.; Kost, J.; Lapidot, S. A. *Biotechnology and Bioengineering* **2003,** 84, 20-28.

9. Traitel, T.; Cohen, Y.; Kost, J. *Biomaterials* **2000,** 21, 1679-1687.

10. Yuk, S. H.; Cho, S. H.; Lee, S. H. *Macromolecules* **1997,** 30, 6856-6859.

11. Kroupova, J.; Horak, D.; Pachernik, J.; Dvorak, P.; Slouf, M. *Journal of Biomedical Materials Research, Part B: Applied Biomaterials* **2006,** 76B, 315-325.

12. Siegel, R. A.; Firestone, B. A. *Macromolecules* **1988,** 21, 3254-9.

13. Dong, L.; Agarwal, A. K.; Beebe, D. J.; Jiang, H. *Nature* **2006,** 442, 551-554.

14. Satish, C. S.; Shivakumar, H. G. *Journal of Macromolecular Science, Part A: Pure and Applied Chemistry* **2007,** 44, 379-387.

15. Kopecek, J.; Yang, J. *Polymer International* **2007,** 56, 1078-1098.

16. Topham, P. D.; Howse, J. R.; Crook, C. J.; Gleeson, A. J.; Bras, W.; Armes, S. P.; Jones, R. A. L.; Ryan, A. J. *Macromolecular Symposia* **2007,** 256, 95-104.

17. Stoltz, M. J.; Brazel, C. S. *Journal of Applied Polymer Science* **2003,** 88, 2974-2981.

18. Triftaridou, A. I.; Hadjiyannakou, S. C.; Vamvakaki, M.; Patrickios, C. S. *Macromolecules* **2002,** 35, 2506-2513.

19. Nykaenen, A.; Nuopponen, M.; Laukkanen, A.; Hirvonen, S.-P.; Rytelae, M.; Turunen, O.; Tenhu, H.; Mezzenga, R.; Ikkala, O.; Ruokolainen, J. *Macromolecules* **2007,** 40, 5827-5834.

20. Victorov, A. *Fluid Phase Equilibria* **2005,** 227, 9-17.

21. Guice, K. B.; Loo, Y.-L. *Macromolecules* **2006,** 39, 2474-2480.

22. Guice, K. B.; Loo, Y.-L. *Macromolecules* **2007,** 40, 9053 -9058.

23. Krasia, T. C.; Patrickios, C. S. *Macromolecules* **2006,** 39, 2467-2473.

24. Achilleos, M.; Krasia-Christoforou, T.; Patrickios, C. S. *Macromolecules* **2007,** 40, 5575-5581.

25. Themistou, E.; Patrickios, C. S. *Macromolecules* **2007,** 40, 5231-5234.

26. Triftaridou, A. I.; Kafouris, D.; Vamvakaki, M.; Georgiou, T. K.; Krasia, T. C.; Themistou, E.; Hadjiantoniou, N.; Patrickios, C. S. *Polymer Bulletin* **2007,** 58, 185-190.

27. Triftaridou, A. I.; Vamvakaki, M.; Patrickios, C. S. *Biomacromolecules* **2007,** 8, 1615-1623.

28. Vamvakaki, M.; Patrickios, C. S.; Lindner, P.; Gradzielski, M. *Langmuir* **2007,** 23, 10433-10437.

29. Shibayama, M.; Hashimoto, T.; Kawai, H. *Macromolecules* **1983,** 16, 16-28.

30. Brannon-Peppas, L.; Peppas, N. A. *Polymer Bulletin* **1988,** 20, 285-9.

31. Polymer Handbook, 4th Ed. In Brandrup, J.; Immergut, E. H.; Grulke, E. A., Eds. Wiley-Interscience: New York, 1999, VI-203.

32. Martin-Gomis, L.; Cuervo-Rodriguez, R.; Fernandez-Monreal, M. C.; Madruga, E. L.; Fernandez-Garcia, M. *Journal of Polymer Science, Part A: Polymer Chemistry* **2003,** 41, 2659-2666.

33. Kishi, H.; Naitou, T.; Matsuda, S.; Murakami, A.; Muraji, Y.; Nakagawa, Y. *Journal of Polymer Science, Part B: Polymer Physics* **2007,** 45, 1425-1434.

34. Bendejacq, D.; Ponsinet, V.; Joanicot, M. *European Physical Journal E: Soft Matter* **2004,** 13, 3-13.

35. Cohen, Y.; Thomas, E. L. *Macromolecules* **2003,** 36, 5265-5270.

36. Flory, P. J.; Rehner, J., Jr. *Journal of Chemical Physics* **1943,** 11, 521-6.

37. Dong, W.; Xu, Y.; Yuan, C. *Cellulose* **2007,** 14, 331-336.

38. Ozden, B. O.; Florence, A. T. *European Polymer Journal* **1995,** 31, 135-144.

39. Asakawa, N.; Sato, D.; Sakurai, M.; Inoue, Y. *Journal of Physical Chemistry A* **2000,** 104, 2716-2723.

40. Porod, G., The Principles of Diffraction, Section 1, General Theory. In *Small-Angle X-ray Scattering*, Glatter, O., Kratky, O., Ed. Academic Press: London, 1982, pp. 17-51.

41. Sanchez, I. C.; Lacombe, R. H. *Macromolecules* **1978,** 11, 1145-56.

42. Suevegh, K.; Domjan, A.; Vanko, G.; Ivan, B.; Vertes, A. *Macromolecules* **1998,** 31, 7770-7775.

43. Emileh, A.; Vasheghani-Farahani, E.; Imani, M. *European Polymer Journal* **2007,** 43, 1986-1995.

Chapter 6. Temperature Responsive Hydrogels from Diblock Copolymers Containing PHD

INTRODUCTION

The study of block copolymer gels has enabled the investigation of a wide range of morphological transitions,[1-9] and the observation of several morphologies that are not common in diblock copolymer melts.[5] For example, Lodge et al. observed alternating lamellae, bicontinuous cubic gyroid, hexagonally-packed cylinders, spheres organized in face-centered- and body-centered-cubic lattices in a symmetric polystyrene-*b*-polyisoprene, PS/PI, diblock copolymer by changing both temperature and the amount of diethyl phthalate (a selective solvent for PS) that is present.[6] In addition to PS/PI in a variety of other organic solvents,[1,3,4,6,8,10] other common polymer-solvent combinations used in the investigation of block copolymer gels include poly(ethylene oxide)-based amphiphilic block copolymers in water.[2,7,9,11] In all of the above mentioned systems, the block copolymer-solvent interactions are only weakly affected by external stimuli, e.g., temperature or pH. Drastic changes in polymer concentration are thus necessary to access different morphologies. The incorporation of stimuli-responsive units within block copolymer architectures should provide an added dimension of tunability, allowing access to further morphological richness and kinetic complexity in the phase behavior of block copolymer gels. For example, poly(DMAEMA) is pH-responsive[12] and exhibits a LCST in water.[13] Block copolymers hydrogels containing DMAEMA should provide a greater temperature response thereby allowing the investigation of a wider range of morphological transformations by tuning temperature alone.

Controlled free-radical polymerization techniques, such as atom transfer radical polymerization (ATRP),[14] have been shown to yield well-defined DMAEMA-containing

homo- and block copolymers.[15-21] It has been suggested, however, that the use of LCST-exhibiting polymers to investigate the phase behavior of block copolymer gels might limit accessible morphological transitions due to their weak temperature response above and below the LCST.[8] As such, it is more suitable to copolymerize DMAEMA with a second monomer in order to better control the degree of temperature response. To this end, we demonstrated the statistical copolymerization of HEMA and DMAEMA at their compositional azeotrope in DMF,[15] or over a broad range of compositions in DMSO.[16] Block copolymer hydrogels comprised of statistical copolymers of HEMA and DMAEMA at varying DMAEMA content, chemically linked to a hydrophobic but rubbery block, should exhibit significant morphological richness that is accessible by tuning temperature and pH.

In this chapter, we present model block copolymer hydrogels of PMA/PHD that undergo thermally reversible morphological transformations over a large phase space but over a narrow temperature window. PMA was chosen as a second block because it does not sorb water significantly,[22] and has a glass transition temperature below room temperature (T_g = 12.5ºC). The low glass transition temperature of PMA enables the diblock copolymers to reorganize at and above ambient temperatures. As such, we can reversibly access multiple morphological transitions in a single block copolymer hydrogel by changing temperature alone.

RESULTS AND DISCUSSION

All the block copolymers studied in this chapter adopt the alternating lamellar morphology in the solid state. Specifically, we refer to Figure 4.6 (PMA/PHD_{75} 13/11, PMA/PHD_{63} 10.0/9.7, PMA/PHD_{50} 12/15, and PMA/PHD_{28} 8.0/13), Figure 5.5 (PS/PHD_{28} 6.8/5.8), and Figure 4.12 (P*t*BA/PHD_{28} 15/18) for relevant SAXS profiles of the block copolymers in the solid state.

Reversible phase transformations of PMA/PHD$_{75}$ 13/11

A previously-annealed, SAXS-verified ordered PMA/PHD$_{75}$ 13/11 sample (0.08 g) was placed in approximately 50 mL of deionized water and was allowed to equilibrate for 24 to 48 h. PMA/PHD$_{75}$ 13/11 swells significantly but does not dissolve in water. At room temperature, the swollen sample consists of approximately 70% water by total mass. The water uptake at specific temperatures appears to be independent of the amount of water the specimen is immersed in. It has been previously demonstrated that the swellability of PS-*b*-poly(acrylic acid), PS/PAA, diblock copolymers at temperatures above the glass transition temperature of the PS block is determined by the hydrophobicity of PS and the degree of ionization of PAA.[23,24] In our system, PMA is the hydrophobic component that prevents the diblock copolymer from dissolution in water. Additionally, since poly(HEMA) only swells and is not completely soluble in water, its incorporation within the PHD block further suppresses solubility. When immersed in water for extended periods of time, PMA/PHD$_{75}$ 13/11 remains optically clear and homogenous.

We can, however, ionize the DMAEMA units within the PHD block when we immerse PMA/PHD$_{75}$ 13/11 in an aqueous buffer below the pKa of DMAEMA at 7.5.[12] Swelling the diblock copolymer under these circumstances results in macroscopic disintegration and dissolution of the sample. This observation is in contrast with our observations of PS/PHD$_{75}$ 6.7/14 during pH studies in Chapter 5 (Figure 5.4), where PS/PHD$_{75}$ 6.7/14 only disintegrated into multiple smaller pieces but did not completely dissolve upon immersion in phosphate buffers below pH 7.5. That PS/PHD$_{75}$ 6.7/14 did not completely dissolve was attributed to the high glass transition temperature of PS (T_g = 105°C). In PS/PHD$_{75}$ 6.7/14, the lamellar microdomains are preserved because PS is glassy during swelling, thereby preventing complete dissolution of PS/PHD$_{75}$ 6.7/14. In

contrast, because PMA is rubbery (T_g = 12.5ºC), it is not able to prevent the solubilization of PMA/PHD_{75} 13/11 under conditions of more extreme swelling, such as when the majority of DMAEMA units are ionized.

Figure 6.1 contains the SAXS profiles of the PMA/PHD_{75} 13/11 swollen in water at three representative temperatures (22ºC, 37ºC, 52ºC). The SAXS profile of PMA/PHD_{75} 13/11 in the solid state (Figure 6.1a) is also included for comparison. The SAXS profiles acquired at a specific temperature are identical whether we approach this temperature by heating or cooling. The SAXS profile collected on the PMA/PHD_{75} 13/11 hydrogel at 22ºC (Figure 6.1b) exhibits a primary peak at q* = 0.128 nm^{-1}, which is significantly lower than the primary peak position in the SAXS profile acquired on PMA/PHD_{75} 13/11 in the solid state (q* = 0.290 nm^{-1}). The SAXS profile in Figure 6.1b also exhibits a broad bump between q = 0.24 – 0.33 nm^{-1}. This bump is consistent with a form factor maximum for spheres with an average radius of 22 nm (dashed curve).[25] Given that water is only absorbed in the PHD phase and not in PMA, PMA must constitute spheres in a PHD matrix. The absence of higher-order structure factor peaks in combination with the breadth of the primary peak ($W_{0.5}$ = 0.074 nm^{-1}; compared to $W_{0.5}$ = 0.046 nm^{-1} for PMA/PHD_{75} 13/11 in the solid state) in the SAXS profile at 22ºC indicates that the specimen is disordered. Characteristically similar SAXS profiles have previously been described as a disordered, interacting micellar morphology, D.[8]

The SAXS profile collected at 37ºC (Figure 6.1c) exhibits a primary peak at q* = 0.190 nm^{-1} ($W_{0.5}$ = 0.066 nm^{-1}) with higher-order reflections at q/q* ratios of √3 and √4, suggestive of a hexagonally-packed cylindrical morphology, H.[26] Since PMA does not sorb water,[22] PMA must form the discrete cylinders in the water-swollen PHD matrix. The morphological transformation from disordered micelles to ordered PMA cylinders on increasing temperature is indicative of a decrease in the relative volume fraction of the

PHD phase with increasing temperature. A decrease in the relative volume fraction of the PHD phase strongly suggests reduced water uptake at 37°C compared to that at 22°C. We attribute this deswelling in the PHD matrix to a decrease in hydrophilicity of the DMAEMA units with increasing temperature.[27] In aqueous poly(DMAEMA) homopolymer solutions, this decrease in hydrophilicity gives rise to the presence of an LCST at 46°C,[13] below which the solution is homogenous and above which the polymer becomes completely insoluble and precipitates out of solution.[27] In PMA/PHD_{75} 13/11, the PMA block and the HEMA units in the PHD block serve to limit the solubility of the diblock copolymer in water. We are thus able to reversibly access the different morphologies associated with states of intermediate water uptake.

We have attempted to track the kinetics of transformation from D to H in PMA/PHD_{75} 13/11 and found the transition to be fast. D to H transformations are generally completed in less than 1 h (the time required to acquire a single SAXS profile). We show successive SAXS traces (1 h each) collected on the PMA/PHD_{75} 13/11 solution during a temperature ramp from 22°C to 37°C, with a temperature equilibration time of less than 30 min, in Figure 6.2a. We also compiled the primary peak position extracted from each SAXS profile, as a function of time from the start of the temperature ramp, in Figure 6.2b. The primary peak position is constant after the first scan, and we see no further change in the higher-order reflections (Figure 6.2a) after this time. That we see no changes in the SAXS profile after the first profile suggests that the morphological transformation is complete shortly after temperature equilibration at 37°C.

Subsequent cooling of the PMA/PHD_{75} 13/11 solution to 37ºC or 22ºC results in a morphological transition back to H or D, respectively. The transition back to H or D, however, is significantly slower compared to the morphological transformations we observe on heating, occurring over a period >10 h. We monitored the morphological

evolution of the PMA/PHD_{75} 13/11 hydrogel while cooling from of 37ºC or 22ºC, wherein the temperature equilibrated at 22°C after approximately 1.25 h. SAXS profiles were acquired for 1 h each successively over 8 h, and a final SAXS profile was collected after equilibration overnight. Each of the collected SAXS profiles is shown in Figure 6.3a, with the time evolution of the primary peak position shown in Figure 6.3b. In contrast to the morphological transition on heating (Figure 6.2), the transition on cooling is significantly slower. Drastically different rates of phase transformation on heating and cooling have previously been reported for PS/PI and PS/polydimethylsiloxane block copolymers in selective solvents.[1,28] However, the rate of phase transformation was faster upon disordering for both of these examples.[1,28] In our case, we speculate that the faster transformation on ordering (heating) occurs because PMA/PHD_{75} 13/11 squeezes water out due to increased hydrophobicity in the PHD_{75} phase. Conversely, the slower transformation on disordering (cooling) is diffusion limited due to the fact that PMA/PHD_{75} 13/11 exists at a more collapsed state at the beginning of the cooling experiment.

The SAXS profile of the PMA/PHD_{75} 13/11 hydrogel collected at 52ºC (Figure 6.1c) exhibits a primary peak at $q^* = 0.269$ nm^{-1} ($W_{0.5} = 0.047$ nm^{-1}) and higher-order reflections at q/q^* ratios of 2 and 3. The primary peak position at 52°C now approaches that of the diblock copolymer in the solid state. The spacing of the higher-order reflections indicates that the PMA/PHD_{75} 13/11 solution adopts a lamellar morphology at 52°C and suggests that the sample has undergone a second morphological transition from H to alternating lamellae (L) on heating.[26] Previous reports on phase transformations in block copolymer gels have relied on tuning both the polymer concentration and temperature,[1-9] so multiple samples at varying concentrations were required to access changes in morphologies. In our case, we have been able to traverse a large phase space

(from D to H to L) with a single PMA/PHD_{75} 13/11 hydrogel by changing temperature alone. We attribute the expanded range of morphological transitions in the PMA/PHD_{75} 13/11 hydrogel to the presence of functional DMAEMA units within the PHD block. Specifically, the change in hydrophilicity of the DMAEMA units as a function of temperature augments the swelling characteristics; we are thus able to access multiple morphologies over a narrow temperature window ($\Delta T = 30°C$). As with the transition from D to H, the H to L transition is also completed in less than 1 h, whereas transitions from L to H upon cooling are considerably slower.

In Figure 6.4, we have plotted the interdomain spacing of the swollen PMA/PHD_{75} 13/11 as a function of temperature. Each data point represents an individual SAXS profile. The data points are labeled D, H, or L depending on which morphology the sample exhibits at the specified temperatures. Figure 6.4 shows the succession from D to H to L with increasing temperature; these phases are accessible reversibly as the individual SAXS profiles were collected at random on both heating and cooling. At low temperatures ($T < 32ºC$), the PMA/PHD_{75} 13/11 hydrogel forms disordered micelles with average correlation distances between micelles of greater than 40nm. This correlation distance decreases with increasing temperature at a rate of -1.45nm/ºC. At intermediate temperatures ($32ºC < T < 42ºC$), the block copolymer hydrogel adopts a hexagonally-packed cylindrical morphology. The characteristic hexagonal spacing decreases with increasing temperature, at a rate of -0.85nm/ºC. At high temperatures ($T > 42ºC$), the PMA/PHD_{75} 13/11 hydrogel adopts an alternating lamellar morphology; its characteristic lamellar spacing also decreases with increasing temperature, at a rate of -0.26nm/ºC. While gels of PS/PI in selective solvents and poly(ethylene oxide)-*b*-poly(propylene oxide), PEO/PPO, in water swell with increasing temperature,[11] hydrogels of poly(ethylene oxide)-*b*-poly(butylene oxide), PEO/PBO, have been reported to deswell

with increasing temperature due to the hydrophobicity of the BO segments.[7] In addition to the hydrophobicity of the MA segments, we attribute the deswelling in the PMA/PHD$_{75}$ 13/11 hydrogel to a decrease in hydrophilicity of the DMAEMA units with increasing temperature.[13] As reference, we have also plotted the characteristic lamellar spacing of PMA/PHD$_{75}$ 13/11 in the solid state (L^d) as a function of temperature in Figure 6.4. In PMA/PHD$_{75}$ 13/11, the characteristic spacing also decreases with increasing temperature, due to a decreasing χ with temperature (Figure 4.7). The decrease in d in solid state, however, is significantly smaller (-0.02nm/^{o}C) compared to those observed for the different morphologies in swollen PMA/PHD$_{75}$ 13/11.

Temperature response in PMA/PHD$_{63}$ 10/9.7, PMA/PHD$_{50}$ 12/15, and PMA/PHD$_{28}$ 8.0/13 hydrogels

It has been reported that the temperature-sensitive nature of poly(DMAEMA) can be tailored by copolymerizing DMAEMA with other hydrophilic monomers.[13] To demonstrate the tunability of PMA/PHD, we carried out temperature-response experiments on hydrogels of PMA/PHD$_{63}$ 10/9.7, PMA/PHD$_{50}$ 12/15, and PMA/PHD$_{28}$ 8.0/13, where the molecular weights of the block copolymers are nominally the same but the DMAEMA content in the PHD block varies (indicated by subscript). All PMA/PHD diblock copolymers in this study adopt an alternating lamellar morphology in the solid state. Unlike the PMA/PHD$_{75}$ 13/11 hydrogel, which exhibits a disordered micellar phase, these block copolymers readily adopt the H morphology when swollen with water at room temperature. As an example, the SAXS profile of the PMA/PHD$_{50}$ 12/15 hydrogel, collected at 22^{o}C is shown in Figure 6.5. The SAXS profile exhibits a primary peak at q* = 0.211 nm^{-1}, with higher-order reflections at q/q* = $\sqrt{4}$, $\sqrt{7}$, and $\sqrt{9}$. The higher-order reflections are consistent with the H morphology.[26] In Chapter 4, the SAXS profile collected on PMA/PHD$_{50}$ 12/15 in the solid state (Figure 4.19c) did not reveal any higher-order reflections and showed noticeable curvature at higher q, which was

attributed to a low electron density contrast (ratio of electron densities = 1.005) and to the fact that the block copolymer is not particularly strongly segregated.[29] As water is a selective solvent for PHD_{50}, the incorporation of water into PMA/PHD_{50} 12/15 resulted in a net increase in the interblock segregation strength between PHD_{50} (aqueous) and PMA.

The interdomain spacings of each of the PMA/PHD hydrogels decrease with increasing temperature. We have chosen to focus on the thermal response of PMA/PHD hydrogels in the H phase. For each block copolymer, we compared the interdomain spacing of the hexagonal lattice at given temperatures, d, with the interdomain spacing of the block copolymer hydrogel when it first exhibited the H phase during our temperature ramp experiments, $d_{H,o}$. $d_{H,o}$ is the interdomain spacing of the block copolymer hydrogel at 22°C for PMA/PHD_{63} 10/9.7, PMA/PHD_{50} 12/15, and PMA/PHD_{28} 8.0/13, while $d_{H,o}$ is the interdomain spacing at 32°C for PMA/PHD_{75} 13/11. The normalized interdomain spacings, $d/d_{H,o}$, for all four block copolymer hydrogels in the H phase are plotted in Figure 6.6. We have connected successive data points with dashed lines for clarity. The temperature dependence of deswelling within the H phase appears to be strongest in PMA/PHD_{75} 13/11, and it weakens with decreasing DMAEMA content. Decreasing the DMAEMA content in the block copolymers thus dramatically influences the temperature response of the deswelling characteristics within a single phase.

In addition, the DMAEMA content within the PHD block determines the number of morphological transitions that can be observed over the selected temperature window. The PMA/PHD_{50} 12/15 and PMA/PHD_{28} 8.0/13 hydrogels retain the H morphology over the entire temperature window. In contrast, PMA/PHD_{63} 10/9.7 undergoes a phase transformation from H to L at 54°C. SAXS profiles collected on the PMA/PHD_{63} 10/9.7 hydrogel at 37°C and at 57°C are shown in Figure 6.7. The SAXS profile collected at

37°C (Figure 6.7a) exhibits a primary peak at q* = 0.261 nm^{-1}, with higher-order reflections at q/q* = √3, √4, and √7. The locations of the higher-order reflections are consistent with the H morphology.[26] The SAXS profile collected at 57°C (Figure 6.7b) exhibits a primary peak at q* = 0.331 nm^{-1} and a higher-order reflection at q/q* = 2, which is consistent with the L morphology.[26] While no morphological transitions are observed for PMA/PHD_{50} 12/15 and PMA/PHD_{28} 8.0/13, one H to L transition is observed for PMA/PHD_{63} 10/9.7, and two transitions (D to H to L) are observed for PMA/PHD_{75} 13/11. The number of observed morphological transitions over a given temperature range thus also increases with increasing DMAEMA content.

Temperature response of PS/PHD_{28} 6.8/5.8 and P*t*BA/PHD_{28} 15/18

During the pH studies on the lamella-forming diblock copolymer PS/PHD_{28} 6.8/5.8, we observed that the block copolymer hydrogel maintained its lamellar morphology, which we attributed to the presence of glassy PS microdomains that preserve the lamellar structure during swelling. Similarly, the PS/PHD_{28} 6.8/5.8 hydrogel maintains its lamellar morphology when swollen in deionized water. The temperature response of swollen PS/PHD_{28} 6.8/5.8 was characterized by SAXS, and the data are shown in Figure 6.8 (▼). For ease of comparison, we plotted the interdomain spacing of the block copolymer, relative to that of the lamellar block copolymer hydrogel at the lowest temperature ($d_{L,o}$), as a function of temperature. We also replotted the swelling data from PMA/PHD28 8.0/13 (□; from Figure 6.6) in Figure 6.8, for comparison. We observe no change in the interdomain spacing of PS/PHD_{28} 6.8/5.8 hydrogel with increasing temperature. By comparison, the interdomain spacing of the PMA/PHD_{28} 8.0/13 hydrogel immersed in deionized water decreases by 12% as the sample is heated from T = 22°C to T = 63°C (Figure 6.6). PS/PHD_{28} 6.8/5.8 and PMA/PHD_{28} 8.0/13 both have the same composition ($\overline{F_D}$ = 0.28) in the PHD block, and both block copolymer

adopt the alternating lamellar morphology in the solid state. The primary difference between the two block copolymers is the choice of the hydrophobic block. The swelling of PHD_{28} microdomains in the PS/PHD_{28} 6.8/5.8 hydrogel is anchored by glassy PS microdomains, resulting in a lamellar hydrogel at all temperatures. In contrast, rubbery PMA microdomains allow for morphological transformation from L to H in the PMA/PHD_{28} 8.0/13 hydrogel when immersed in deionized water. Because PHD_{28} swells to occupy the matrix in PMA/PHD_{28} 8.0/13, the block copolymer is capable of imbibing more water than the lamellar PS/PHD_{28} 6.8/5.8.[30] We speculate that the absence of a temperature response in the PS/PHD_{28} 6.8/5.8 hydrogel is associated with reduced water uptake at lower temperatures (compared to that of PMA/PHD_{28} 8.0/13), which is a consequence of having glassy PS lamellar microdomains during swelling.

As a final comparison, we explored the temperature response of a hydrogel containing P*t*BA/PHD_{28} 15/18, an amphiphilic block copolymer that forms lamellae in the solid state. Like PS, P*t*BA is hydrophobic and glassy at ambient conditions (T_g = 41°C; Figure 4.4). However, P*t*BA has a glass transition temperature that is experimentally accessible. As such, P*t*BA/PHD hydrogels should behave like PS/PHD hydrogels at temperatures below 41°C, but they should behave like PMA/PHD hydrogels when heated above the glass transition temperature of P*t*BA. SAXS profiles collected on P*t*BA/PHD_{28} 15/18 in the solid state, and of the P*t*BA/PHD_{28} 15/18 hydrogel immersed in deionized water at 20°C and at 63°C, and then subsequently cooled to 20°C are shown in Figure 6.8. The SAXS profile collected on P*t*BA/PHD_{28} 15/18 in the solid state (Figure 6.8a) exhibits a primary peak at q* = 0.211 nm^{-1}, with higher-order reflections at q/q* = 2, 3, 4. The positions of the higher-order reflections are consistent with the L morphology.[26] The SAXS profile of the P*t*BA/PHD_{28} 15/18 hydrogel immersed at 20°C (Figure 6.8b) exhibits a primary peak at q* = 0.182 nm^{-1}, which is shifted to a lower q

compared to that of the sample in the solid state (d/d_o = 1.16), with higher-order reflections[26] at q/q* = 2 and 4. The positions of the higher-order reflections are consistent with the L morphology.[26] Immersion of P*t*BA/PHD_{28} 15/18 in water, at temperatures below the glass transition temperature of P*t*BA, results in swelling of the PHD_{28} microdomains but no structural rearrangement of the lamellar hydrogel.

Upon heating to 63°C, the SAXS profile of the P*t*BA/PHD_{28} 15/18 hydrogel (Figure 6.8c) exhibits a primary peak at q* = 0.161 nm^{-1}, which is shifted to a lower q compared to that of the block copolymer hydrogel at 20°C. A decrease in the primary peak position upon heating is different from what had been observed with PMA/PHD block copolymer hydrogels, which generally exhibit a decrease in characteristic spacing with increasing temperature. In the SAXS profile of the P*t*BA/PHD_{28} 15/18 hydrogel at 63°C, we also observe a higher-order reflection at q/q* = $\sqrt{3}$ and two large bumps with maxima at q ≈ 0.57 nm^{-1} and q ≈ 0.85 nm^{-1}. The location of the higher-order reflections in Figure 6.10c is consistent with the H morphology.[26] To account for the bumps in the SAXS profile at 63°C, we fitted the data to the form factor equation for cylinders (Equation 2.18),[31] with a cylindrical radius of 9.3 nm (dashed curve). A minimum in the form factor curve near q/q* = $\sqrt{7}$ explains the absence of this higher-order reflection in the SAXS profile. While we do not have enough data to explicitly determine the exact radius of P*t*BA cylinders because we cannot determine an apparent v_{PHD} of the swollen block copolymer, we find reasonable agreement between the bumps observed on the SAXS profile and peak maxima from the form factor curve for cylinders with a radius of 9.3 nm. Taken together, the SAXS data suggest that P*t*BA/PHD_{28} 15/18 undergoes a morphological transition from L to H upon heating, with hydrophobic P*t*BA transforming into cylinders with radii of 9.3 nm in a PHD_{28} matrix in the H morphology. We attribute this morphological transition to the devitrification of P*t*BA microdomains when the

hydrogel is heated above the glass transition temperature of P*t*BA (T_g = 41°C) which in turn enables P*t*BA/PHD_{28} 15/18 to structurally rearrange.[30]

Upon cooling of the P*t*BA/PHD_{28} 15/18 hydrogel back to 20°C, and allowing the sample to equilibrate in deionized water at 20°C overnight, the primary peak in the SAXS profile (Figure 6.8d) shifts to an even lower q* of 0.145 nm^{-1} (d/d_o = 1.46). The SAXS profile exhibits higher-order reflections at $q/q^* = \sqrt{3}$ and $\sqrt{4}$, which are consistent with the H morphology.[26] The profile also exhibits two broad bumps with maxima at $q \approx 0.57$ nm^{-1} and $q \approx 0.85$ nm^{-1}. These bumps occur in the same positions in the SAXS profile as the form factor maxima (dashed curve) we previously attributed to isolated P*t*BA cylinders with 9.3 nm radii (Figure 6.8c), which further confirms that the hydrogel exhibits the H morphology with cylinders of the same radius upon cooling to 20°C. Given that the P*t*BA/PHD_{28} 15/18 hydrogel exhibits the H morphology at 63°C and upon cooling to 20°C, we can directly compare the characteristic domain spacings of the hydrogel, extracted from the primary peak positions in the SAXS profiles collected at each temperature. The interdomain spacing of the H-forming P*t*BA/PHD_{28} 15/18 hydrogel collected at 63°C is 10% smaller than that at 20°C. This temperature-dependent change in the characteristic spacing of the P*t*BA/PHD_{28} 15/18 hydrogel is similar to that observed in the PMA/PHD_{28} 8.0/13 hydrogel. Devitrification of the P*t*BA microdomains in the P*t*BA/PHD_{28} 15/18 hydrogel thus enables us to obtain the temperature response that we had previously observed for PMA/PHD hydrogels.

CONCLUSIONS

We investigated the temperature response of a series of PMA/PHD amphiphilic diblock copolymer hydrogels with varying DMAEMA content. These diblock copolymers hydrogels deswell with increasing temperature, due to a decrease in hydrophilicity of the DMAEMA units within the PHD block with temperature.

Accordingly, the extent of change in swelling due to a change in temperature for PMA/PHD block copolymer hydrogels depends strongly on the DMAEMA content within the PHD block. PMA/PHD diblock copolymer hydrogels are able to undergo reversible morphological transformations in response to changes in temperature. Specifically, we observed reversible morphological transitions from disordered, interacting spherical micelles to hexagonally-packed cylinders to alternating lamellae in a PMA/PHD hydrogel by varying temperature alone. The number of morphological transitions that are observed over a specific temperature range is also related to the DMAEMA content. By tuning the composition of the PHD block, we successfully designed block copolymers hydrogels that exhibit zero, one, or two morphological transformations over a narrow temperature range of 30°C.

We also demonstrated that the choice of the hydrophobic block in PHD-containing amphiphilic diblock copolymers presents additional room to tune the temperature response of the diblock copolymers in water. While PMA/PHD diblock copolymers deswell with increasing temperature, PS/PHD diblock copolymer hydrogels exhibit limited swelling due to the presence of glassy PS lamellae. Accordingly, PS/PHD is not temperature responsive when immersed in water.

P*t*BA/PHD diblock copolymer hydrogels also exhibit limited swelling when initially immersed in deionized water at ambient conditions, due to the presence of glassy P*t*BA lamellar microdomains. By heating a P*t*BA/PHD diblock copolymer hydrogel above the glass transition temperature of P*t*BA, however, we successfully induced an L to H transformation. Subsequent cooling of the P*t*BA/PHD hydrogel demonstrated that, upon transformation into H, the block copolymer hydrogel was temperature responsive in a similar manner to PMA/PHD diblock copolymers.

FIGURES

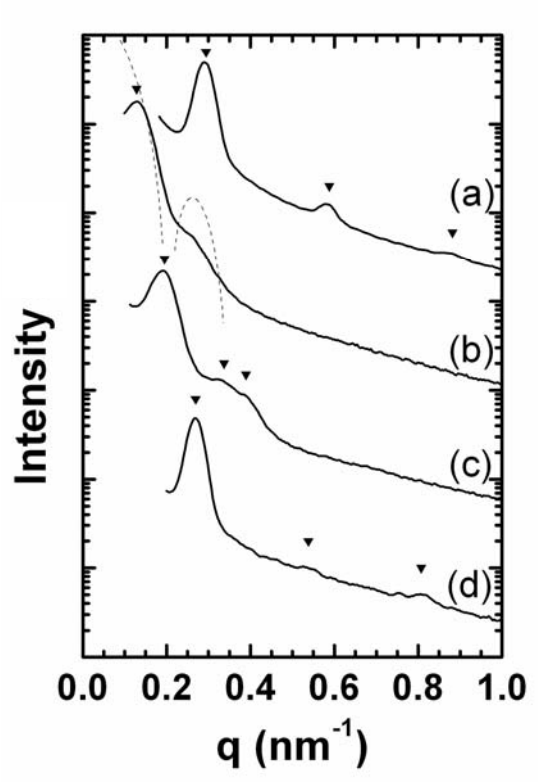

Figure 6.1. Small-angle x-ray scattering profiles of PMA/PHD_{75} 13/11 in the solid state (**a**; alternating lamellae, with ▼ placed at q/q* ratios of 1, 2, and 3), and as a hydrogel at T = 22ºC (**b**; disordered micelles, with form factor for 22 nm spheres shown as dashed curve), at T = 37ºC (**c**; hexagonally-packed cylinders, with ▼ placed at q/q* ratios of 1, √3, and √4), and at T = 52ºC (**d**; alternating lamellae, with ▼ placed at q/q* ratios of 1, 2, and 3).

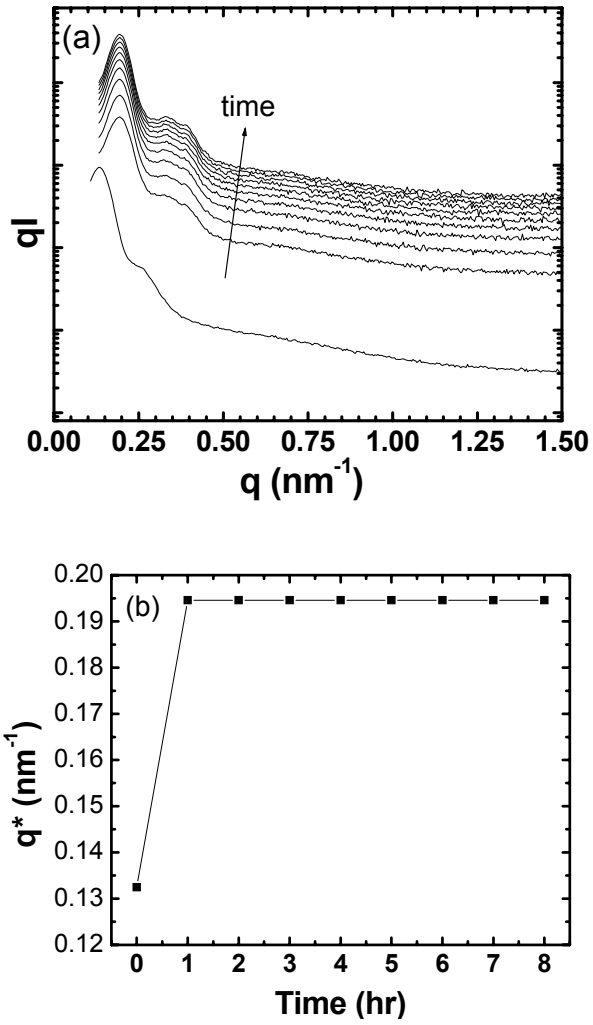

Figure 6.2. (a) Small-angle x-ray scattering profiles of swollen PMA/PHD$_{75}$ 13/11 during a heating experiment from 22ºC to 37ºC. The first scan was acquired at the beginning of the temperature ramp. The temperature equilibrated at 37ºC after approximately 30 min. (b) Position of the primary peak (q*) extracted from the SAXS profiles in (a), shown as a function of time from start of the temperature ramp.

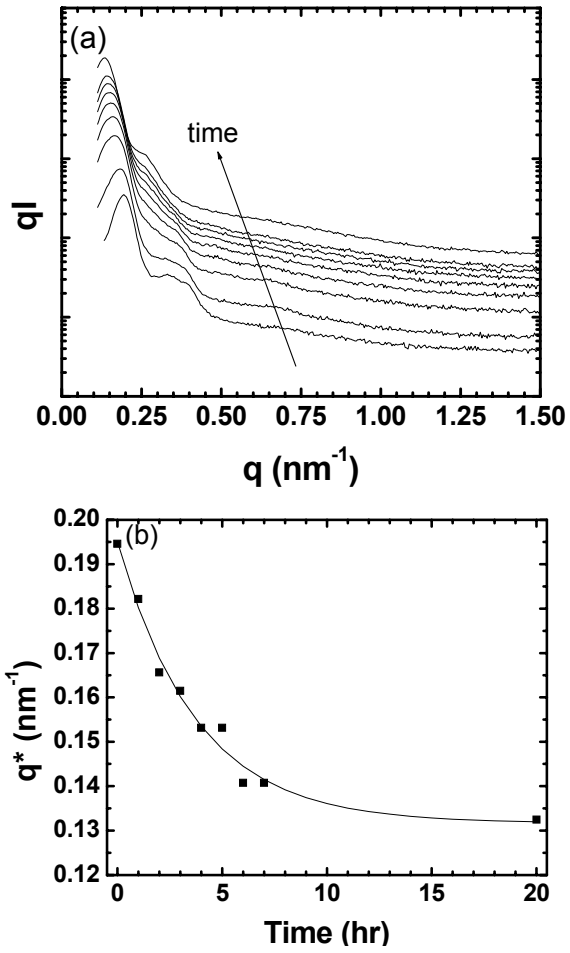

Figure 6.3. (a) Small-angle x-ray scattering profiles of swollen PMA/PHD$_{75}$ 13/11 during a cooling experiment from 37ºC to 22ºC. The first scan was acquired at the beginning of cooling. The temperature equilibrated at 22ºC after approximately 1.25 h. (b) The position of the primary peak (q*) extracted from the SAXS profiles in (a), shown as a function of time from start of the experiment. A curve was imposed on the data in order to guide the eye.

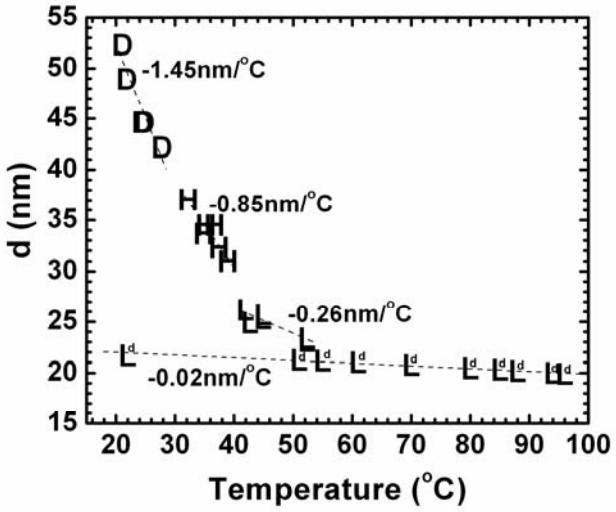

Figure 6.4. The interdomain spacing of the of the PMA/PHD$_{75}$ 13/11 hydrogel at different temperatures. D indicates a disordered, micellar morphology, while H and L represent hexagonally-packed cylindrical and lamellar morphologies, respectively. L^d represents data points that were collected on PMA/PHD$_{75}$ 13/11 in the solid state as a function of temperature.

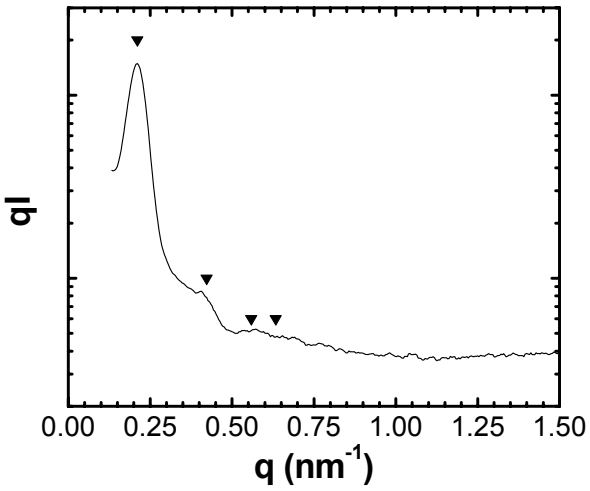

Figure 6.5. Small-angle x-ray scattering profile of the PMA/PHD$_{50}$ 12/15 block copolymer hydrogel at T = 22ºC, with ▼ placed at q/q* ratios of 1, √4, √7, and √9.

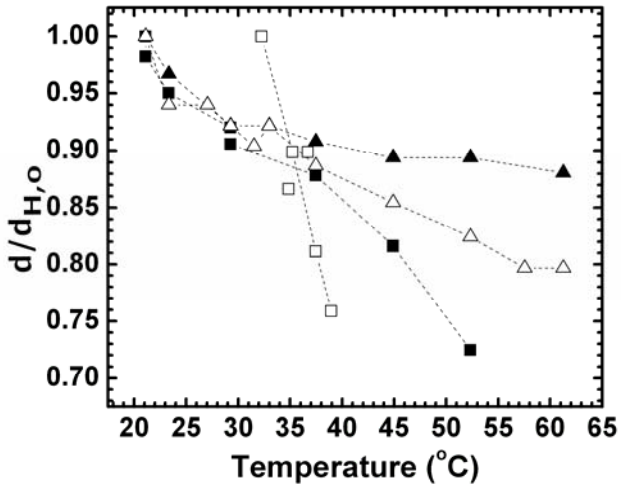

Figure 6.6. Normalized interdomain spacings of PMA/PHD diblock copolymer hydrogels at different temperatures: □ = PMA/PHD$_{75}$ 13/11; ■ = PMA/PHD$_{63}$ 10/9.7; Δ = PMA/PHD$_{50}$ 12/15; ▲ = PMA/PHD$_{28}$ 8.0/13. The reference characteristic spacing, $d_{H,o}$, is taken at the temperature at which H is first observed in each hydrogel. Dashed lines are added for clarity.

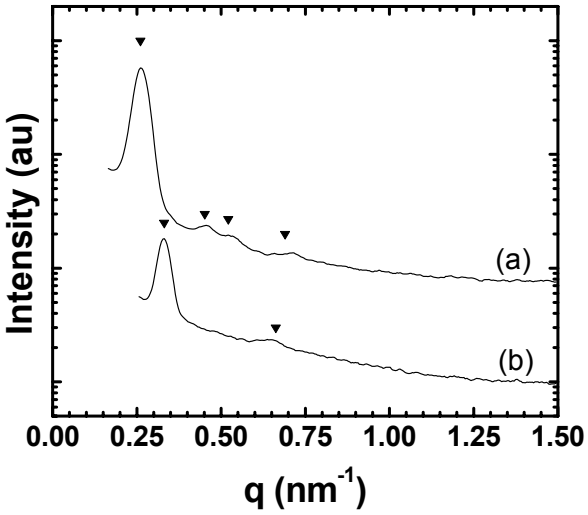

Figure 6.7. Small-angle x-ray scattering profiles of the PMA/PHD_{63} 10/9.7 hydrogel (a) at T = 37ºC (H; ▼ placed at q/q* ratios of 1, √3, √4, and √7) and (b) at T = 57ºC (L; ▼ placed at q/q* ratios of 1 and 2).

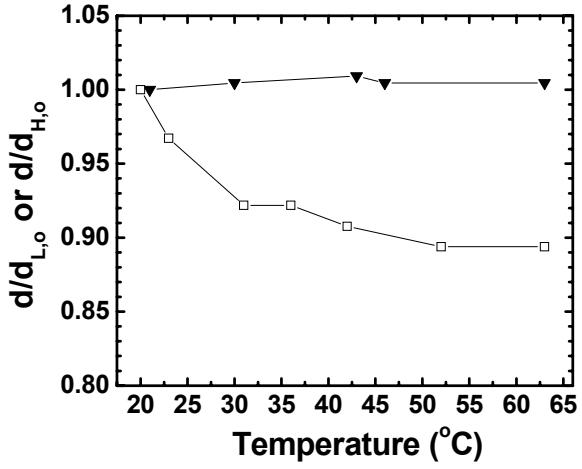

Figure 6.8. Normalized interdomain spacings of PS/PHD$_{28}$ 6.8/5.8 (d/d$_{H,o}$; ▼) and PMA/PHD$_{28}$ 8.0/13 (d/d$_{H,o}$; □) hydrogels at different temperatures. The reference interdomain spacing, d$_{L,o}$ or d$_{H,o}$, is taken at the temperature at which L or H is first observed in each hydrogel. Lines are added for clarity.

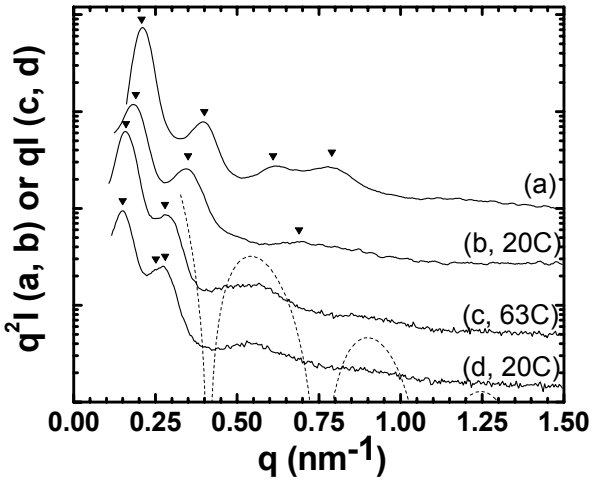

Figure 6.9. Small-angle x-ray scattering profiles of P*t*BA/PHD$_{28}$ 15/18 in the solid state **(a)**, and the P*t*BA/PHD$_{28}$ 15/18 hydrogel immersed in deionized water at T = 20ºC **(b)**, T = 63 ºC **(c)**, and then cooled back to T = 20ºC **(d)**. Markers (▼) are placed at q/q* ratios of 1, 2, 3, and 4 in **(a)**, at ratios of 1, 2, and 4 in **(b)**, at ratios of 1, and √3 in **(c)**, and at ratios of 1, √3, and √4 in **(d)**. The form factor[31] for cylinders of radius 9.3 nm is also shown (dashed curve).

REFERENCES

1. Park, M. J.; Char, K.; Lodge, T. P.; Kim, J. K. *Journal of Physical Chemistry B* **2006,** 110, 15295-15301.

2. Battaglia, G.; Ryan, A. J. *Macromolecules* **2006,** 39, 798-805.

3. Park, M. J.; Char, K.; Bang, J.; Lodge, T. P. *Macromolecules* **2005,** 38, 2449-2459.

4. Park, M. J.; Bang, J.; Harada, T.; Char, K.; Lodge, T. P. *Macromolecules* **2004,** 37, 9064-9075.

5. Bang, J.; Lodge, T. P. *Journal of Physical Chemistry B* **2003,** 107, 12071-12081.

6. Lodge, T. P.; Pudil, B.; Hanley, K. J. *Macromolecules* **2002,** 35, 4707-4717.

7. Hamley, I. W.; Mai, S.-M.; Ryan, A. J.; Fairclough, J. P. A.; Booth, C. *Physical Chemistry Chemical Physics* **2001,** 3, 2972-2980.

8. Hanley, K. J.; Lodge, T. P.; Huang, C.-I. *Macromolecules* **2000,** 33, 5918-5931.

9. Alexandridis, P.; Olsson, U.; Lindman, B. *Langmuir* **1998,** 14, 2627-2638.

10. Lai, C.; Russel, W. B.; Register, R. A. *Macromolecules* **2002,** 35, 4044-4049.

11. Alexandridis, P.; Zhou, D.; Khan, A. *Langmuir* **1996,** 12, 2690-2700.

12. Van de Wetering, P.; Moret, E. E.; Schuurmans-Nieuwenbroek, N. M. E.; Van Steenbergen, M. J.; Hennink, W. E. *Bioconjugate Chemistry* **1999,** 10, 589-597.

13. Fournier, D.; Hoogenboom, R.; Thijs, H. M. L.; Paulus, R. M.; Schubert, U. S. *Macromolecules* **2007,** 40, 915-920.

14. Matyjaszewski, K.; Xia, J. *Chemical Reviews* **2001,** 101, 2921-2990.

15. Guice, K. B.; Loo, Y.-L. *Macromolecules* **2006,** 39, 2474-2480.

16. Teoh, R. L.; Guice, K. B.; Loo, Y.-L. *Macromolecules* **2006,** 39, 8609-8615.

17. Monge, S.; Darcos, V.; Haddleton, D. M. *Journal of Polymer Science, Part A: Polymer Chemistry* **2004,** 42, 6299-6308.

18. Jin, X.; Shen, Y.; Zhu, S. *Macromolecular Materials and Engineering* **2003,** 288, 925-935.

19. Lee, S. B.; Russell, A. J.; Matyjaszewski, K. *Biomacromolecules* **2003,** 4, 1386-1393.

20. Mao, B.; Gan, L.-H.; Gan, Y.-Y.; Li, X.; Ravi, P.; Tam, K.-C. *Journal of Polymer Science, Part A: Polymer Chemistry* **2004,** 42, 5161-5169.

21. Zhang, X.; Xia, J.; Matyjaszewski, K. *Macromolecules* **1998,** 31, 5167-5169.

22. Gomez Ribelles, J. L.; Monleon Pradas, M.; Gallego Ferrer, G.; Peidro Torres, N.; Perez Gimenez, V.; Pissis, P.; Kyritsis, A. *Journal of Polymer Science, Part B: Polymer Physics* **1999,** 37, 1587-1599.

23. Bendejacq, D. D.; Ponsinet, V.; Joanicot, M. *Langmuir* **2005,** 21, 1712-1718.

24. Bendejacq, D.; Joanicot, M.; Ponsinet, V. *European Physical Journal E: Soft Matter* **2005,** 17, 83-92.

25. Castelletto, V.; Hamley, I. W. *Current Opinion in Colloid & Interface Science* **2002,** 7, 167-172.

26. Shibayama, M.; Hashimoto, T.; Kawai, H. *Macromolecules* **1983,** 16, 16-28.

27. Stoltz, M. J.; Brazel, C. S. *Journal of Applied Polymer Science* **2003,** 88, 2974-2981.

28. Abbas, S.; Li, Z.; Hassan, H.; Lodge, T. P. *Macromolecules* **2007,** 40, 4048-4052.

29. Guice, K. B.; Loo, Y.-L. *Macromolecules* **2007,** 40, 9053 -9058.

30. Nykaenen, A.; Nuopponen, M.; Laukkanen, A.; Hirvonen, S.-P.; Rytelae, M.; Turunen, O.; Tenhu, H.; Mezzenga, R.; Ikkala, O.; Ruokolainen, J. *Macromolecules* **2007,** 40, 5827-5834.

31. Porod, G., The Principles of Diffraction, Section 1, General Theory. In *Small-Angle X-ray Scattering*, Glatter, O., Kratky, O., Ed. Academic Press: London, 1982, pp. 17-51.

Chapter 7. Conclusions and Future Work

This thesis documents the synthesis and investigation of model pH- and temperature- responsive block copolymer hydrogels containing statistical copolymers of HEMA and DMAEMA. We demonstrated that control over the monomer sequence distribution during the copolymerization of HEMA and DMAEMA can be accomplished by the selection of an appropriate polymerization medium and monomer feed composition. Specifically, polymerization of statistical copolymers of HEMA and DMAEMA in DMF can be achieved at the azeotropic composition ($\overline{F_D}$ = 0.28), which is dictated by the reactivity ratios of HEMA and DMAEMA in DMF.[1] In contrast, polymerizations at monomer feed compositions outside the compositional azeotrope result in pronounced drift in the monomer sequence distribution along the length of the polymer chain. The reactivity ratios of HEMA and DMAEMA in DMSO are both near unity. Consequently, DMSO is an ideal solvent for the copolymerization of HEMA and DMAEMA, as statistical PHD copolymers with uniform sequence distributions can be synthesized at any composition in DMSO.[2]

Using ATRP, we can control the molecular weight and molecular weight distribution of PHD statistical copolymers and block copolymers containing PHD. Using a macroinitiation strategy, we synthesized PS/PHD_{28}, PtBA/PHD_{28}, and PCL/PHD_{28} block copolymers in DMF, and we also synthesized PMA/PHD at a variety of PHD compositions in DMSO. Using RAFT, we also synthesized a series of PS/PHD diblock and PS/PHD/PS triblock copolymers with varying PHD compositions.

We investigated the pH response of lamella-forming model block copolymer hydrogels comprised of PHD statistical copolymers and PS. The swelling in these hydrogels increases with decreasing pH and with increasing DMAEMA content.

Because PS is hydrophobic and glassy, its presence ensures that the lamellar structure within the block copolymer hydrogels is preserved during swelling of PHD. It has been generally assumed that PS/PHD/PS triblock copolymers are necessary to preserve the network structure during swelling. We demonstrated, however, that lamellar PS/PHD diblock copolymer hydrogels also maintain their lamellar microstructures during swelling. Moreover, we demonstrated that PS/PHD_{28} diblock copolymers with low DMAEMA content ($\overline{F_D} = 0.28$) maintain their macroscopic integrity and swell similarly to their triblock copolymer equivalents.

PMA/PHD diblock copolymer hydrogels exhibit decreased swelling with increasing temperature due to a hydrophilic-to-hydrophobic transition of DMAEMA. Accordingly, the swelling response of PHD-containing block copolymer hydrogels increases with increasing DMAEMA content. Moreover, because PMA has a glass transition temperature below ambient temperature, changes in the degree of swelling within PHD at temperatures above room temperature can induce morphological transitions in the PMA/PHD hydrogel, with the number of morphological transitions and the temperature range over which the transitions occur dependent on the DMAEMA content within PHD. Specifically, we observed reversible morphological transitions from disordered micelles to hexagonally-packed cylinders to alternating lamellae over a narrow temperature window (30^oC) for a PMA/PHD_{75} block copolymer hydrogel with a high DMAEMA content ($\overline{F_D} = 0.75$)

FUTURE WORK

Nanoporous Hydrogels

One of the major drawbacks of current hydrogel technology is the response time of the materials, which is diffusion limited ($D_{gel} \approx 10^{-7}$ cm^2/sec).[3] For applications in which fast response times are required, traditional hydrogels are thus largely unsuitable.

To overcome this problem, porogens are often incorporated during the synthesis of traditional hydrogels.[4,5] Incorporation of porogens into hydrogels during synthesis, however, generally results in pores that are large and frequently not uniformly distributed throughout the hydrogel.[4,5] By covalently linking hydrogel components, such as HEMA and DMAEMA, with degradable materials, one can exploit the self-assembly characteristics learned from this thesis to create nanopores that are periodically spaced within a hydrogel matrix. The regularity and size of pores are tunable at the onset of polymer synthesis, and the resulting materials can potentially exhibit improved diffusion rates relative to other porous or traditional hydrogel materials. The ability to evoke a change in swelling in these hydrogels by temperature or pH should provide additional tunability of diffusion rates.

One attractive polymer for degradation is PCL, which undergoes main chain scission during acid hydrolysis to result in monomer and oligomer.[6] In Chapter 4, we demonstrated the synthesis and characterization of PCL/PHD_{28} 9.0/17.8, a cylinder-forming block copolymer. The PCL cylindrical microdomains can potentially be degraded to produce regularly-spaced, monodisperse cylindrical pores. Prior to degradation, the PHD matrix should be lightly crosslinked to preserve structural integrity. One possible crosslinking agent is glutaraldehyde, which reacts when catalyzed by a small amount of acid.[7]

The investigation of porous PHD networks with tunable swelling and diffusion properties requires the synthesis and investigation of PCL/PHD block copolymers across a range of PHD compositions. PCL, however, is not soluble in DMSO, the preferred solvent for the polymerization of statistical PHD copolymers. As such, the ability to synthesize PCL/PHD block copolymers using a macroinitiator or macro-CTA approach is limited. To overcome this synthetic limitation, one might synthesize PCL and PHD

separately, then couple the two polymer chains to yield a block copolymer. One of the more popular coupling reactions is 'click' chemistry, which utilizes a Huisgen cycloaddition process between an azide and an alkyne to achieve a triazole linkage.[8-13] The 'click' coupling reaction is shown schematically in Figure 7.1. The reaction is catalyzed by copper (CuI is used in the Figure), and R_1 and R_2 can be any two compounds that one is interested in coupling.[8-13] In the case of the coupling reaction of PCL and PHD, R_1 and R_2 represent PCL and PHD that are functionalized with alkyne and azide terminal groups, respectively. With appropriate endgroup modification, 'click' techniques have been previously extended to the efficient coupling of azide- and alkyne-functionalized polymer chains that were originally synthesized by ROP,[13] ATRP,[10,14] or RAFT.[9] A variety of ATRP initiators and RAFT CTAs can be synthesized with alkyne or azide functionalities.[9,10] In addition, terminal hydroxyls[13] (from ROP) or alkyl halides[16] (from ATRP) can be converted into the requisite functionalities. Using these techniques, PCL and PHD can be synthesized and functionalized separately before they are linked in a mutual solvent (e.g., DMF) to achieve PCL/PHD block copolymers across a wide range of PHD compositions.

Amphoteric Block Copolymer Nanostructures

We are also interested in the design of amphoteric block copolymers with cationic and anionic functionalities localized in discrete microdomains. The formation of these structures can be potentially achieved using P*t*BA/PHD block copolymers synthesized for the work described in this thesis. Specifically, P*t*BA/PHD block copolymers can be induced to phase separate in the solid state before the pendant *tert*-butyl group is cleaved from P*t*BA, leaving poly(acrylic acid), PAA.[15] The conversion of P*t*BA into PAA has been previously demonstrated in microphase-separated P*t*BA/PS diblock copolymers.[15] In our case, it is likely necessary to first crosslink the PHD phase to prevent complexation

of AA and DMAEMA groups. Further, PHD/P*t*BA/PHD triblock copolymers can be used to ensure that PAA microdomains are sufficiently anchored by chemically crosslinked PHD microdomains to prevent complexation. We previously demonstrated the synthesis of PHD_{28}/P*t*BA/PHD_{28} 8.5/16/8.5 by ATRP. The synthesis of PHD/P*t*BA/PHD triblock copolymers at other PHD compositions requires new synthetic techniques, as P*t*BA is not soluble in DMSO. We propose that 'click' chemistry techniques can be used to achieve a wider range of PHD/P*t*BA/PHD triblock copolymers. Specifically, P*t*BA can be synthesized from a bifunctional initiator by ATRP, and the alkyl halide endgroups can be subsequently converted into azide functionalities with NaN_3.[10,14] Alkyne-functionalized ATRP initiators or RAFT CTAs can be used for the synthesis of PHD in DMSO.[19] Finally, the PHD statistical copolymers can be 'clicked' to the bifunctional P*t*BA to yield PHD/P*t*BA/PHD triblock copolymers.

Role of Sequence Distribution on LCST behavior

In Figure 3.18, we demonstrated that the LCST of PHD statistical copolymers with similar molecular weights and similar molecular weight distributions decreases with increasing HEMA content. By comparison, all PD/PH block copolymers that we have synthesized (Table 4.2) are not soluble in water, even with significant DMAEMA content (e.g., PD/PH 25/5.2, $F_D = 0.8$). These initial results suggest that the sequence distribution of HEMA and DMAEMA can significantly impact the solution behavior of PHD copolymers. We are interested in a more thorough examination of the role of monomer sequence distribution on the solution behavior of PHD copolymers. We have developed techniques for the synthesis of PHD statistical copolymers and PD/PH block copolymers, which represent the two extremes of sequence distributions that might be achieved. Synthesis of PHD copolymers with controlled gradients in sequence distributions might be accomplished by continuous or intermittent monomer feed. Successful synthesis of

controlled gradient PHD copolymers would enable the study of the solution behavior of PHD copolymers over a wider range of composition distributions.

FIGURES

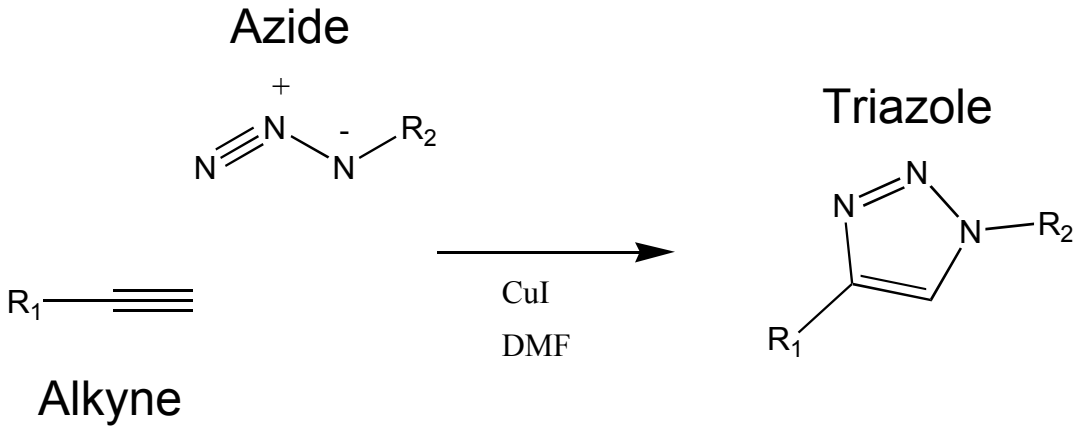

Figure 7.1. 'Click' reaction scheme between a terminal alkyne and an azide, in the presence of CuI, to achieve a triazole linkage.

REFERENCES

1. Guice, K. B.; Loo, Y.-L. *Macromolecules* **2006,** 39, 2474-2480.

2. Teoh, R. L.; Guice, K. B.; Loo, Y.-L. *Macromolecules* **2006,** 39, 8609-8615.

3. Qiu, Y.; Park, K. *Advanved Drug Delivery Reviews* **2001,** 53, 321-339.

4. Kabiri, K.; Omidian, H.; Zohuriann-Mehr, M. J. *Polymer International* **2003,** 52, 1158-1164.

5. Badiger, M. V.; McNeill, M. E.; Graham, N. B. *Biomaterials* **1993,** 14, 1059-1063.

6. Tsuji, H.; Ono, T.; Saeki, T.; Daimon, H.; Fujie, K. *Polymer Degradation and Stability* **2005,** 89, 336-343.

7. Koshiro, Y.; Morone, N.; Fukutomi, T. *Polymer Gels and Networks* **1995,** 3, 59-70.

8. Rostovtsev, V. V.; Green, L. G.; Fokin, V. V.; Sharpless, K. B. *Angewandte Chemie, International Edition* **2002,** 114, 2708-2711.

9. Ting, S. R. S.; Granville, A. M.; Quemener, D.; Davis, T. P.; Stenzel, M. H.; Barner-Kowollik, C. *Australian Journal of Chemistry* **2007,** 60, 405-409.

10. Golas, P. L.; Tsarevsky, N. V.; Sumerlin, B. S.; Walker, L. M.; Matyjaszewski, K. *Australian Journal of Chemistry* **2007,** 60, 400-404.

11. Lutz, J.-F.; Borner, H. G.; Weichenhan, K. *Australian Journal of Chemistry* **2007,** 60, 410-413.

12. Binder, W. H.; Sachsenhofer, R. *Macromolecular Rapid Communications* **2007,** 28, 15-54.

13. Mespouille, L.; Vachaudez, M.; Suriano, F.; Gerbaux, P.; Coulembier, O.; Degée, P.; Flammang, R.; Dubois, P. *Macromolecular Rapid Communications* **2007,** 28, 2151-2158.

14. Opsteen, J. A.; van Hest, J. C. M. *Chemical Communications* **2005,** 1, 57-59.

15. Xu, C.; Fu, X.; Fryd, M.; Xu, S.; Wayland, B. B.; Winey, K. I.; Composto, R. J. *Nano Letters* **2006,** 6, 282-287.

16. Satish, C. S.; Shivakumar, H. G. *Journal of Macromolecular Science, Part A: Pure and Applied Chemistry* **2007,** 44, 379-387.

17. Traitel, T.; Cohen, Y.; Kost, J. *Biomaterials* **2000,** 21, 1679-1687.

18. Brahim, S.; Narinesingh, D.; Guiseppi-Elie, A. *Biomacromolecules* **2003,** 4, 1224-1231.

19. Brahim, S.; Narinesingh, D.; Guiseppi-Elie, A. *Biomacromolecules* **2003,** 4, 497-503.

Bibliography

1. Abbas, S.; Li, Z.; Hassan, H.; Lodge, T. P. *Macromolecules* **2007**, 40, 4048-4052.

2. Achilleos, M.; Krasia-Christoforou, T.; Patrickios, C. S. *Macromolecules* **2007**, 40, 5575-5581.

3. Alexander, L., X-Ray Diffraction Methods in Polymer Science Wiley-Interscience: New York, **1985**.

4. Alexandridis, P.; Olsson, U.; Lindman, B. *Langmuir* **1998**, 14, 2627-2638.

5. Alexandridis, P.; Zhou, D.; Khan, A. *Langmuir* **1996**, 12, 2690-2700.

6. Ando, T.; Kamigaito, M.; Sawamoto, M. *Tetrahedron* **1997**, 53, 15445-15457.

7. Asakawa, N.; Sato, D.; Sakurai, M.; Inoue, Y. *Journal of Physical Chemistry A* **2000**, 104, 2716-2723.

8. Asgarzadeh, F. B., E.; Chaumont, P. *Polym. Prepr. (Am. Chem. Soc., Div. Polym. Chem.)* **1999**, 40, 899-900.

9. ASTM D153-84, Standard Test Methods for Specific Gravity of Pigments **2003**.

10. Badiger, M. V.; McNeill, M. E.; Graham, N. B. *Biomaterials* **1993**, 14, 1059-1063.

11. Bang, J.; Lodge, T. P. *Journal of Physical Chemistry B* **2003**, 107, 12071-12081.

12. Barner-Kowollik, C.; Quinn, J. F.; Morsley, D. R.; Davis, T. P. *Journal of Polymer Science, Part A: Polymer Chemistry* **2001**, 39, 1353-1365.

13. Battaglia, G.; Ryan, A. J. *Macromolecules* **2006**, 39, 798-805.

14. Becke, F. H., H., Badische Anilin & Soda-Fabrik Aktiengesellschaft. Germany, **1968**.

15. Bell, C. L. P., N.A. *Advances in Polymer Science* **1994**, 122, 129-173.

16. Bendejacq, D. D.; Ponsinet, V.; Joanicot, M. *Langmuir* **2005**, 21, 1712-1718.

17. Bendejacq, D.; Joanicot, M.; Ponsinet, V. *European Physical Journal E: Soft Matter* **2005**, 17, 83-92.

18. Bendejacq, D.; Ponsinet, V.; Joanicot, M. *European Physical Journal E: Soft Matter* **2004**, 13, 3-13.

19. Bielawski, C. W.; Louie, J.; Grubbs, R. H. *Journal of the American Chemical Society* **2000**, 122, 12872-12873.

20. Binder, W. H.; Sachsenhofer, R. *Macromolecular Rapid Communications* **2007**, 28, 15-54.

21. Bories-Azeau, X.; Armes, S. P. *Macromolecules* **2002**, 35, 10241-10243.

22. Bougard, F.; Jeusette, M.; Mespouille, L.; Dubois, P.; Lazzaroni, R. *Langmuir* **2007**, 23, 2339-2345.

23. Brahim, S.; Narinesingh, D.; Guiseppi-Elie, A. *Biomacromolecules* **2003**, 4, 1224-1231.

24. Brahim, S.; Narinesingh, D.; Guiseppi-Elie, A. *Biomacromolecules* **2003**, 4, 497-503.

25. Brannon-Peppas, L.; Peppas, N. A. *Polymer Bulletin* **1988**, 20, 285-9.

26. Bucholz, T. L.; Li, S. P.; Loo, Y.-L. *Journal of Materials Chemistry* **2008**, 18, 530-536.

27. Bucholz, T. L.; Loo, Y.-L. *Macromolecule*s **2006**, 39, 6075-6080.

28. Burke, S. A.; Ritter-Jones, M.; Lee, B. P.; Messersmith, P. B. *Biomedical Materials* **2007**, 2, 203-210.

29. Cai-yuan, P.; Chun-yan, H., Synthesis and Characterizations of Block Copolymers Prepared via Controlled Radical Polymerization Methods. In Developments in Block Copolymer Science and Technology, Hamley, I. W., Ed. John Wiley & Sons: Chichester, **2004**; pp 71-126.

30. Castelletto, V.; Hamley, I. W. *Current Opinion in Colloid & Interface Science* **2002**, 7, 167-172.

31. Caykara, T.; Ozyurek, C.; Kantoglu, O.; Guven, O. *Journal of Polymer Science, Part B: Polymer Physics* **2002**, 40, 1995-2003.

32. Cho, S. H.; Jhon, M. S.; Yuk, S. H.; Lee, H. B. *Journal of Polymer Science, Part B: Polymer Physics* **1997**, 35, 595-598.

33. Cohen, Y.; Thomas, E. L. *Macromolecules* **2003**, 36, 5265-5270.

34. Coote, M. L.; Davis, T. P., Copolymerization Kinetics. In Handbook of Radical Polymerization, Matyjaszewski, K.; Davis, T. P., Eds. Wiley-Interscience: New York, **2002**; pp 263-300.

35. Cowie, J. M. G.; McEwen, I. J.; Yule, D. J. *European Polymer Journal* **2000**, 36, 1795-1803.

36. Czerwinski, W. K. *Polymer* **1997**, 39, 183-187.

37. Deb, P. C. *Polymer* **2007**, 48, 4932-4935.

38. Dias, M. L.; Mano, E. B.; Azuma, C. *European Polymer Journal* **1997**, 33, 559-564.

39. Dong, L.; Agarwal, A. K.; Beebe, D. J.; Jiang, H. *Nature* **2006**, 442, 551-554.

40. Dong, W.; Xu, Y.; Yuan, C. *Cellulose* **2007**, 14, 331-336.

41. dos Santos, A. M.; Pohn, J.; Lansalot, M.; D'Agosto, F. *Macromolecular Rapid Communications* **2007**, 28, 1325-1332.

42. Du, R.; Zhao, J. *Journal of Applied Polymer Science* **2004**, 91, 2721-2728.

43. Dubin, P. L.; Koontz, S.; Wright, K. L., III. *Journal of Polymer Science, Polymer Chemistry Edition* **1977**, 15, 2047-2057.

44. Emileh, A.; Vasheghani-Farahani, E.; Imani, M. *European Polymer Journal* **2007**, 43, 1986-1995.

45. Even, M.; Haddleton, D. M.; Kukulj, D. *European Polymer Journal* **2003**, 39, 633-639.

46. Fernandez-Monreal, C.; Martinez, G.; Sanchez-Chaves, M.; Madruga, E. L. *Journal of Polymer Science, Part A: Polymer Chemistry* **2001**, 39, 2043-2048.

47. Fineman, M.; Ross, S. D. *Journal of Polymer Science* **1950**, 5, 259-262.

48. Fischer, H. *Journal of Polymer Science, Part A: Polymer Chemistry* **1999**, 37, 1885-1901.

49. Flory, P. J.; Rehner, J., Jr. *Journal of Chemical Physics* **1943**, 11, 521-6.

50. Fournier, D.; Hoogenboom, R.; Thijs, H. M. L.; Paulus, R. M.; Schubert, U. S. *Macromolecules* **2007**, 40, 915-920.

51. Fox, T. G. *Bulletin of the American Physical Society* **1956**, 1, 123.

52. Fukuda, T.; Goto, A.; Tsujii, Y., Kinetics of Living Radical Polymerization. In Handbook of Radical Polymerization, Matyjaszewski, K.; Davis, T. P., Eds. Wiley-Interscience: New York, **2002**; pp 407-462.

53. Golas, P. L.; Tsarevsky, N. V.; Sumerlin, B. S.; Walker, L. M.; Matyjaszewski, K. *Australian Journal of Chemistry* **2007**, 60, 400-404.

54. Gomez Ribelles, J. L.; Monleon Pradas, M.; Gallego Ferrer, G.; Peidro Torres, N.; Perez Gimenez, V.; Pissis, P.; Kyritsis, A. *Journal of Polymer Science, Part B: Polymer Physics* **1999**, 37, 1587-1599.

55. Gomez, E. D.; Das, J.; Chakraborty, A. K.; Pople, J. A.; Balsara, N. P. *Macromolecules* **2006**, 39, 4848-4859.

56. Guice, K. B.; Loo, Y.-L. *Macromolecules* **2006**, 39, 2474-2480.

57. Guice, K. B.; Loo, Y.-L. *Macromolecules* **2007**, 40, 9053 -9058.

58. Hamley, I. W., Introduction to Block Copolymers. In Developments in Block Copolymer Science and Technology, Hamley, I. W., Ed. John Wiley & Sons: Chichester, **2004**; pp 1-30.

59. Hamley, I. W.; Mai, S.-M.; Ryan, A. J.; Fairclough, J. P. A.; Booth, C. *Physical Chemistry Chemical Physics* **2001**, 3, 2972-2980.

60. Handlin, D. L., Jr.; Thomas, E. L. *Macromolecules* **1983**, 16, 1514-25.

61. Hanley, K. J.; Lodge, T. P.; Huang, C.-I. *Macromolecules* **2000**, 33, 5918-5931.

62. Haraguchi, K.; Takehisa, T. *Advanced Materials* **2002**, 14, 1120-1124.

63. Hill, D. J. T.; Lang, A. P.; O'Donnell, J. H.; O'Sullivan, P. W. *European Polymer Journal* **1989**, 25, 911-15.

64. Huglin, M. B.; Zakaria, M. B. *Polymer* **1984**, 25, 797-802.

65. Jin, X.; Shen, Y.; Zhu, S. *Macromolecular Materials and Engineering* **2003**, 288, 925-935.

66. Johnson, J. A.; Lewis, D. R.; Diaz, D. D.; Finn, M. G.; Koberstein, J. T.; Turro, N. J. *Journal of the American Chemical Society* **2006**, 128, 6564-6565.

67. Kabiri, K.; Omidian, H.; Zohuriann-Mehr, M. J. *Polymer International* **2003**, 52, 1158-1164.

68. Kajiwara, A.; Matyjaszewski, K.; Kamachi, M. *Macromolecules* **1998**, 31, 5695-5701.

69. Kelen, T.; Tudos, F. *Journal of Macromolecular Science, Chemistry* **1975**, A9, 1-27.

70. Kishi, H.; Naitou, T.; Matsuda, S.; Murakami, A.; Muraji, Y.; Nakagawa, Y. *Journal of Polymer Science, Part B: Polymer Physics* **2007**, 45, 1425-1434.

71. Klumperman, B.; Kraeger, I. R. *Macromolecules* **1994**, 27, 1529-1534.

72. Klumperman, B.; O'Driscoll, K. F. *Polymer* **1993**, 34, 1032-1037.

73. Kopecek, J.; Yang, J. *Polymer International* **2007**, 56, 1078-1098.

74. Koshiro, Y.; Morone, N.; Fukutomi, T. *Polymer Gels and Networks* **1995**, 3, 59-70.

75. Krasia, T. C.; Patrickios, C. S. *Macromolecules* **2006**, 39, 2467-2473.

76. Kroupova, J.; Horak, D.; Pachernik, J.; Dvorak, P.; Slouf, M. *Journal of Biomedical Materials Research, Part B: Applied Biomaterials* **2006**, 76B, 315-325.

77. Kwok, A. Y.; Qiao, G. G.; Solomon, D. H. *Polymer* **2004**, 45, 4017-4027.

78. Lai, C.; Russel, W. B.; Register, R. A. *Macromolecules* **2002**, 35, 4044-4049.

79. Lee, J.; Aoai, T.; Kondo, S. I.; Miyagawa, N.; Takahara, S.; Yamaoka, T. *Journal of Polymer Science, Part A: Polymer Chemistry* **2002**, 40, 1858-1867.

80. Lee, S. B.; Russell, A. J.; Matyjaszewski, K. *Biomacromolecules* **2003**, 4, 1386-1393.

81. Leibler, L. *Macromolecules* **1980**, 13, 1602-17.

82. Liu, Q.; Yu, Z.; Ni, P. *Colloid and Polymer Science* **2004**, 282, 387-393.

83. Liu, R.; Oppermann, W. *Macromolecules* **2006**, 39, 4159-4167.

84. Liu, W.; Nakano, T.; Okamoto, Y. *Polymer* **2000**, 41, 4467-4472.

85. Lodge, T. P.; Pudil, B.; Hanley, K. J. *Macromolecules* **2002**, 35, 4707-4717.

86. Loo, Y.-L. Controlled polymer crystallization through block copolymer self-assembly, Ph.D. Dissertation, Princeton University, Princeton, N.J. **2001**, p. 42.

87. Loo, Y.-L.; Register, R. A.; Ryan, A. J. *Macromolecules* **2002**, 35, 2365-2374.

88. Lowe, A. B.; McCormick, C. L. *Progress in Polymer Science* **2007**, 32, 283-351.

89. Lutz, J.-F.; Borner, H. G.; Weichenhan, K. *Australian Journal of Chemistry* **2007**, 60, 410-413.

90. Malkoch, M.; Vestberg, R.; Gupta, N.; Mespouille, L.; Dubois, P.; Mason, A. F.; Hedrick, J. L.; Liao, Q.; Frank, C. W.; Kingsbury, K.; Hawker , C. J. *Chemical Communications* **2006**, 26, 2774-2776.

91. Mao, B.; Gan, L.-H.; Gan, Y.-Y.; Li, X.; Ravi, P.; Tam, K.-C. *Journal of Polymer Science, Part A: Polymer Chemistry* **2004**, 42, 5161-5169.

92. Mao, R.; Huglin, M. B. *Polymer* **1994**, 35, 3525-9.

93. Martin-Gomis, L.; Cuervo-Rodriguez, R.; Fernandez-Monreal, M. C.; Madruga, E. L.; Fernandez-Garcia, M. *Journal of Polymer Science, Part A: Polymer Chemistry* **2003**, 41, 2659-2666.

94. Mathew-Krotz, J.; Mahadevan, V. *Macromolecular Chemistry and Physics* **1997**, 198, 1597-1604.

95. Matsen, M. W.; Bates, F. S. *Macromolecules* **1996**, 29, 1091-1098.

96. Matyjaszewski, K., General Concepts and History of Living Radical Polymerization. In Handbook of Radical Polymerization, Matyjaszewski, K.; Davis, T. P., Eds. Wiley-Interscience: New York, **2002**; pp 361-406.

97. Matyjaszewski, K.; Nanda, A. K.; Tang, W. *Macromolecules* **2005**, 38, 2015-2018.

98. Matyjaszewski, K.; Patten, T. E.; Xia, J. *Journal of the American Chemical Society* **1997**, 119, 674-680.

99. Matyjaszewski, K.; Shipp, D. A.; Wang, J.-L.; Grimaud, T.; Patten, T. E. *Macromolecules* **1998**, 31, 6836-6840.

100. Matyjaszewski, K.; Xia, J. *Chemical Reviews* **2001**, 101, 2921-2990.

101. Matyjaszewski, K.; Xia, J., Fundamentals of Atom Transfer Radical Polymerization. In Handbook of Radical Polymerization, Matyjaszewski, K.; Davis, T. P., Eds. Wiley-Interscience: New York, **2002**; pp 523-628.

102. Meng, F.; Xu, Z.; Zheng, S. *Macromolecules* **2008**, 41, 1411-1420.

103. Mespouille, L.; Vachaudez, M.; Suriano, F.; Gerbaux, P.; Coulembier, O.; Degée, P.; Flammang, R.; Dubois, P. *Macromolecular Rapid Communications* **2007**, 28, 2151-2158.

104. Miller, P. J.; Matyjaszewski, K. *Macromolecules* **1999**, 32, 8760-8767.

105. Moad, G.; Chiefari, J.; Chong, Y. K.; Krstina, J.; Mayadunne, R. T. A.; Postma, A.; Rizzardo, E.; Thang, S. H. *Polymer International* **2000**, 49, 993-1001.

106. Moad, G.; Rizzardo, E.; Thang, S. H. *Australian Journal of Chemistry* **2005**, 58, 379-410.

107. Monge, S.; Darcos, V.; Haddleton, D. M. *Journal of Polymer Science, Part A: Polymer Chemistry* **2004**, 42, 6299-6308.

108. Mori, H.; Wakisaka, O.; Hirao, A.; Nakahama, S. *Macromolecular Chemistry and Physics* **1994**, 195, 3213-24.

109. Nykaenen, A.; Nuopponen, M.; Laukkanen, A.; Hirvonen, S.-P.; Rytelae, M.; Turunen, O.; Tenhu, H.; Mezzenga, R.; Ikkala, O.; Ruokolainen, J. *Macromolecules* **2007**, 40, 5827-5834.

110. Oae, S. Y., T.; Okabe, T. . *Tetrahedron* **1972**, 28, 3203-3216.

111. Odian, G., Principles of Polymerization. 4th ed.; Wiley-Interscience: New York, **2004**.

112. Opsteen, J. A.; van Hest, J. C. M. *Chemical Communications* **2005**, 1, 57-59.

113. Ozden, B. O.; Florence, A. T. *European Polymer Journal* **1995**, 31, 135-144.

114. Park, M. J.; Bang, J.; Harada, T.; Char, K.; Lodge, T. P. *Macromolecules* **2004**, 37, 9064-9075.

115. Park, M. J.; Char, K.; Bang, J.; Lodge, T. P. *Macromolecules* **2005**, 38, 2449-2459.

116. Park, M. J.; Char, K.; Lodge, T. P.; Kim, J. K. *Journal of Physical Chemistry B* **2006**, 110, 15295-15301.

117. Park, S. Y.; Cho, S. H.; Yuk, S. H.; Jhon, M. S. *European Polymer Journal* **2001**, 37, 1785-1790.

118. Podzimek, S. *Journal of Applied Polymer Science* **1994**, 54, 91-103.

119. Polymer Handbook, 4th Ed. In Brandrup, J.; Immergut, E. H.; Grulke, E. A., Eds. Wiley-Interscience: New York, **1999**, VI-203.

120. Porod, G., The Principles of Diffraction, Section 1, General Theory. In *Small-Angle X-ray Scattering*, Glatter, O., Kratky, O., Ed. Academic Press: London, 1982, pp. 17-51.

121. Qiu, Y.; Park, K. *Advanved Drug Delivery Reviews* **2001**, 53, 321-339.

122. Rostovtsev, V. V.; Green, L. G.; Fokin, V. V.; Sharpless, K. B. *Angewandte Chemie, International Edition* **2002**, 114, 2708-2711.

123. Sahnoun, M.; Charreyre, M.-T.; Veron, L.; Delair, T.; D'Agosto, F. *Joural of Polymer Science, Part A: Polymer Chemistry* **2005**, 43, 3551-3565.

124. Sakurai, S.; Momii, T.; Taie, K.; Shibayama, M.; Nomura, S.; Hashimoto, T. *Macromolecules* **1993**, 26, 485-491.

125. Sanchez, I. C.; Lacombe, R. H. *Macromolecules* **1978**, 11, 1145-56.

126. Satish, C. S.; Shivakumar, H. G. *Journal of Macromolecular Science, Part A: Pure and Applied Chemistry* **2007**, 44, 379-387.

127. Schellekens, M. A. J.; de Wit, F.; Klumperman, B. *Macromolecules* **2001**, 34, 7961-7966.

128. Senshu, K.; Yamashita, S.; Ito, M.; Hirao, A.; Nakahama, S. *Langmuir* **1995**, 11, 2293-2300.

129. Shibayama, M.; Hashimoto, T.; Kawai, H. *Macromolecules* **1983**, 16, 16-28.

130. Siegel, R. A.; Firestone, B. A. *Macromolecules* **1988**, 21, 3254-9.

131. Skeist, I. *Journal of the American Chemical Society* **1946**, 68, 1781-1784.

132. Snijder, A.; Klumperman, B.; van der Linde, R. *Macromolecules* **2002**, 35, 4785-4790.

133. Stoltz, M. J.; Brazel, C. S. *Journal of Applied Polymer Science* **2003**, 88, 2974-2981.

134. Suevegh, K.; Domjan, A.; Vanko, G.; Ivan, B.; Vertes, A. *Macromolecules* **1998**, 31, 7770-7775.

135. Tang, W.; Matyjaszewski, K. *Macromolecules* **2006**, 39, 4953-4959.

136. Teodorescu, M.; Matyjaszewski, K. *Macromolecules* **1999**, 32, 4826-4831.

137. Teoh, R. L.; Guice, K. B.; Loo, Y.-L. *Macromolecules* **2006**, 39, 8609-8615.

138. Themistou, E.; Patrickios, C. S. *Macromolecules* **2007**, 40, 5231-5234.

139. Tidwell, P. W.; Mortimer, G. A. *Journal of Polymer Science, Part A: General Papers* **1965**, 3, 369-387.

140. Ting, S. R. S.; Granville, A. M.; Quemener, D.; Davis, T. P.; Stenzel, M. H.; Barner-Kowollik, C. *Australian Journal of Chemistry* **2007**, 60, 405-409.

141. Topham, P. D.; Howse, J. R.; Crook, C. J.; Gleeson, A. J.; Bras, W.; Armes, S. P.; Jones, R. A. L.; Ryan, A. J. *Macromolecular Symposia* **2007**, 256, 95-104.

142. Traitel, T.; Cohen, Y.; Kost, J. *Biomaterials* **2000**, 21, 1679-1687.

143. Traitel, T.; Kost, J.; Lapidot, S. A. *Biotechnology and Bioengineering* **2003**, 84, 20-28.

144. Triftaridou, A. I.; Hadjiyannakou, S. C.; Vamvakaki, M.; Patrickios, C. S. *Macromolecules* **2002**, 35, 2506-2513.

145. Triftaridou, A. I.; Kafouris, D.; Vamvakaki, M.; Georgiou, T. K.; Krasia, T. C.; Themistou, E.; Hadjiantoniou, N.; Patrickios, C. S. *Polymer Bulletin* **2007**, 58, 185-190.

146. Triftaridou, A. I.; Vamvakaki, M.; Patrickios, C. S. *Biomacromolecules* **2007**, 8, 1615-1623.

147. Tsarevsky, N. V.; Matyjaszewski, K. *Chemical Reviews* **2007**, 107, 2270-2299.

148. Tsarevsky, N. V.; Pintauer, T.; Matyjaszewski, K. *Macromolecules* **2004**, 37, 9768-9778.

149. Tsuji, H.; Horikawa, G.; Itsuno, S. *Journal of Applied Polymer Science* **2007**, 104, 831-841.

150. Tsuji, H.; Ono, T.; Saeki, T.; Daimon, H.; Fujie, K. *Polymer Degradation and Stability* **2005**, 89, 336-343.

151. Vamvakaki, M.; Patrickios, C. S.; Lindner, P.; Gradzielski, M. *Langmuir* **2007**, 23, 10433-10437.

152. Van de Wetering, P.; Moret, E. E.; Schuurmans-Nieuwenbroek, N. M. E.; Van Steenbergen, M. J.; Hennink, W. E. *Bioconjugate Chemistry* **1999**, 10, 589-597.

153. Van Tomme, S. R.; van Steenbergen, M. J.; De Smedt, S. C.; van Nostrum, C. F.; Hennink, W. E. *Biomaterials* **2005**, 26, 2129-2135.

154. Victorov, A. *Fluid Phase Equilibria* **2005**, 227, 9-17.

155. Victorov, A. I. *Fluid Phase Equilibria* **2006**, 241, 334-343.

156. Wang, T.-L.; Liu, Y.-Z.; Jeng, B.-C.; Cai, Y.-C. *Journal of Polymer Research* **2005**, 12, 67-75.

157. Weaver, J. V. M.; Bannister, I.; Robinson, K. L.; Bories-Azeau, X.; Armes, S. P.; Smallridge, M.; McKenna, P. *Macromolecules* **2004**, 37, 2395-2403.

158. Xiong, Q.; Ni, P.; Zhang, F.; Yu, Z. *Polymer Bulletin* **2004**, 53, 1-8.

159. Xu, C.; Fu, X.; Fryd, M.; Xu, S.; Wayland, B. B.; Winey, K. I.; Composto, R. J. *Nano Letters* **2006**, 6, 282-287.

160. Yilmaz, Z.; Akkas, P. K.; Sen, M.; Guven, O. *Journal of Applied Polymer Science* **2006**, 102, 6023-6027.

161. Young, R. J.; Lovell, P. A., Introduction to Polymers. 2nd ed.; Chapman & Hall: London, **1991**.

162. Yuk, S. H.; Cho, S. H.; Lee, S. H. *Macromolecules* **1997**, 30, 6856-6859.

163. Zhang, H.; Klumperman, B.; Ming, W.; Fischer, H.; van der Linde, R. *Macromolecules* **2001**, 34, 6169-6173.

164. Zhang, X.; Xia, J.; Matyjaszewski, K. *Macromolecules* **1998**, 31, 5167-5169.

Vita

Kyle Brandon Guice was born on April 29, 1982, in Ruston, Louisiana. Kyle is the second son of Dr. Leslie and Kathy Guice. Kyle graduated from Ruston High School in 2000. In 2004, Kyle earned his Bachelor of Science in Chemical Engineering from Louisiana Tech University. Kyle participated in undergraduate research under the direction of Dr. Michael J. McShane, where he researched fluorescence sensors for biological applications based on the electrostatic self-assembly of polyelectrolytes, publishing three peer-reviewed articles on the subject. After graduation from Louisiana Tech University, Kyle married Ginger McBride, also from Ruston, Louisiana. In 2004, Kyle entered the Ph.D. program in Chemical Engineering at the University of Texas at Austin where, under the direction of Dr. Yueh-Lin Loo, he researched block copolymer hydrogels containing statistical copolymers of 2-dimethylaminoethyl methacrylate and 2-hydroxyethyl methacrylate. Upon completion of his doctorate degree, Kyle will begin work with the ExxonMobil Upstream Research Company in Houston, Texas.

Permanent address: 210 Audubon Drive, Ruston, LA 71270

This dissertation was typed by Kyle Guice.